Advancing Fetoscopic Repair of Complex Gastroschisis

Proof of Principle for a Novel Closure Method Using a Silicone Ring with Membrane

Nynke Ansems

Master Thesis

Erasmus MC

TU Delft

Advancing Fetoscopic Repair of Complex Gastroschisis

Proof of Principle for a Novel Closure Method Using a Silicone Ring with Membrane

by

Nynke Ansems

a thesis in partial fulfillment of the requirements for the degree of

Master of Science
in Biomedical Engineering

at the Delft University of Technology,
to be defended publicly on Tuesday October 3, 2023 at 3:45 PM.

Student number:	5366496	
Thesis committee:	Prof. dr. J.J. van den Dobbelsteen	TU Delft, supervisor
	Dr. P.L.J. DeKoninck	Erasmus MC, supervisor
	Prof. dr. M. van der Elst	TU Delft
	Dr. ir. F.J.H. Gijsen	TU Delft

This thesis is confidential and cannot be made public until October 3, 2025

TU Delft

Abstract

Gastroschisis, a congenital abdominal wall defect located to the right of the intact umbilical cord (UC), results in the herniation of fetal abdominal organs into the amniotic cavity without a protective membrane covering these structures. Complex gastroschisis (CG), comprising approximately 10% of cases, is associated with significantly higher morbidity and mortality rates compared to simple gastroschisis. Fetoscopic repair of CG offers the potential to improve gastrointestinal health at birth, but thus far, no procedure has been successfully demonstrated as safe and feasible. Therefore, the goal of this graduation project was to provide a proof of principle for a novel dedicated method that enables the swift closure of the abdominal wall defect during a fetoscopic repair procedure for CG.

The development of this method began with an analysis of the clinical context, including the characteristics of the abdominal wall defect, the adjacent umbilical cord and vessels, and the fetoscopic surgical setup, which provided a clear design direction. After generating various concept solutions, the key concept — a silicone ring with membrane — was selected using the Harris Profile methodology. This concept was designed for insertion into the fetal abdominal cavity, with the membrane effectively covering the opening of the defect.

Eight configurations of the silicone ring with a membrane were then prototyped through injection molding of liquid silicone rubber in a 3D-printed mold. The rings varied in shape (round or rusk), diameter (20 mm and 30 mm), and stiffness (shore hardness A25 and A40). Additionally, a validation model simulating a 24-week-old fetus with CG was developed with input from medical experts.

The validation experiments demonstrated that the silicone ring with a membrane securely remained in place, effectively closing the abdominal wall defect under intra-abdominal pressure conditions ranging from 0 to 40 mmHg. These experiments, conducted using the validation model, simulated conditions during and immediately after fetal intervention in a 24-week-old fetus with CG following intestinal repositioning. These experiments provided proof of principle for the silicone ring with membrane as a novel method that enables the swift closure of the abdominal wall defect in CG during a fetoscopic repair procedure. Notably, round-shaped rings were favored, and larger diameters allowed for coverage of larger defects. However, it's noteworthy that the 20 mm round ring effectively covered an oval-shaped defect measuring 13.5 $\times$ 12.7 mm, aligning with the reported mean defect size in CG. Furthermore, the experiments demonstrated the feasibility of introducing the rings through a 12 Fr (20 mm rings) or 14 Fr (30 mm rings) surgical port, aligning with the preferred surgical setup.

Future research is required to clinically investigate the defect diameter in CG and optimize the silicone ring with membrane's design. Additionally, enhancing the validation model to serve dual purposes as both a validation and training model will facilitate user tests. Moreover, developing an instrument for introducing the ring into the uterus and refining the surgical technique for precise ring positioning will be essential steps toward the clinical application of this innovative approach.

Contents

List of Abbreviations vii

1 Introduction 1
- 1.1 Fetoscopic Surgery in Gastroschisis . . . 1
- 1.2 State-of-the-Art . . . 2
  - 1.2.1 Literature Review . . . 2
  - 1.2.2 Progressive Insight Based on Unpublished Research . . . 2
- 1.3 Problem Definition . . . 3
- 1.4 Project Goal . . . 4
- 1.5 Project Approach and Thesis Outline . . . 4

2 Concept Design 5
- 2.1 Clinical Context Analysis . . . 5
  - 2.1.1 Abdominal Wall Defect . . . 5
  - 2.1.2 Umbilical Cord and Vessels . . . 6
  - 2.1.3 Surgical Setup . . . 7
- 2.2 Design Direction . . . 8
  - 2.2.1 Key Properties . . . 8
  - 2.2.2 List of Requirements . . . 9
- 2.3 Concept Design . . . 10
  - 2.3.1 Ideation . . . 10
  - 2.3.2 Most Promising Concepts . . . 10
  - 2.3.3 Concept Selection . . . 11

3 Prototyping 13
- 3.1 First Prototyping Round . . . 13
  - 3.1.1 Introduction . . . 13
  - 3.1.2 Methods . . . 13
  - 3.1.3 Results . . . 16
  - 3.1.4 Discussion . . . 18
- 3.2 Final Prototyping Round . . . 19
  - 3.2.1 Introduction . . . 19
  - 3.2.2 Methods . . . 19

4 Validation Model Development 23
- 4.1 Objective and Requirements . . . 23
  - 4.1.1 List of Requirements . . . 24
- 4.2 Additional Clinical Context Analysis . . . 24
  - 4.2.1 Dimensions Abdominopelvic Cavity . . . 24
  - 4.2.2 Intra-Abdominal Pressure . . . 25
- 4.3 Initial Version Validation Model . . . 25
  - 4.3.1 3D-Printed Components . . . 26
  - 4.3.2 Abdominal Wall . . . 26
  - 4.3.3 Umbilical Cord and Vessels . . . 27
  - 4.3.4 Intra-Abdominal Pressure . . . 27
  - 4.3.5 Validation and Feedback Medical Experts . . . 27
- 4.4 Refinement Model Components . . . 28
  - 4.4.1 Abdominal Wall . . . 28
  - 4.4.2 Intra-Abdominal Pressure Regulation . . . 29
  - 4.4.3 Redesign 3D-Printed Components . . . 29

4.5 Final Version Validation Model . . . 31
4.5.1 Requirements Evaluation . . . 32

5 Validation Experiments **35**
5.1 Experiment 1: Proof of Principle . . . 35
5.1.1 Introduction . . . 35
5.1.2 Methods . . . 36
5.1.3 Results . . . 38
5.2 Experiment 2: Increase Abdominal Wall Defect Diameter . . . 40
5.2.1 Introduction . . . 40
5.2.2 Methods . . . 40
5.2.3 Results . . . 42
5.3 Experiment 3: Compatibility Surgical Ports . . . 42
5.3.1 Introduction . . . 42
5.3.2 Methods . . . 43
5.3.3 Results . . . 44

6 Discussion **45**
6.1 Validation Experiment 1 and 2: Proof of Principle . . . 45
6.1.1 Interpretation of the Results . . . 45
6.1.2 Implications . . . 47
6.1.3 Limitations . . . 47
6.2 Validation Experiment 3: Compatibility Surgical Ports . . . 48
6.2.1 Interpretation of the Results . . . 48
6.2.2 Implications . . . 48
6.2.3 Limitations . . . 49
6.3 Requirements Evaluation . . . 49
6.4 Future Recommendations . . . 51
6.4.1 Clinical Research . . . 51
6.4.2 Silicone Ring Design Parameters . . . 51
6.4.3 Validation Model . . . 51
6.4.4 Introducing the Ring . . . 52
6.4.5 Placing the Ring . . . 52
6.5 Conclusion . . . 52

References **53**

A Clinical Interview **57**

B Ultrasound Image Analysis **59**

C Dutch Fetal Biobank **63**

D Gastroschisis Newborn Examination **65**

E Ideated Concepts and Harris Profiles **67**

F Production Protocol Silicone Rings **71**

G Dimensions Umbilical Cord and Vessels **77**

H Technical Specifications 3D-Printed Mold **79**

I Dimensions Fetal Abdominopelvic Cavity **83**

J Abdominal Wall Prototypes **85**

K Production Protocol Abdominal Wall **87**

L Technical Specifications 3D-Printed Components Validation Model **91**

M Assembly Instructions Validation Model **95**

List of Abbreviations

ACS abdominal compartment syndrome

CG complex gastroschisis

EC experimental condition

EU experimental unit

GA gestational age

IABD intra-abdominal bowel dilation

IAP intra-abdominal pressure

IPA isopropyl alcohol

LSR liquid silicone rubber

MRI magnetic resonance imaging

PLA polylactic acid

SBA spina bifida aperta

SG simple gastroschisis

UA umbilical artery

UC umbilical cord

US ultrasound

UV umbilical vein

1

Introduction

1.1. Fetoscopic Surgery in Gastroschisis

Gastroschisis is a congenital abdominal wall defect that occurs in approximately 3 per 10,000 births in Europe and 4.3 per 10,000 in the USA [1]. The defect is usually located just to the right of the intact umbilical cord (UC), causing the fetus' abdominal organs to herniate from the abdomen into the amniotic cavity without a membrane covering the structures as illustrated in Figure 1.1 [2], [3]. A clinical differentiation is made between simple gastroschisis (SG) and complex gastroschisis (CG). CG accounts for approximately 10% of gastroschisis cases [4] and is characterized by one or more of the following complications at birth: intestinal atresia, perforation, volvulus or necrosis [1]. As newborns with CG have significantly higher rates of morbidity and mortality than newborns with SG, multiple authors have argued that CG is a candidate condition for fetal surgery [3]–[5].

The rationale behind this intervention is that coverage or (partial) repositioning of the bowels in utero could improve or reverse the natural history of the condition. This is achieved by reducing or preventing secondary bowel damage caused by (1) ischemic constriction at the site of the defect, and (2) inflammation due to exposure of the bowel to amniotic fluid [5]. Furthermore, intrauterine reduction of the bowel herniation could ensure that the abdominal cavity grows more proportionally with the intestines, thereby guaranteeing that the abdomen is large enough to accommodate for the entire bowel [3]. If such a fetal intervention would be successfully performed, gastrointestinal health at birth will improve, preventing the need for multiple neonatal surgeries and general anesthesia. Consequently, this would minimize the medical and emotional burden on patients and their families [5].

Figure 1.1: Illustration of a newborn with gastroschisis. Source: Adapted from [6]

Fetoscopy has emerged as the preferred surgical approach in fetal surgery for gaining fetal access. This preference is evident in the advancements made in the fetal spina bifida aperta (SBA) intervention, where newly developed fetoscopic techniques have shown a reduction in maternal and neonatal complications compared to the previously employed open hysterotomy approach [7], [8].

1.2. State-of-the-Art

1.2.1. Literature Review

Prior to this graduation project, a comprehensive literature review was conducted to examine the current state of research on fetoscopic surgery for gastroschisis. The few studies that have been published on this subject - conducted using ovine models - conclude that it is not feasible to reposition the intestines into the fetal abdominal cavity as both the defect and the fetal abdominal cavity are too small to return the large volume of eviscerated bowel [9], [10].

However, one study employed an alternative approach by using a fetoscopic technique to cover the intestines with a bag, yielding positive outcomes. The application of these bags resulted in improved bowel histology and reduced bowel peel formation [11]. Nonetheless, at the end of gestation, the sutures used to secure the bags to the fetal abdominal wall became torn or grew out of the fetal skin. Consequently, the bags became partially or completely dislocated [12].

1.2.2. Progressive Insight Based on Unpublished Research

After conducting the literature review, the FDA approval of a phase 1 clinical trial for fetoscopic repair of CG was announced during a webinar presented by Baylor College of Medicine and Texas Children's Hospital (Houston, Texas, USA) [13], [14]. The trial will employ a laparotomy-assisted fetoscopic 2-port technique on an exteriorized uterus, which is equivalent to the fetoscopic SBA intervention developed at the same hospital [7]. The procedure, depicted in Figure 1.2, involves repositioning the intestines into the fetal abdominal cavity using standard 3 mm fetoscopic instrumentation (Karl Storz, Tuttlingen, Germany). The abdominal wall defect will then be closed using polydioxanone sutures.

Prior to this human trial, researchers at KU Leuven (Belgium) developed and validated a fetal lamb model of CG. They initially demonstrated the safety and efficacy of open fetal repair and subsequently established the feasibility and safety of fetoscopic repair [13]. However, it should be noted that the aforementioned studies have not been published at the time of writing this thesis.

The fetoscopic intervention is scheduled to be performed between 20 to 26 weeks of gestation [14]. The lower limit of 20 weeks aligns with the typical timing of gastroschisis detection during the routine 20-week ultrasound (US) examination [4]. The upper limit of 26 weeks, although not explicitly discussed, is presumably based on the understanding that the earlier the intervention is carried out, the likelier it is that secondary bowel damage is prevented. Additionally, as the gestational age (GA) progresses, repositioning the rapidly growing intestines into the abdomen may become more challenging due to their increasing volume. Furthermore, the timing of the intervention aligns with the well-studied studied fetal SBA procedure [15].

To identify CG fetuses eligible for the trial, an inclusion criterion of intra-abdominal bowel dilation (IABD) $\geq$10 mm at 20-24 weeks GA is used, as this US marker has shown to be the most reliable predictor of CG (specificity = 95.6%, sensitivity = 51.8%) [1].

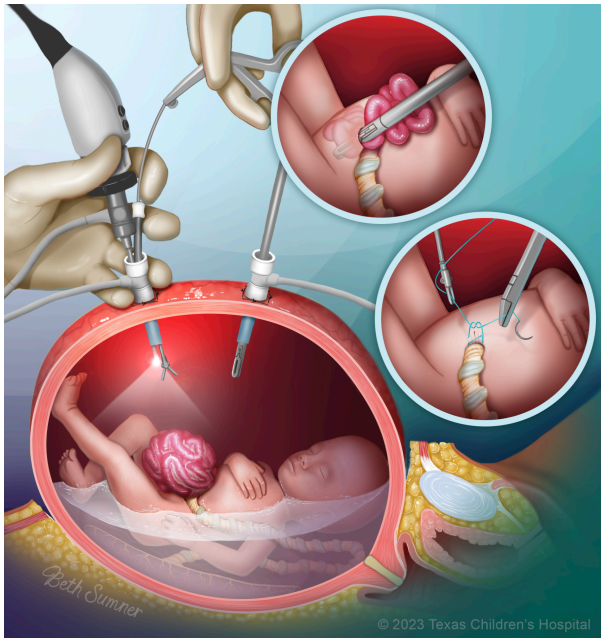

Figure 1.2: Illustration of the laparotomy-assisted fetoscopic 2-port technique on an exteriorized uterus employed in the fetal gastroschisis repair procedure during the clinical trial at Texas Children's Hospital (Houston, Texas, USA). The procedure involves the use of two ports, one for an endoscopic camera and a fetoscopic working instrument, and another for a fetoscopic working instrument. The eviscerated intestines are repositioned into the abdominal cavity using atraumatic graspers, followed by closure of the abdominal wall defect using polydioxanone sutures. Source: [16]

1.3. Problem Definition

Ideally, a fetoscopic repair procedure for gastroschisis addresses both causes of secondary bowel damage: (1) ischemic constriction at the site of the defect, and (2) inflammation due to exposure of the bowel to amniotic fluid, while minimizing maternal and fetal risk.

The procedure that will be studied in the FDA-approved phase 1 clinical trial for fetoscopic repair of CG strives to do both [14]. Nonetheless, the results of the clinical trial must be awaited to determine whether this procedure is safe and feasible to perform on humans. Besides, even if the results were positive, suturing up the defect remains a time-intensive task to perform fetoscopically (as demonstrated by the fetoscopic SBA procedure [7]). Because prolonged operative time significantly increases the likelihood of complications, a reduction in operative duration is desired to minimize maternal and fetal risk [17]. In addition to the aspect of time, the location of the defect - right next to the UC - causes the area to be especially delicate to operate on.

The other approach that was studied by Bergholz *et al.*, fetoscopic coverage of the intestines with a bag, protects the bowels from the amniotic fluid, but does not tackle the issue of ischemic constriction [12]. Furthermore, a sufficient fixation technique that keeps the bag in place until birth has not been established. Therefore, the problem definition is defined as follows:

Problem Definition

Fetoscopic repair of complex gastroschisis holds the potential to enhance gastrointestinal health at birth. However, thus far, no procedure has been successfully demonstrated as safe, feasible, and capable of addressing both causes of secondary bowel damage while minimizing risks to both the mother and the fetus.

1.4. Project Goal

Erasmus MC (Rotterdam, The Netherlands), serving as the client for this graduation project, is seeking to develop an innovative fetoscopic repair procedure for CG as an alternative to the procedure currently under evaluation at Texas Children's Hospital (outlined in Section 1.2). Building upon the unpublished research conducted at KU Leuven [13], which indicates the feasibility of fetoscopically reducing eviscerated intestines into the abdomen, and in line with the problem definition outlined in Section 1.3, Erasmus MC presented the following project assignment: *Design a method that enables swift closure of the abdominal wall defect, following the reduction of eviscerated intestines in CG using fetoscopy, eliminating the reliance on suturing while ensuring the stability of the closure until the end of the pregnancy.*

To ensure a clear scope for this graduation project, it was essential to address the numerous variables associated with a fetoscopic procedure. Firstly, it was determined that the procedure for gaining surgical access to the fetus would align with existing techniques, specifically the laparotomy-assisted fetoscopic 2-port technique on an exteriorized uterus, originally developed for fetal SBA repair [7]. The procedural aspects relevant to this project will be discussed in Section 2.1.3.

Additionally, it was decided that the project would exclusively focus on the development of a novel closure method, excluding the development of any new instruments that might be required for implementing the closure method. However, if the closure method required the use of a non-existing instrument, it had to be feasible to produce it based on the already existing fetoscopic or laparoscopic instrumentation. Based on these considerations, the project goal was formulated as follows:

Project Goal

To provide a proof of principle for a novel dedicated method that enables the swift closure of the abdominal wall defect during a fetoscopic repair procedure for complex gastroschisis.

1.5. Project Approach and Thesis Outline

At the outset of this project, it became evident that three distinct research paths had to be pursued to demonstrate a proof of principle for a novel dedicated closure method. These paths included: (1) designing a concept for the closure method, (2) producing a prototype of the designed concept, and (3) developing a validation model to assess the functionality of the produced prototype.

As these paths represent distinct components of the project, each one is outlined in a dedicated chapter (Chapter 2, 3 and 4, respectively), facilitating a comprehensive understanding of their individual contributions. Subsequently, in Chapter 5, the validation experiments and results are presented, followed by a comprehensive discussion in Chapter 6.

2

Concept Design

This chapter presents the systematic process for designing the concept of the novel dedicated closure method. It begins with an analysis of the relevant clinical context for the design in Section 2.1. Following this, Section 2.2 establishes the design direction. Lastly, Section 2.3 elaborates on the actual concept design process.

2.1. Clinical Context Analysis

The clinical context considered relevant to the design encompassed the anatomy and size of the abdominal wall defect throughout gestation, vital structures surrounding the defect (with a focus on the UC and its vessels), and the surgical setup for the fetoscopic procedure.

In addition to the literature, this section draws from a clinical interview (Appendix A), analysis of US images (Appendix B), examination of a gastroschisis fetus from the Dutch Fetal Biobank (Appendix C), and examination of a gastroschisis newborn at Erasmus MC (Appendix D).

2.1.1. Abdominal Wall Defect

Anatomy of the Defect

As discussed in Section 1.1, a newborn with gastroschisis exhibits an anterior abdominal wall defect, resulting in a circular opening located just to the right of the UC. This defect, situated between the pair of rectus abdominis muscles, encompasses all layers of the abdominal wall, including the skin, two fatty layers, multiple fascia layers, and the parietal peritoneum (Figure 2.1).

Pediatric surgeons at Erasmus MC noted that, in postnatal examinations, they can palpate a firm ring along the edges of the defect (see Appendix A). This firmness primarily stems from the deep fascia layers that constitute the rectus sheath, composed of dense and organized connective tissue [18].

Size of the Defect

The size of the abdominal wall defect in CG lacks comprehensive study, resulting in limited conclusive dimensions from existing literature. Mazzoni *et al.* reported defect sizes based on US analysis at diagnosis, with a mean defect size of 15 mm (n = 16) for SG and 12 mm (n = 5) for CG (range 12-14 mm) [19]. This study reported a median defect size at birth as 27 mm, without distinguishing between SG and CG, implying an increase in defect size during gestation.

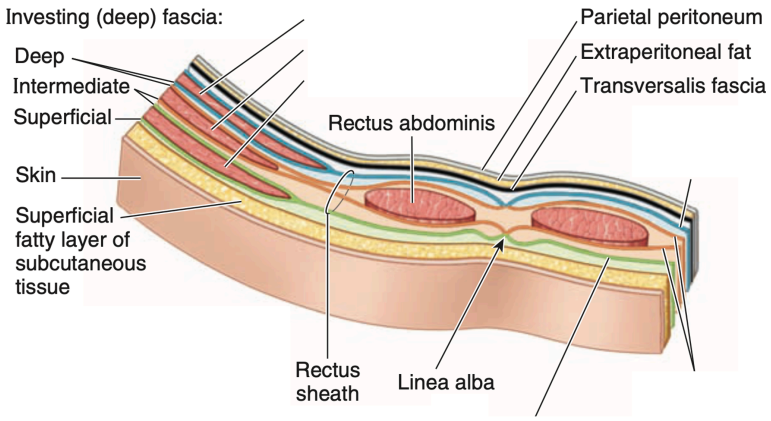

Figure 2.1: Structure of the anterior abdominal wall. Superior view of the transverse section superior to umbilicus. Source: Adapted from: [18]

Notably, in CG cases, it seems the defect size remains stable or may even narrow, resulting in smaller defects at birth compared to SG. This hypothesis emerged from a fetal MRI study, indicating that the process of bowel segments protruding into the amniotic cavity during the second trimester halts due to a narrowed abdominal wall defect, leading to intestinal stenosis/atresia characteristic of CG [20].

Supporting this difference in defect size at birth, Gelas *et al.* reported a mean defect size of 23 mm (n = 61) in SG compared to a smaller 12 mm (n = 8) in CG [21]. Additionally, patients with bowel atresia, a complication specific to CG, presented with significantly smaller defect sizes compared to those without (21 mm vs. 37 mm) [22].

Due to the lack of definitive conclusions in the literature regarding defect size, additional retrospective US analysis and examination of a gastroschisis newborn were performed at Erasmus MC as part of this project (see Appendix B and D). The US analysis indicated a consistent defect size of approximately 10 mm for a GA of 20 to 25 weeks. However, data regarding the defect size before week 20 or after week 25, as well as information on postnatal outcomes, were unavailable for these cases. Examination of the defect in a newborn with SG (36 weeks GA) showed a defect size of 20 mm both before and after repositioning of the intestines (see Appendix D).

In summary, existing literature does not conclusively establish the size of the defect in CG, but the defect size at birth appears to range from 12 mm to 21 mm. The self-conducted US examinations revealed a defect size of approximately 10 mm for a GA of 20 to 25 weeks, though additional data was lacking. Nevertheless, literature suggests that in CG cases, the defect diameter typically remains stable or narrows during gestation, potentially leading to increased intestinal compression and complications like atresia and stenosis.

2.1.2. Umbilical Cord and Vessels

During the clinical interview (Appendix A), it became evident that the proximity of the UC and the umbilical vessels to the abdominal wall defect requires careful consideration. Pediatric surgeons at Erasmus MC noted that the UC is positioned in a manner that it is ”almost inside the defect.” This clinical observation found further support through the examination of a gastroschisis fetus at the Dutch Fetal Biobank (see Appendix C) and a gastroschisis newborn at Erasmus MC (see Appendix D), both of which confirmed direct adjacency between the defect and the UC.

Typically, the UC comprises the umbilical vein (UV) and two umbilical arteries (UAs), all embedded

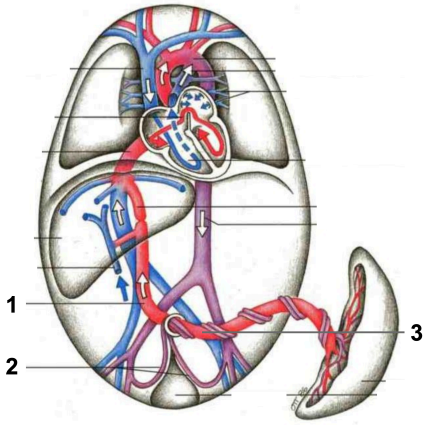

Figure 2.2: Schematic representation of the fetal circulatory system, illustrating the oxygen gradient indicated by color. *Labels:* (1) Umbilical vein, (2) Umbilical artery, (3) Umbilical cord. Source: Adapted from: [24]

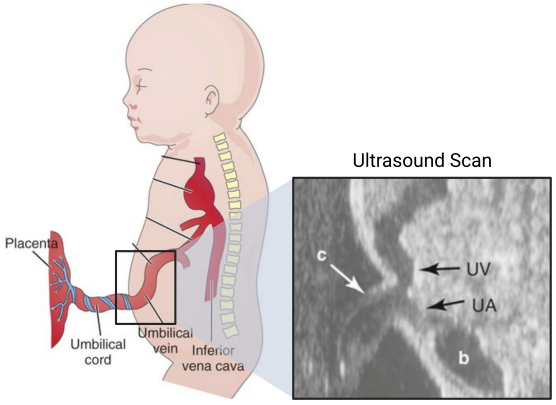

Figure 2.3: Schematic illustration of the course of the umbilical vein in the sagittal plane, accompanied by an ultrasound scan demonstrating the umbilical cord and the trajectory of its vessels in the fetus. *Labels:* (b) Bladder, (c) Umbilical cord, (DV) Ductus venosus, (UA) Umbilical artery, (UV) Umbilical vein. Created with BioRender.com. Source: Adapted from: [23]

within the Wharton's jelly, a mucous connective tissue. The umbilical vessels, also enveloped in mucous connective tissue, naturally extend into the abdominal cavity, with the UV carrying oxygen-rich blood towards the liver, while the UAs return medium-oxygenated blood from the internal iliac arteries back to the placenta (see Figure 2.2) [23].

The anatomical trajectory of the UV and UAs within the fetal body can be observed in Figure 2.2 (anterior aspect) and Figure 2.3 (sagittal plane). Any disruption to the blood flow through the UC or its associated vessels poses a significant risk to the fetus's viability.

2.1.3. Surgical Setup

The FDA-approved phase 1 clinical trial for fetoscopic repair of CG, discussed in Section 1.2, employs a laparotomy-assisted fetoscopic 2-port technique. The novel dedicated closure method should align with this technique. During this procedure, the maternal abdomen is opened via a transverse lower abdominal incision, and the uterus is exteriorized. Under US guidance, the fetus is carefully manipulated into position. Prior to introducing a 12 Fr port (Cook Inc., Bloomington, IN, USA) (illustrated in Figure 2.4) into the amniotic cavity using the Seldinger technique, plication sutures are placed to secure the membranes to the uterine wall. Approximately 300 to 500 mL of amniotic fluid is then withdrawn, and CO_2 is insufflated into the uterus via a heater/humidifier. By inserting an endoscope into the gas pocket via the port, visualization is achieved. An additional working instrument can be introduced through this port. Additionally, a second 12 Fr port is inserted under direct visualization to accommodate further instrumentation [15].

Erasmus MC, the client of this project, intends to employ the novel closure method in the alternative fetoscopic procedure using a maximum of two 12 Fr (4 mm) ports. However, they are willing to consider a port with a maximum diameter of 14 Fr (≈4.7 mm) if the former option is not feasible. Furthermore, they aim for the alternative fetoscopic procedure to have a maximum in utero time of 30 minutes (see Appendix A).

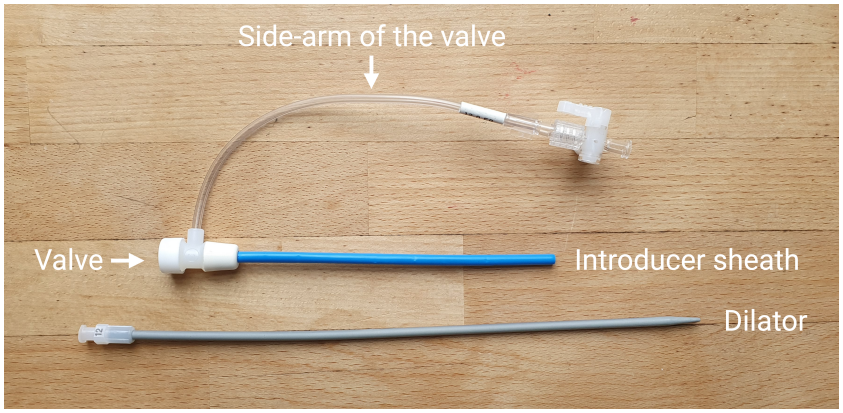

Figure 2.4: 12 Fr Performer™Introducer Set (Cook Inc., Bloomington, IN, USA) comprising an introducer sheath equipped with a valve to prevent CO_2 leakage and a dilator.

2.2. Design Direction

This section presents the design direction by defining the key properties and the full list of requirements that the design should fulfill. The design direction aligns with the project goal discussed in Section 1.4 and builds upon the clinical context analysis conducted in Section 2.1.

2.2.1. Key Properties

A list of key properties was formulated which served as guiding principles throughout the design process. During the ideation phase, they played a crucial role in quickly evaluating the suitability and feasibility of ideas. This proved to be particularly valuable as assessing a concept against the complete list of requirements was challenging at such an early stage.

- **Efficient Closure:** The design should ensure a efficient closure of the defect, preventing the intestines from protruding into the amniotic cavity and shielding them from exposure to the amniotic fluid.
- **Functionality in Wet Environment:** The design should function effectively within the amniotic fluid.
- **Fetal Growth Compatibility:** The design should account for the growth and development of the fetus, maintaining its intended functionality until birth.
- **Safety Umbilical Cord and Vessels:** The design should not compromise the blood flow through the UC or its vessels.
- **Surgical Setup Compatibility:** The design should be compatible with the current surgical setup used for fetal surgery, ensuring ease of implementation.
- **Compact Size:** The design should be compact, allowing for the use of surgical ports with minimal diameters to minimize the risk of premature birth.
- **Quick Procedure:** The design should facilitate a quick surgical procedure, reducing both maternal and fetal risks associated with prolonged operations.
- **Manufacturability:** The design should be easily manufacturable, considering factors such as the production processes, availability of materials, and cost-effectiveness.

2.2.2. List of Requirements

A comprehensive list of requirements was developed which served a dual purpose: firstly, as a guideline during the development of the new design, and secondly, as a tool for evaluating the produced prototype. The list underwent regular review and updates to ensure its accuracy and relevance.

Performance

- ☐ The design should prevent the intestines from protruding into the amniotic cavity.
- ☐ The design should shield the intestines from exposure to amniotic fluid.
- ☐ The design should maintain its intended functionality from the fetal intervention (20-25 weeks GA) until birth (38-40 weeks GA).
- ☐ The design should be suitable for abdominal wall defects with diameters ranging from 12 mm to 20 mm.
- ☐ The design should function effectively in the wet environment of the amniotic fluid.

Safety

- ☐ The design should not compromise the blood flow through the UC or its vessels.
- ☐ All materials used in the design should comply with biological safety standards as defined in ISO 10993-1 [25].
- ☐ The design should be capable of undergoing terminal sterilization, as defined in EN 556-1 [26].

Surgical Context

- ☐ The design should facilitate a surgical procedure with a maximum in utero time of 30 minutes.
- ☐ The design should be operable solely with indirect visual feedback provided by an endoscopic camera.
- ☐ The design should require the use of a maximum of two working instruments simultaneously, excluding the endoscopic camera.
- ☐ The design should be compatible with surgical ports with a maximum inner diameter of 14 Fr (≈4.7 mm), with a preference for 12 Fr (4.0 mm) or smaller.

Manufacturing Process

- ☐ The materials and equipment required for producing the design should be readily available commercially.
- ☐ The manufacturing process for the design should be replicable to ensure consistent quality.

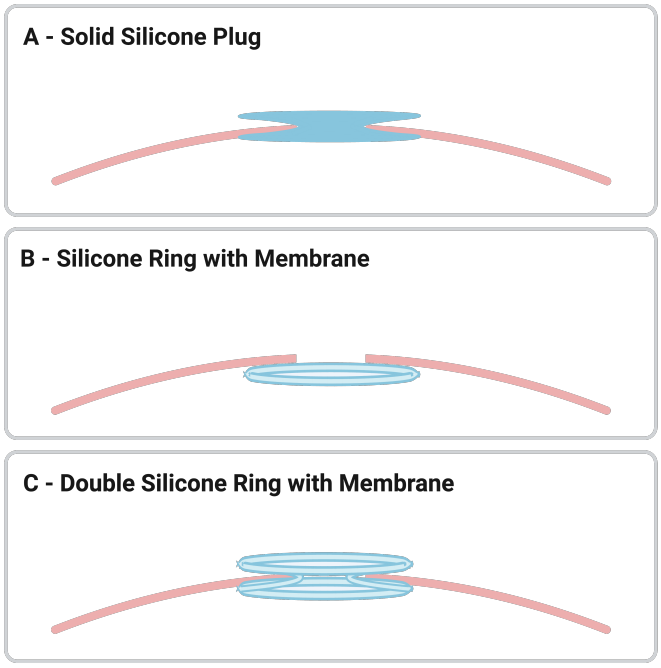

Figure 2.5: The three most promising concept solutions (A-C), depicted in relation to a simplified transverse view of an abdominal wall with a gastroschisis defect. Created with BioRender.com

2.3. Concept Design

This section presents the actual concept design phase, starting with an exploration of the ideation process in Section 2.3.1. The subsequent focus is directed to the three most promising concept solutions that arose from the ideation phase in Section 2.3.2. Additionally, the rationale behind the concept selection is discussed in Section 2.3.3.

2.3.1. Ideation

A brainstorming session was conducted to explore and generate a diverse set of concept solutions. Following this ideation process, each concept underwent evaluation using the Harris Profile methodology [27], taking into account the key properties outlined in Section 2.2.1. This evaluation enabled a swift and efficient visual comparison of all concept solutions, which facilitated the decision-making process regarding which concepts to proceed with in the design process. For an overview of all concept solutions created during the ideation process and their corresponding Harris profiles, please refer to Appendix E.

2.3.2. Most Promising Concepts

After evaluating all ideated concepts using the Harris profiles, the three most promising concepts were chosen for further development. Figure 2.5 visually represents these selected concepts.

Concept A is a solid silicone plug designed in the shape of a diabolo, with one end inserted inside the fetal abdomen and the other end extending into the amniotic cavity. The narrowest part of the plug is positioned at the level of the abdominal wall. The narrow section can be adjusted to be very narrow, suitable for small defect sizes, while the heads can be larger to cover larger defects.

Concept B involves a silicone ring that encompasses a thin silicone membrane. The entire device

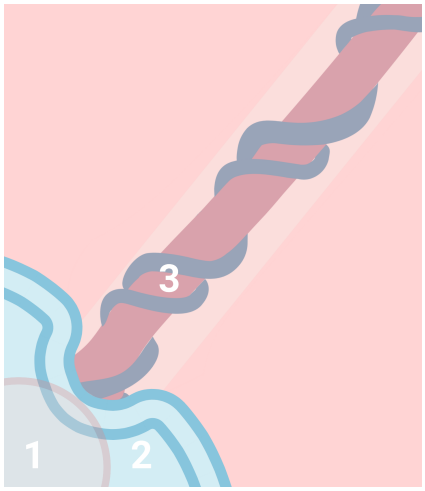

Figure 2.6: Schematic illustration showcasing how concept solutions A, B, and C incorporate a cut-out design to prevent interference with the umbilical cord while effectively covering the abdominal wall defect. (1) Abdominal wall defect. (2) Silicone ring or plug. (3) Umbilical cord. Created with BioRender.com

is meant to be fully inserted into the fetal abdominal cavity, with the ring in direct contact with the abdominal wall and the membrane covering the opening of the defect. The pressure exerted by the intestines against the abdominal wall helps to keep the ring in place.

Concept C combines elements of both *Concept A* and *Concept B*. It features a double silicone ring with membranes, similar to a diabolo plug, where the two rings enclose thin membranes connected only at the midpoint. This design aims to close the defect in a manner similar to *Concept A*.

All these concepts were specifically designed to function effectively within the amniotic fluid. Additionally, they did not require direct attachment to the abdominal wall, eliminating the risk of sutures, hooks, or glue detaching due to fetal growth.

To minimize the risk to the fetus, all the concepts avoided using sharp edges or hooks. Additionally, they were designed to be made from a flexible silicone rubber to avoid compressing of the UC and its vessels, ensuring unimpeded blood flow. Figure 2.6 visually demonstrates how all the concepts could include a cut-out in the ring or plug to prevent the compression of the UC and vessels while effectively covering the defect.

All the concepts were designed to be compact and made from a flexible material, making it easier to insert them through a surgical port. The goal was for them to be swiftly positioned using a maximum of two surgical instruments, relying solely on visual feedback provided by an endoscopic camera.

Silicone rubber was selected as the material for these concepts because liquid silicone rubbers (LSRs) are readily available commercially, relatively inexpensive, and suitable for prototyping through injection molding. Additionally, 'biomedical grade' LSRs find extensive use in the medical industry due to their inert properties (minimal biological reactivity when implanted in the body), high mechanical durability, and suitability for sterilization processes [28]–[30].

2.3.3. Concept Selection

After conducting an evaluation of the Harris Profiles for the most promising concepts (as depicted in Figure 2.7) and consulting with TU Delft research engineer Jan van Frankenhuyzen regarding manufacturing possibilities, the decision was made to move forward with *Concept B* for prototyping and testing.

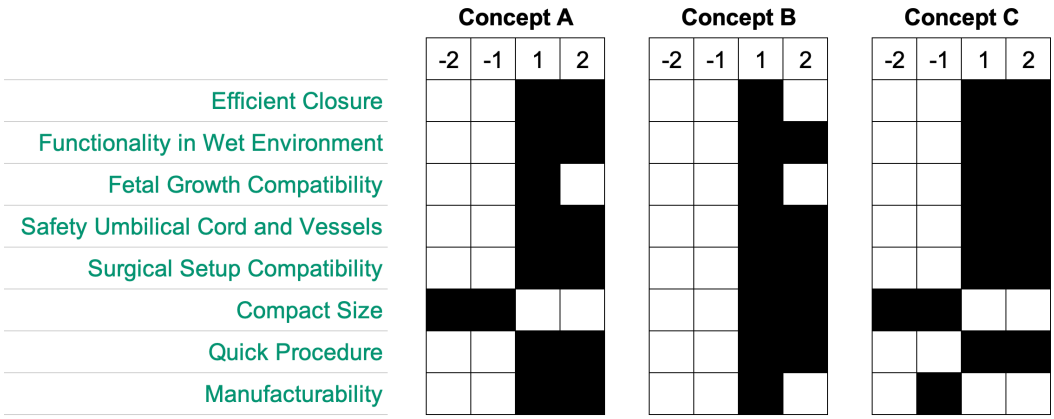

Figure 2.7: The Harris Profiles of the three most promising concepts with respect to the key properties the design needs to possess. A score of -2 indicates poor performance in the evaluated key property, while +2 signifies excellent performance. *Concepts:* A, Solid Silicone Plug. B, Silicone Ring with Membrane. C, Double Silicone Ring with Membrane.

Although *Concept A* received a higher score in terms of efficient closure and manufacturability compared to *Concept B*, it was not selected due to its relatively large size and lack of compressibility, which would have posed challenges for insertion through a 14 Fr port.

While *Concept C* outperformed *Concept B* in terms of efficient closure and compatibility with fetal growth, *Concept B* was chosen due to its more compact size, which was expected to facilitate easier insertion through a small port. Additionally, the simplicity of *Concept B's* design was anticipated to simplify the production process.

3

Prototyping

This chapter outlines the prototyping process for the silicone rings with membranes. It commences with the first prototyping round in Section 3.1, where the focus was on evaluating the concept's manufacturability and conducting preliminary tests. The chapter then proceeds to the second and final prototyping round in Section 3.2, which led to the production of the silicone rings utilized in the validation experiments detailed in Chapter 5.

3.1. First Prototyping Round

3.1.1. Introduction

The initial round of prototyping focused primarily on evaluating the manufacturability of the selected concept, which involved a silicone ring with a thin membrane. Various configurations of the concept were designed and produced to explore its manufacturing feasibility, encompassing different cord sizes and stiffness levels. Subsequently, preliminary tests were performed with the initial version of the validation model to demonstrate an initial proof of principle and evaluate the selected characteristics of the ring. Furthermore, preliminary tests were conducted using the fabricated rings to assess their suitability for introduction through a 14 Fr port. The outcomes from both the manufacturing phase of the first prototyping round and the preliminary tests served as the foundation for the design decisions made in the subsequent and final prototyping round.

3.1.2. Methods

Design Rings and Mold

The ring's characteristics were chosen as follows: a circular shape, an outer diameter of 20 mm — expected to effectively cover abdominal wall defects up to 16 mm in size - and a membrane thickness of 0.4 mm, deemed the thinnest feasible membrane achievable through injection molding using a 3D-printed mold [31]. In the first round of prototyping, the decision was made not to incorporate a cut-out in the ring design. This deliberate choice aimed to prioritize testing the manufacturability of the simplest design iteration before introducing additional complexities.

Three distinct configurations of the ring were developed, each featuring different cord sizes: 1.5 mm, 2.0 mm, and 2.5 mm. This allowed for evaluating various cord dimensions and their potential

Table 3.1: Specifications of the silicone rubbers used in the molding process of the silicone rings with membrane.

Silicone rubber	Shore hardness [36]	Proportion components[a]
Flexible	A25	1A:1B
Semi-flexible	- [b]	1A:1B:0.5H
Stiff	A40	1A:1B:1H

[a] PlatSil® Gel-25 Part A and Part B, and PlatSil® Part H Hardener (Polytek® Development Corp., Easton, PA, USA).
[b] The shore hardness of this mixing proportion is not provided in the technical bulletin for PlatSil® Gels [36].

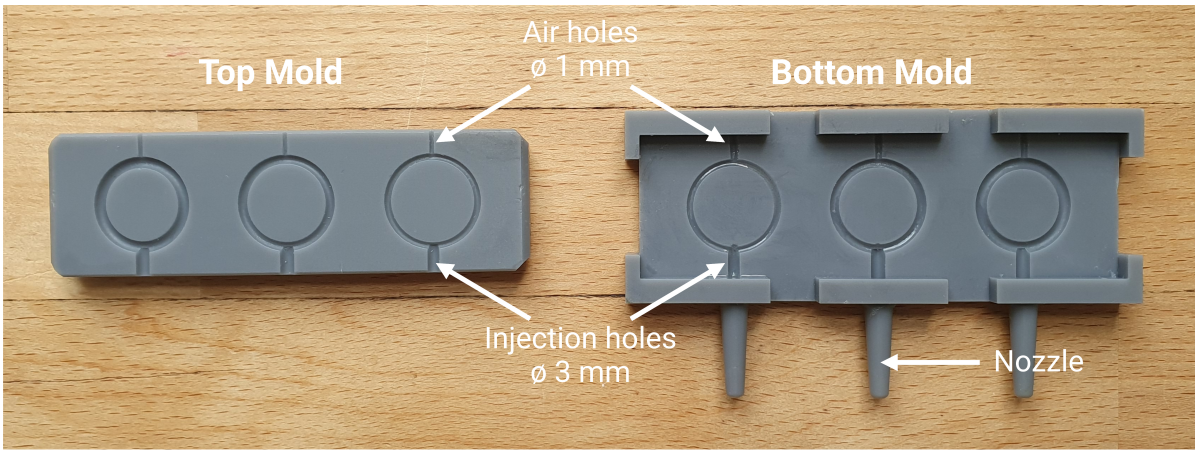

Figure 3.1: Interior surface of both the top and bottom mold used for producing three configurations of the silicone ring with membrane during the first prototyping round. The outer diameter of all rings is consistent at 20 mm and the membrane thickness at 0.4 mm. The rings exhibit varying cord sizes of 1.5 mm, 2.0 mm, and 2.5 mm.

impact on the ring's functionality.

The mold required for manufacturing these rings was created using the CAD software SolidWorks. It consisted of two parts: the top mold and the bottom mold. Each part contained a negative impression of half of the three rings. These impressions were connected to an injection hole with a diameter of 3 mm, which terminated in a nozzle, and an air hole with a diameter of 1 mm.

To materialize the design, the mold was produced using materials and equipment from Formlabs Inc. (Somerville, MA, USA). Specifically, the mold was created through 3D printing using Grey Resin material and a Form 3 printer [31]–[33]. Following the printing process, the mold underwent thorough cleaning with isopropyl alcohol (IPA) in the Form Wash for a duration of 10 minutes [34]. Subsequently, it was subjected to a 30-minute curing process in the Form Cure at a temperature of 60 °C [35]. These post-processing steps resulted in the final mold, as illustrated in Figure 3.1.

Production Silicone Rings with Membrane

To produce silicone rings with varying degrees of stiffness, a combination of the LSRs components PlatSil® Gel-25 (Part A and Part B) and PlatSil® Part H Hardener, all from Polytek® Development Corp. (Easton, PA, USA), was utilized to prepare the silicone rubbers for injection molding. Table 3.1 outlines the distinct silicone rubbers employed during the first prototyping round. The *flexible* silicone rubber employed in the prototyping process represents the highest level of flexibility achievable with PlatSil® Gel-25 without the incorporation of a deadener. In contrast, the *stiff* silicone rubber represents the maximum level of stiffness attainable using PlatSil® Gel-25 in combination with a hardener.

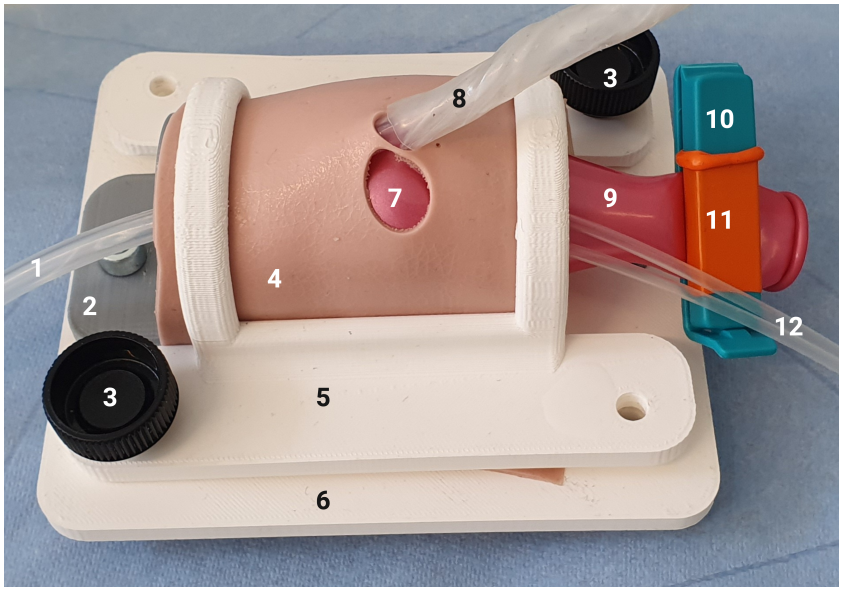

Figure 3.2: Experimental setup used in the preliminary test that intended to establish an initial proof of principal, using the initial version of the validation model. *Labels:* (1) Umbilical vein, (2) 3D-printed superior cap, (3) Knurled-head thumb screw, (4) Abdominal wall, (5) 3D-printed top, (6) 3D-printed base, (7) Abdominal wall defect, (8) Umbilical cord, (9) Balloon, (10) Sealing clip, (11) Cut-out balloon, (12) Umbilical arteries.

The initial production protocol went through a trial-and-error phase during the first prototyping round, where various adjustments and modifications were tested to determine the optimal approach. The final production protocol, refined for the second and final prototyping round, is provided in Appendix F. It outlines the precise steps for consistent and reliable silicone ring production.

Preliminary Test: Proof of Principle

To offer an initial proof of principle, a preliminary test was conducted using the semi-flexible rings with cord sizes of 1.5 mm, 2.0 mm, and 2.5 mm. The choice of these specific rings was primarily influenced by their availability during the testing period. For the test, the initial version of the validation model, described in detail in Section 4.3, was employed, with only the superior cap attached. The base was covered by stretching the abdominal wall (AWL1, refer to Appendix J) over it, and then the top was positioned over the abdominal wall. The top was securely fastened in place using two bolts and nuts, ensuring a tight fit. The UC was positioned within the abdominal wall, with the UV inserted through the hole in the superior cap. Subsequently, a balloon was gently inserted into the abdomen from the bottom, lightly inflated, and secured using a sealing clip. To prevent any air leakage, a cut-out balloon was placed around the sealing clip. Figure 3.2 illustrates the setup used for the preliminary test.

To simulate the amniotic fluid and intestinal mucus, the abdominal wall, balloon, and ring were lubricated with a water-based lubricant (EasyGlide, Veendam, The Netherlands). The ring was cautiously inserted into the defect manually, and pressure in the abdomen was increased by pressing the balloon from the bottom. This pressure was alternately applied by pressing and releasing the balloon. Throughout this process, close attention was paid to the behavior of the ring.

Preliminary Test: Compatibility Surgical Ports

To assess the feasibility of introducing different configurations of the silicone ring through a 14 Fr port or smaller, a precisely crafted aluminum block was utilized. The block, measuring 20 mm in height, was specifically designed to have three holes, each meticulously drilled and scraped to possess the following diameters: 3.5 mm, 4.0 mm, and 4.5 mm, as depicted in Figure 3.3.

Figure 3.3: Aluminum block featuring three holes of varying diameters (3.5 mm, 4.0 mm, and 4.5 mm). Used to assess the feasibility of inserting the different configurations of silicone rings.

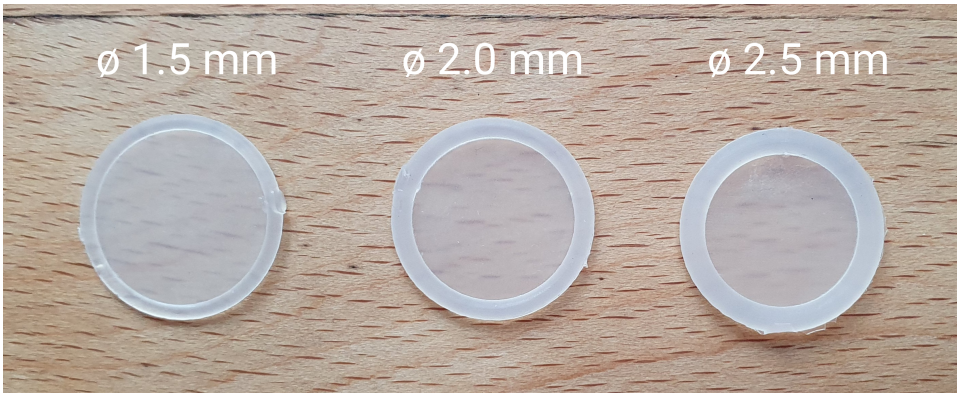

Figure 3.4: Three configurations of the silicone ring with membrane produced during the first prototyping round with varying cord sizes (1.5 mm, 2.0 mm, and 2.5 mm). Notably, the 1.5 mm ring displays visible air bubbles as well as a remnant of the cut rod originating from the injection hole. Additionally, the 2.5 mm ring exhibits slight traces of silicone on its outer surface.

For testing purposes, only undamaged and air bubble-free copies of the rings were employed. The holes in the aluminum block were initially moistened with a water-based lubricant (EasyGlide, Veendam, The Netherlands). Similarly, the ring itself was lubricated and rolled up by hand. It was then manually guided through the hole using twisting and pushing actions. The different holes were tested using the same ring, starting with the 4.5 mm hole and progressing to the smallest diameter hole. The smallest attainable diameter for successful ring insertion was documented and recorded during the testing process for each ring configuration.

3.1.3. Results

Manufacturability

Table 3.2 showcases the manufacturing outcomes for each injection molding attempt, represented by + (positive), ~ (neutral), or − (negative) signs, indicating the quality of the produced rings. The quality of the rings was mainly affected by the presence of air bubbles or textural imperfections. Additionally, all rings, to varying degrees, exhibited remnants of silicone from the cut rods that originated from the injection hole, as they could not be trimmed cleanly. Figure 3.4 illustrates the configurations of the silicone rings that were manufactured.

Table 3.2: Manufacturing outcomes for each injection molding attempt, represented by + (positive), ≀ (neutral), or − (negative) signs to indicate the quality of the produced silicone rings with membrane.

Injection molding attempt	Silicone rubber	Cord size ring (mm)		
		1.5	2.0	2.5
1	Flexible	≀	+	+
2	Stiff	−	−	−
3	Stiff	≀	≀	≀
4	Stiff	+	+	+
5	Semi-flexible	≀	+	+
6	Flexible	≀	≀	+

Table 3.3: Smallest achievable hole diameter (mm) for successful ring insertion for each configuration of the silicone ring with membrane produced in the first prototyping round.

Cord size	Silicone rubber		
	Flexible	Semi-flexible	Stiff
1.5 mm	- [a]	4.0	4.0
2.0 mm	4.5	4.5 [b]	4.5
2.5 mm	- [c]	- [c]	- [c]

[a] No undamaged ring available for this configuration.
[b] Membrane ruptured during manipulation into 4.0 mm hole.
[c] Could not be inserted into the 4.5 mm hole.

Preliminary Test: Proof of Principle

During the test, it was observed that the abdominal wall defect, initially measuring 12 mm in diameter, stretched to 20 mm in diameter under increased intra-abdominal pressure (IAP). Despite the stretching of the abdominal wall, all rings remained in place throughout multiple cycles of increasing and decreasing IAP. However, eventually, the rings popped out of the defect. Notably, the ring with a cord size of 1.5 mm remained in place for the longest duration, while the ring with a cord size of 2.5 mm popped out the quickest.

Additionally, it was observed that all rings had a higher tendency to protrude through the defect on the side of the UC.

Preliminary Test: Compatibility Surgical Ports

Table 3.3 displays the smallest achievable port diameter for each configuration of the silicone ring. No differences in insertion feasibility were observed between rings of varying flexibility.

It was noted that manually rolling up the rings posed a challenge due to their small size and their tendency to revert back to their original form.

3.1.4. Discussion

Manufacturability

The first round of prototyping demonstrated the feasibility of manufacturing a 20 mm silicone ring with a 0.4 mm membrane, featuring various cord sizes (1.5 mm, 2.0 mm, and 2.5 mm), and differing levels of stiffness through injection molding. This was achieved using a specifically designed 3D-printed mold, along with a relatively straightforward production protocol.

Thorough cleaning of the mold after each molding cycle proved essential to maintain the ring quality due to the rings' small dimensions. Consequently, the use of a release agent before each subsequent use became necessary to facilitate the rings' successful extraction from the mold.

The silicone remnants that originated from the injection hole could be attributed to the relatively large diameter of the injection hole (3 mm) when compared to the cord size of the rings.

Preliminary Test: Proof of Principle

The preliminary tests provided the initial proof of principle for the silicone ring. Among the various cord sizes, the 1.5 mm ring demonstrated the longest duration of remaining in place despite alternating increases and decreases in IAP.

Two factors appeared to contribute to this finding: (1) All rings had the same outer diameter, but the 2.5 mm and 2.0 mm cord size rings had a relatively smaller membrane, making them more prone to protruding from the defect with slight displacements. (2) The 2.5 mm and 2.0 mm rings displayed a stronger tendency to return to their original shape when a portion protruded from the defect.

Due to the stretching of the abdominal wall defect, none of the silicone rings could completely cover the defect under increased IAP. This observation influenced the refinement of the abdominal wall in the final version of the validation model, which will be discussed in Section 4.4.1.

It's important to note that the conclusions from these preliminary tests are limited for several reasons. Firstly, only rings with a single stiffness level were tested, preventing a comparison of their influence. Secondly, IAP values were not strictly regulated, potentially affecting the comparison between different cord sizes. Lastly, IAP values could not be correlated with clinically relevant values.

Preliminary Test: Compatibility Surgical Ports

The preliminary tests showcased the feasibility of inserting the rings through a port with a diameter of 14 Fr (4.7 mm) or less. To be precise, the 2.0 mm ring could be inserted through a 4.5 mm hole, while the 1.5 mm ring could fit through a 4.0 mm hole.

The successful insertion of the rings faced limitations due to the challenge of manually rolling them up. This process could vary among researchers and, consequently, could lead to minor variations in results when the test is replicated.

Conclusion

In summary, the first round of prototyping successfully demonstrated the feasibility of manufacturing a 20 mm silicone ring with a 0.4 mm membrane, featuring various cord sizes (1.5 mm, 2.0 mm, and 2.5 mm), and varying levels of stiffness through injection molding. These preliminary tests provided the initial proof of concept for the silicone ring. Notably, among the different cord sizes tested, the 1.5 mm ring exhibited the longest duration of remaining in place, even when subjected to alternating increases and decreases in IAP. Additionally, it was confirmed that it is possible to insert the 2.0 mm ring through a 14 Fr port and the 1.5 mm ring through a 12 Fr port.

3.2. Final Prototyping Round

3.2.1. Introduction

Building upon the successful outcomes of the first prototyping round, which established the feasibility of manufacturing the silicone ring with membrane, and considering the encouraging results of the preliminary tests that provided initial proof of concept and confirmed the compatibility of these rings with surgical ports of 14 Fr or smaller, the second and final prototyping round was dedicated to creating new configurations of silicone rings. These configurations included variations in shape, diameter, and stiffness and were specifically intended for the validation experiments.

It's essential to clarify that this section exclusively presents the methods employed for designing and manufacturing these rings. The validation experiments conducted with these rings and their corresponding results are detailed in Chapter 5, followed by a comprehensive discussion of the findings in Chapter 6.

3.2.2. Methods

Design Rings and Mold

All ring configurations were designed with a consistent cord size of 1.5 mm and a membrane thickness of 0.4 mm. To explore the impact of diameter on the ring's performance and its feasibility of being introduced through a 14 Fr port, the choice was made to vary the rings' diameters, considering the range of defect sizes. The selected diameters were specifically 20 mm and 30 mm.

Additionally, the ring's shape was diversified to incorporate a rusk-shaped ring with a cut-out, as suggested in Section 2.3.2, to accommodate the umbilical vessels' initiation. The size of the cut-out in the rusk-shaped ring was established after a careful analysis of the UC and vessels' cross-sectional area during gestation, as depicted in Appendix G. This examination led to the conclusion that the cut-out should have a diameter of 11 mm to offer sufficient space for the umbilical vessels, which collectively attain a maximum diameter of around 10.7 mm at approximately 34-35 weeks of gestation. The outer shape of the rings, with their corners yet to be rounded, was determined as illustrated in Figure 3.5.

The mold required for manufacturing the four configurations of the ring was designed using the CAD software SolidWorks. It consisted of two parts: the top and the bottom mold. Each part featured a negative impression of half of the four ring configurations. These impressions were connected to an injection hole with a diameter of 1.5 mm, increasing to 2 mm towards the nozzle, and an air hole with a diameter of 1 mm. The technical specifications of the mold can be found in Appendix H.

To materialize the design, the mold was produced using materials and equipment from Formlabs Inc. (Somerville, MA, USA). Specifically, the mold was created through 3D printing using Grey Resin material and a Form 3 printer [31]–[33]. Following the printing process, the mold underwent thorough cleaning with IPA in the Form Wash for a duration of 10 minutes [34]. Subsequently, it was subjected to a 30-minute curing process in the Form Cure at a temperature of 60 °C [35].

Following the post-processing steps, an unintentional diagonally striped pattern was observed on the top mold. To address this issue, the mold underwent light sanding to rectify the pattern. These actions resulted in the final mold, which is illustrated in Figure 3.6.

Production Silicone Rings

To achieve varying levels of stiffness in the silicone rings, a combination of the LSRs components PlatSil® Gel-25 (Part A and Part B) and PlatSil® Part H Hardener, all sourced from Polytek® Development Corp. (Easton, PA, USA), was used to prepare the silicone rubbers for injection molding.

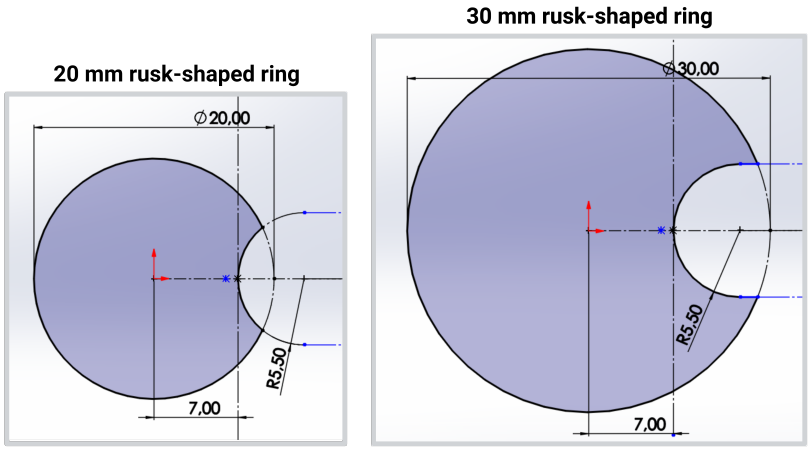

Figure 3.5: Sketch depicting the outer shape of the rusk-shaped rings with diameters of 20 mm and 30 mm, with their corners still unrounded. Both rings include a cut-out with a diameter of 11 mm, positioned at a distance of 7 mm from the midpoint of the ring.

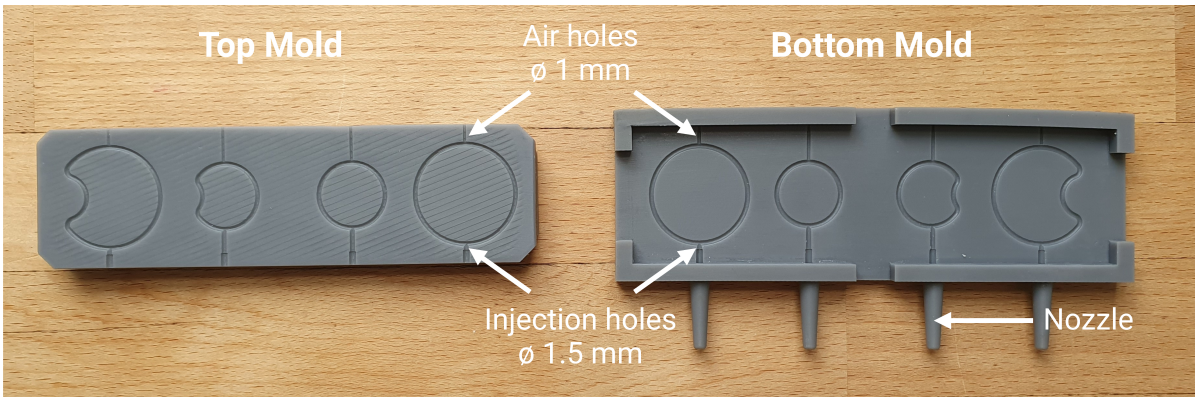

Figure 3.6: Interior surface of both the top and bottom mold used for producing four configurations of the silicone ring with membrane during the final prototyping round. The membrane thickness for all rings is consistent at 0.4 mm. The rings exhibit two different shapes: round or rusk (with a cut-out). The rings exhibit varying diameters of 20 mm and 30 mm. Note that the top mold unintentionally exhibits a diagonally striped pattern.

For the final prototyping round, it was decided to focus on producing rings with two distinct levels of stiffness, as opposed to the three levels employed in the first prototyping round. This decision was made to facilitate a more straightforward interpretation of the results from the subsequent validation experiments. Consequently, the minimum and maximum levels of stiffness achievable with the PlatSil® Gel-25 in combination with a hardener were utilized during the final prototyping round, corresponding to the *flexible* and *stiff* silicone rubbers outlined in Table 3.1.

A detailed description of the production protocol employed during the final prototyping can be found in Appendix F. Figure 3.7 illustrates the four configurations of the silicone ring with membrane that were manufactured during the final prototyping round.

Figure 3.7: The four configurations of the silicone ring with membrane produced during the final prototyping round with varying shapes (round or rusk) and varying diameters (20 mm or 30 mm). Notably, the membranes exhibit an unintentional striped pattern.

4

Validation Model Development

In this chapter, the development process of the validation model, designed specifically for the validation experiments, is explored. Section 4.1 provides an outline of the objective and requirements of the model. Following that, Section 4.2 presents the additional context analysis necessary for the validation model. In Section 4.3, the initial version of the validation model is detailed. Subsequently, Section 4.4 elucidates the refinement process, focusing on specific components that underwent enhancement. These combined efforts culminate in the presentation of the final version of the validation model in Section 4.5.

4.1. Objective and Requirements

Ideally, to fully validate the functionality of the silicone ring with membrane and ensure it meets all the specified requirements outlined in Section 2.2.2, a validation model would involve a fetus with gastroschisis starting from a GA of 20 weeks and progressing to a 40-week-old fetus within the amniotic cavity. Additionally, the model should allow for performing a fetoscopic procedure on the fetus. However, it is important to note that these physiological characteristics can currently only be simulated using animal models, with the ovine model being the gold standard for fetal surgery [37]. Considering the current stage of the project, where it is not ethically appropriate to use an animal model, a simplified model of the abdominopelvic cavity of a fetus with gastroschisis, focusing on the fetal intervention period, has been developed.

The primary objective of this model was to validate that the silicone ring with a membrane remains within the abdominopelvic cavity during and immediately after the fetoscopic intervention, effectively covering the abdominal wall defect. This validation was aimed at demonstrating the feasibility and efficacy of the closure method, rather than focusing on the specifics of ring placement during the procedure. While the proper placement of the ring during the fetoscopic intervention holds importance, it is considered a secondary aspect compared to the primary objective of establishing the proof of principle. Once this proof of principle is established, future efforts can be dedicated to further refining the fetoscopic procedure for optimal ring placement.

4.1.1. List of Requirements

Given the considerations discussed in the preceding sections and the accessibility of anatomical data, the decision was made to develop a validation model representing a 24-week-old gastroschisis fetus. The following list of requirements was established for the validation model:

Anatomical and Physiological

- ☐ The model should represent the dimensions of the abdominopelvic cavity of a 24-week-old fetus.
- ☐ The model should mimic the tissue characteristics of the fetal abdominal wall in a 24-week-old fetus.
- ☐ The model should represent the anatomical position and dimension of a gastroschisis abdominal wall defect in a 24-week-old fetus.
- ☐ The model should represent the anatomical trajectory and dimensions of the UC and vessels in a 24-week-old fetus.
- ☐ The model should represent the anatomical position of the UC in relation to the abdominal wall defect.
- ☐ The model should simulate the wet environment of the amniotic fluid.
- ☐ The model should accurately simulate and regulate the IAP within a clinically relevant range.

Manufacturing Process

- ☐ The materials and equipment required for producing the model should be readily available commercially.
- ☐ The manufacturing process for the model should be replicable to ensure consistent quality.

4.2. Additional Clinical Context Analysis

To meet the anatomical and physiological requirements of the validation model, further clinical context analysis was conducted in addition to the information presented in Section 2.1. Specifically, the IAP, the dimensions of the abdominopelvic cavity, and the size of the UC and vessels were considered. The analysis of the UC and vessels has been previously referenced and is provided in detail in Appendix G.

4.2.1. Dimensions Abdominopelvic Cavity

To determine the dimensions of the abdominopelvic cavity in a 24-week-old fetus, magnetic resonance imaging (MRI) images of a fetus with SBA and US images of a fetus with gastroschisis, both at 24 weeks of gestation, were analyzed at Erasmus MC. The detailed methodology for this analysis can be found in Appendix I.

The analysis revealed the following dimensions: a length of 55.1 mm, a width of 46.9 mm, and a height of 41.1 mm. The length was measured from the top of the diaphragm to the pelvic floor in the

superior to inferior direction. The width was measured laterally, and the height was determined in the anterior to posterior direction, excluding the spine.

4.2.2. Intra-Abdominal Pressure

To determine the clinically relevant range of IAP that should be simulated in the validation model, a literature search was conducted to gather information on IAP values. This search revealed that the abdomen can be conceptualized as a closed box with a combination of rigid walls (such as the costal arch, spine, and pelvis) and flexible walls (including the abdominal wall and diaphragm). The pressure within the abdomen is influenced by the elasticity of these walls and the nature of its contents. It is important to note that the abdomen and its contents behave as a relatively noncompressible system, primarily consisting of fluid, adhering to Pascal's law[1]. As a result, the IAP is defined as the steady-state pressure concealed within the abdominal cavity [39].

For children and adults, the trans-bladder technique serves as the standard method for measuring IAP [40]. However, this technique cannot be applied to measure fetal IAP, resulting in a lack of available data.

Generally, normal IAP values for children and adults hover around 0 mmHg[2] [39]. Nevertheless, situations like gastroschisis deviate from the norm. Repositioning eviscerated intestines back into the abdomen can increase IAP. For instance, attempting primary closure of the abdominal wall defect in gastroschisis neonates with matted, thickened, and dilated bowel or in cases of abdominovisceral disproportion poses a notable risk of abdominal compartment syndrome (ACS), which is defined as a sustained elevation in IAP exceeding 10 mmHg [40], [42].

Olesevich *et al.* conducted a study aiming to determine the viability of primary closure for gastroschisis neonates based on intraoperative IAP measurements using the trans-bladder technique [43]. Derived from animal studies, the researchers inferred that maintaining adequate visceral and renal blood flow in neonates required an IAP of 20 mmHg or lower. Consequently, during closure of the abdominal wall defect, they closely monitored IAP levels, ensuring they remained at or below 20 mmHg while securing fascial sutures. Sutures were tied if IAP remained within the acceptable range. Notably, a subsequent drop in IAP was often observed within minutes after primary closure and consistently occurring before neonate transfer to the neonatal intensive care unit.

In summary, while data on fetal IAP values is lacking due to measurement constraints, insights from intraoperative IAP measurements in gastroschisis newborns suggest that IAP might range from 0 to 20 mmHg after intestinal repositioning.

4.3. Initial Version Validation Model

Building on the objectives and requirements stated in Section 4.1, and integrating the insights from the additional context analysis presented in Section 4.2, the initial version of the validation model was developed. In the subsequent sections, each component of the initial model will be briefly described, along with the validation process and feedback received from medical experts.

[1] Pascal's law can be expressed as follows: "pressure applied at any point in a contained incompressible fluid is transmitted equally in all directions throughout the entire enclosed fluid" [38].

[2] 1 mmHg = 133.322 Pa = 0.00133322 bar [41].

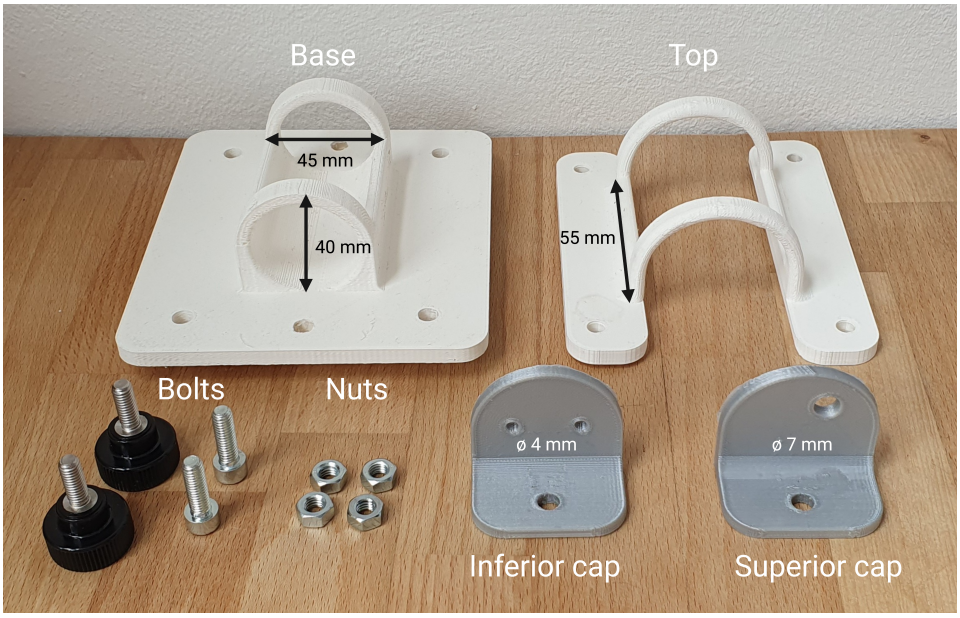

Figure 4.1: The 3D-printed components used in the initial version of the validation model, along with the bolts and nuts used for assembly.

4.3.1. 3D-Printed Components

To achieve a simplified depiction of the fetal abdominopelvic cavity, it was represented as an oval cylinder, with its dimensions derived from the analysis findings outlined in Section 4.2.1.

To construct this cylinder, two components (the base and top) were designed using SolidWorks CAD software. They were then 3D printed using UltiMaker polylactic acid (PLA) White on an UltiMaker S5 printer (Ultimaker B.V., Geldermalsen, The Netherlands) [44], [45]. Rubber caps were glued to each corner on the downside of the base to prevent it from sliding on the surface. The base and top components were designed to function as a clamp, allowing the abdominal wall to be positioned between them.

To achieve a complete seal of the abdominopelvic cavity, two caps (superior and inferior) were designed and printed using a similar process as the base and top components. The superior cap features a single 7 mm hole to accommodate the passage of the UV, while the inferior cap has two 4 mm holes to allow for the passage of the UAs.

Figure 4.1 presents all the 3D-printed components, encompassing the base, top, caps, as well as the bolts and nuts employed for assembly.

4.3.2. Abdominal Wall

The abdominal wall was fabricated using a silicone rubber to mimic the skin and fatty tissue, specifically LSRs components PlatSil® Gel-25 Part A and B (Polytek® Development Corp., Easton, PA, USA). To simulate the fascia layer, PowerMesh fabric (69% polyamide / 31% lycra) was incorporated. The abdominal wall was designed with two circular holes placed at a distance of 1-2 mm from each other. The first hole, with a diameter of 6 mm, was intended for accommodating the UC and its vessels. The second hole, measuring 12 mm in diameter, represented the abdominal wall defect.

Additional information regarding the development of the abdominal wall can be found in Section 4.4.1, which provides a comprehensive outline of the complete prototyping process.

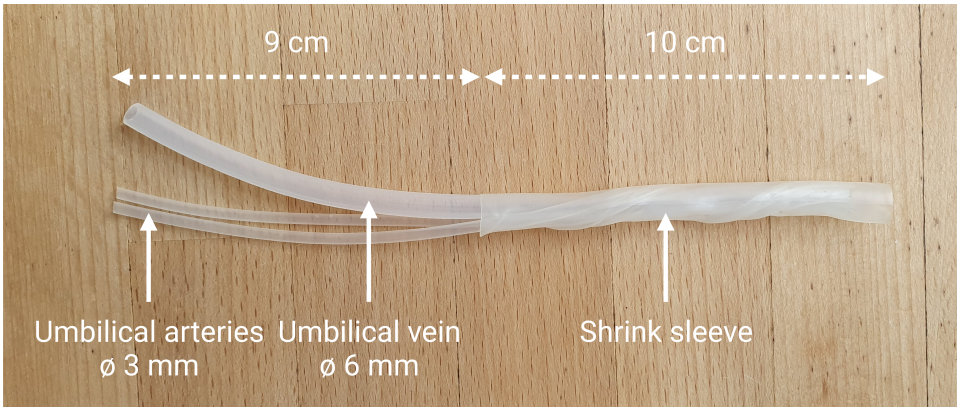

Figure 4.2: Umbilical cord and vessels composed of three silicone tubes, partially enclosed within a shrink sleeve.

4.3.3. Umbilical Cord and Vessels

To simulate the UC and its vessels, two 3 mm silicone tubes were utilized to represent the umbilical arteries, while a single 6 mm silicone tube was used to represent the umbilical vein. These dimensions were determined based on the analysis provided in Appendix G. The two 3 mm tubes were twisted around the 6 mm tube, and then a transparent shrink sleeve was carefully placed over approximately half of the twisted tubes. Using a blow dryer, the shrink sleeve was heated and shrunk until it tightly enclosed the tubes, as illustrated in Figure 4.2.

It was intentionally decided not to invest significant efforts in replicating the tissue characteristics of the Wharton's jelly, as it was deemed unnecessary for the intended purpose of this validation model.

4.3.4. Intra-Abdominal Pressure

To represent the intra-abdominal contents, a latex balloon (30 cm) was used. The balloon was inserted into the model from the side of the inferior cap, without the use of the inferior cap itself. It was partially inflated and secured using a sealing clip. To ensure there was no air leakage, a cut-out balloon was placed around the sealing clip. To mimic the presence of amniotic fluid and intestinal mucus, both the abdominal wall and balloon were lubricated with a water-based lubricant (EasyGlide, Veendam, The Netherlands). Increasing the IAP was achieved by applying pressure to the bottom of the balloon. A photograph showcasing the entire setup of the initial version of the validation model was previously referenced in Chapter 3 (Figure 3.2).

4.3.5. Validation and Feedback Medical Experts

The initial version of the validation model underwent assessment by three medical experts: Prof. dr. R.M.H. Wijnen (pediatric surgeon and head of the department of pediatric surgery, Erasmus MC), Dr. H.R. Langeveld-Benders (pediatric surgeon, Erasmus MC), and Dr. P.L.J. DeKoninck (gynecologist-perinatologist, Erasmus MC), collectively referred to as the *medical experts*.

The feedback received affirmed that the 3D-printed components accurately represented the fetal abdominopelvic cavity for the intended model purpose. Concerning the UC, the experts found the use of silicone tubes with the shrink sleeve to be realistic and suitable. They also considered the trajectory of the umbilical vessels as an accurate representation. Furthermore, the distance between the UC and the abdominal wall defect was judged to be realistic. Regarding the balloon simulating intra-abdominal contents, it was deemed satisfactory. However, a suggestion was made to include clear and adjustable regulation of IAP for experimental purposes.

Detailed feedback regarding the abdominal wall will be presented in Section 4.4.1.

4.4. Refinement Model Components

After incorporating the feedback from the medical experts and considering the observations made during the preliminary tests with the initial version of the validation model, several model components underwent refinement. The following sections will delve into the details of this refinement process.

4.4.1. Abdominal Wall

To ensure the accurate replication of the tissue characteristics of the fetal abdominal wall, multiple prototyping rounds were conducted, followed by feedback from the medical experts. The step-by-step process of this iterative refinement is presented in the following sections.

A detailed overview of the characteristics of all prototypes created throughout the prototyping rounds is provided in Appendix J. The prototypes will be referred to by the names assigned to them in this appendix. The production protocol for the abdominal wall layers produced in the fourth and final prototyping round can be found in Appendix K.

Prototyping Round 1

In the first prototyping round, four configurations of the abdominal wall were developed. All prototypes were crafted using silicone rubber to simulate skin and fatty tissue, and PowerMesh fabric to represent the fascia. The variations among the prototypes primarily centered around the number of silicone and fascia layers incorporated.

The medical experts evaluated the four prototypes and offered positive feedback overall. Among them, prototype AW1 was deemed the most realistic, although the experts noted that, in their view, it was somewhat too thick.

Subsequently, prototype AW1 was integrated into the initial version of the validation model for conducting preliminary tests, as outlined in Section 3.1.2.

Prototyping Round 2

After noting that the abdominal wall defect, initially measuring 12 mm in diameter, expanded to 20 mm in diameter under increased abdominal pressure during preliminary tests, this issue was addressed in the second prototyping round. Three new abdominal wall configurations were developed to mitigate the stretching of the defect. This was pursued through two approaches: Firstly, a different material, specifically a cotton handkerchief, was introduced to simulate the fascia layer. Secondly, a hardener was incorporated into the liquid silicone mixture.

Among the prototypes created in the second prototyping round, prototype AW6 exhibited the greatest success in reducing the stretching of the abdominal wall defect while maintaining required flexibility. However, it's worth noting that prototype AW6 was found to be thicker than the AW1 configuration, which the medical experts had previously considered too thick.

Prototyping Round 3

During the third round of prototyping, enhancements were made to the production protocol for the abdominal wall. The aim was to achieve a more uniform thickness of around 1.0 mm, while retaining the favorable traits of prototype AW6. This effort led to the development of prototype AW8.

Following this, prototype AW1 and AW8 were evaluated by the medical experts. The assessment criteria encompassed the abdominal wall's flexibility under varying IAPs, along with the stretching of the

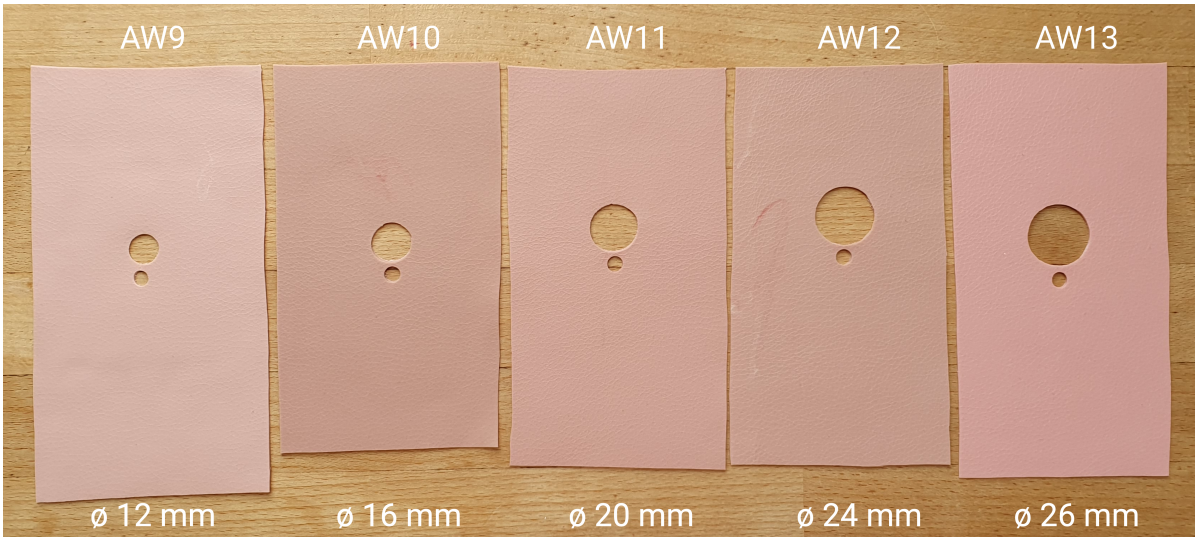

Figure 4.3: Abdominal wall prototypes created during the fourth and final prototyping round with defect sizes ranging from 12 mm to 26 mm. All prototypes include a 6 mm hole for embedding the umbilical cord.

abdominal wall defect. Considering these aspects, prototype AW8 was regarded as the most realistic choice.

Prototyping Round 4

In the fourth and final round of prototyping, the aim was to develop five abdominal wall configurations, akin to AW8, but with distinct defect diameters, tailored for the validation experiments. As a result, abdominal wall layers were produced with defect sizes of 12 mm, 16 mm, 20 mm, 24 mm, and 26 mm, as depicted in Figure 4.3.

4.4.2. Intra-Abdominal Pressure Regulation

To regulate IAP within the clinically relevant range in the validation model, an improved setup was developed, still employing a latex balloon to simulate intra-abdominal contents.

To control and monitor the pressure within the balloon, a manual blood pressure monitor (ST-A211-II, Stalt Medical, Dordrecht, The Netherlands) was partially disassembled by cutting the tube near the arm cuff. The cut end of the tube was then connected to a connection nipple. Subsequently, the open end of the latex balloon (30 cm) was stretched over the connection nipple and secured using two zip ties. Care was taken to position the zip tie heads exactly opposite each other to create a complete seal of the balloon. A visual representation of the complete IAP regulation setup can be seen in Figure 4.4.

The inflation bulb could be used to increase the pressure inside the balloon, while the sphygmomanometer allowed for the measurement of pressure in mmHg. The sphygmomanometer was capable of measuring pressure within a range of 0 to 300 mmHg, with an accuracy of 3 mmHg [46]. The air release valve could be employed to release air from inside the balloon when necessary.

4.4.3. Redesign 3D-Printed Components

The 3D-printed components underwent a redesign to enhance ease of use during the validation experiments, simplify the setup, and improve the overall durability of the model. Similar to the initial version, these parts were designed using SolidWorks CAD software and printed in UltiMaker PLA White on the UltiMaker S5 printer [44], [45]. The technical specifications of the 3D-printed components are presented

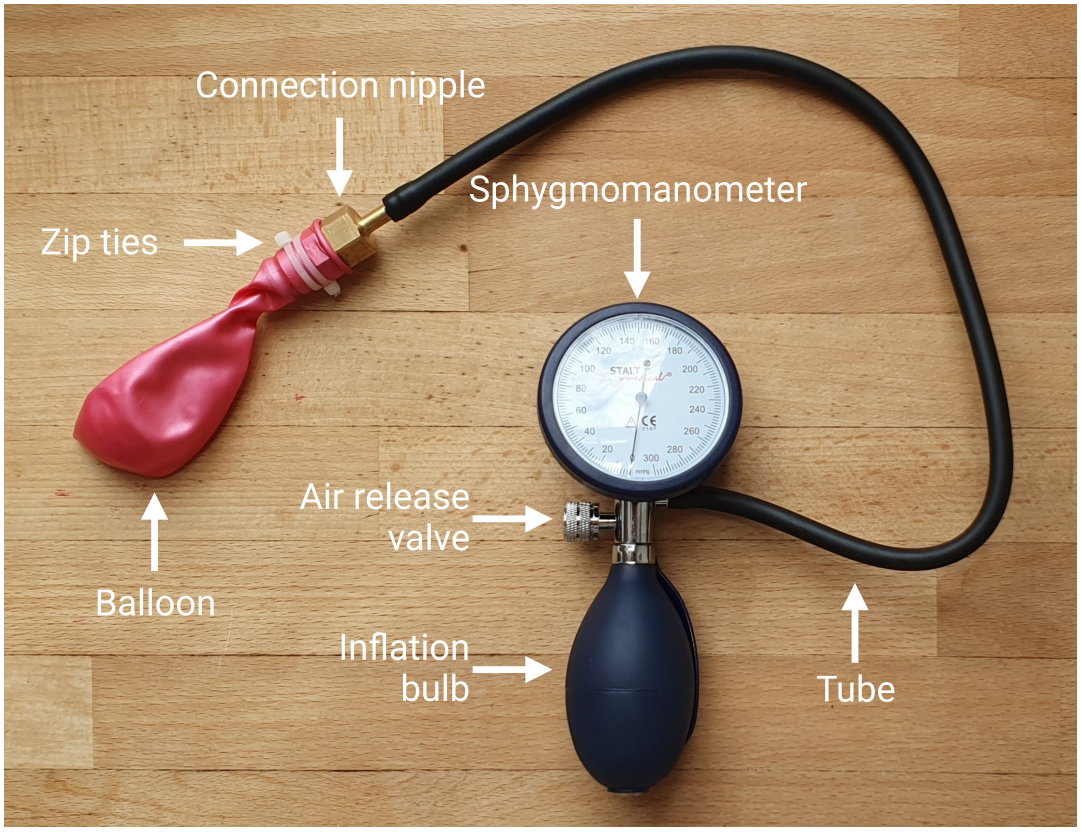

Figure 4.4: Intra-abdominal pressure regulation setup in the final validation model. The setup includes a balloon representing the intra-abdominal contents, connected with zip ties to a connection nipple which, in turn, is linked to a disassembled manual blood pressure monitor. The manual blood pressure monitor incorporates a sphygmomanometer, inflation bulb, air release valve, and tube.

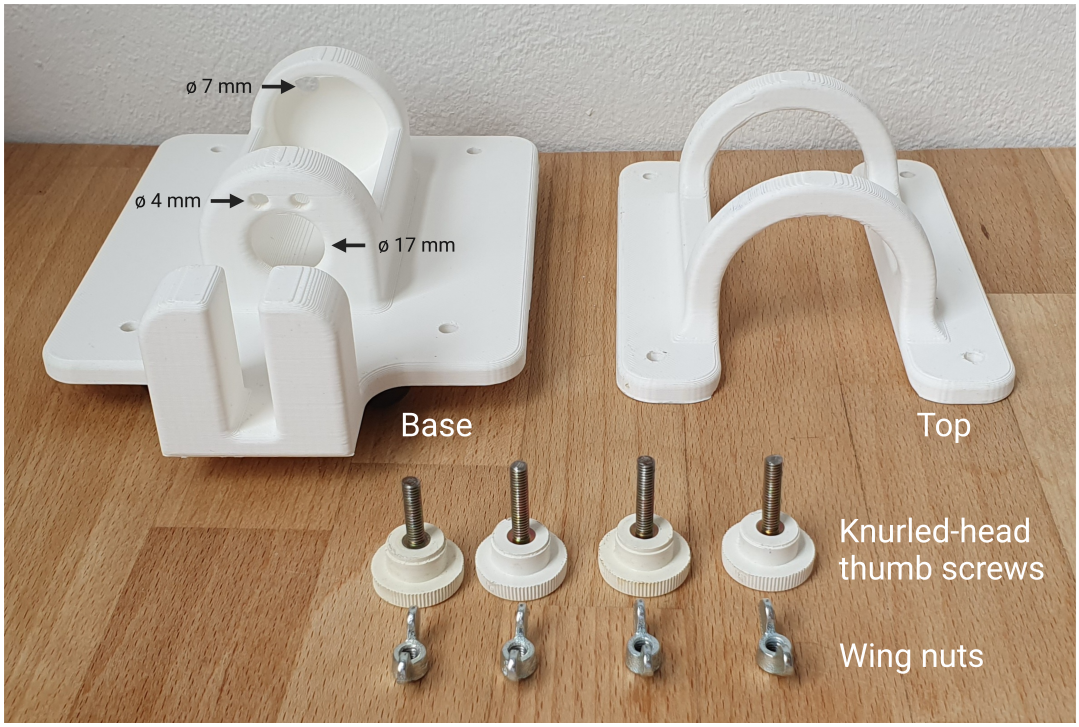

Figure 4.5: Redesigned 3D-printed components used in the final version of the validation model, along with the screws and nuts used for assembly.

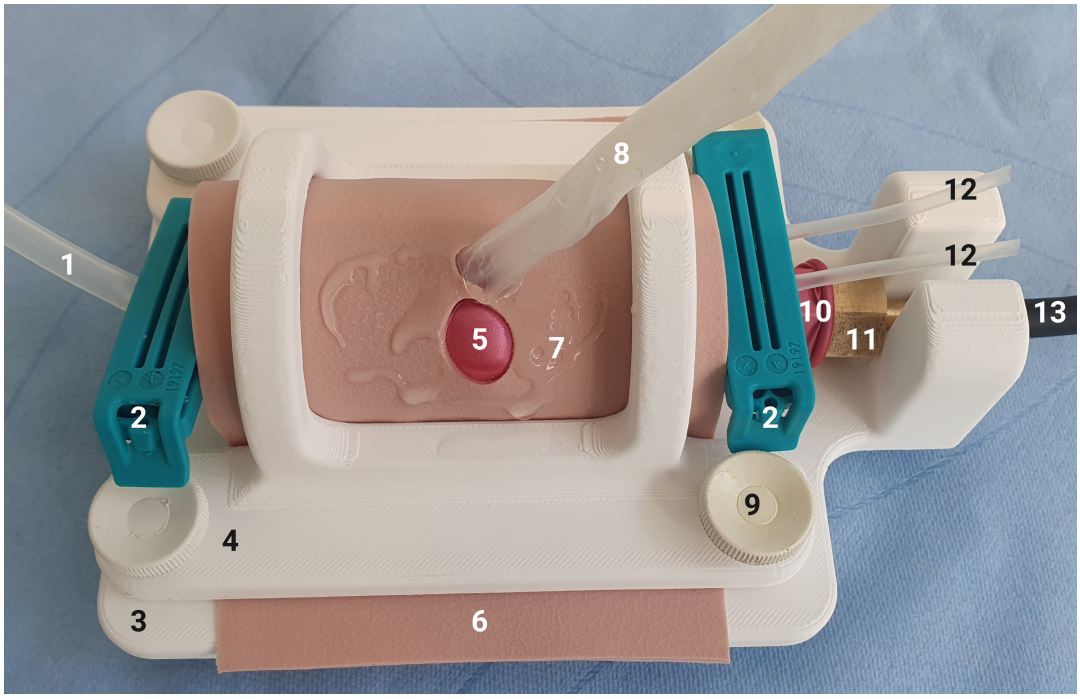

Figure 4.6: Final version of the validation model used during the validation experiments. The sphygmomanometer, connected to the tube, is positioned outside the frame. *Labels:* (1) Umbilical vein, (2) Sealing clip, (3) 3D-printed base (4) 3D-printed top, (5) Abdominal wall defect, (6) Abdominal wall, (7) Water-based lubricant, (8) Umbilical cord, (9) Knurled-head thumb screw, (10) Latex balloon, (11) Connection nipple, (12) Umbilical artery, (13) Tube.

in Appendix L.

While the dimensions of the fetal abdominopelvic cavity remained unchanged, modifications were implemented in the design. The superior and inferior caps were integrated into the base, eliminating the need for separate components. On the inferior side, the two holes accommodating the UAs were repositioned upward to account for the balloon's natural push in that direction during the experiments. Additionally, a new 17 mm hole was added to the inferior side, facilitating easy balloon insertion.

Furthermore, a simple slot was introduced in the base to securely hold the thin part of the connection nipple, preventing accidental dislodging of the balloon from the abdominopelvic cavity during experiments. Lastly, the bands of the top frame were reinforced with increased thickness at the top to ensure a stronger overall structure.

Lastly, both the base and top were designed with four 5 mm holes that aligned to accommodate the screws for fastening the components together. Just as in the initial design, rubber caps were glued to each corner on the downside of the base to prevent it from sliding on the surface.

Figure 4.5 showcases the redesigned 3D-printed components used in the final version of the validation model, along with the screws and nuts utilized for assembly.

4.5. Final Version Validation Model

Following the implementation of improvements to the initial version, the final version of the validation model used during the validation experiments consisted of the following components:

- Redesigned 3D-printed top and base components
- UC and its vessels
- IAP regulation setup

- Abdominal wall
- 2 × Sealing clip (BEVARA Sealing clip (6 cm), IKEA, Delft, The Netherlands)
- 4 × Knurled-head thumb screw (M4, length 20 mm)
- 4 × Wing nut (M4)
- Water-based lubricant (EasyGlide, Veendam, The Netherlands)

Figure 4.6 illustrates the complete setup, excluding the sphygmomanometer, which is positioned outside the photograph. Detailed instructions for constructing and assembling the validation model can be found in Appendix M.

4.5.1. Requirements Evaluation

The final version of the validation model was assessed against the predetermined requirements outlined in Section 4.1.1. The evaluation is presented below, indicating the fulfillment of each requirement by checking the corresponding boxes. Additional explanations, if necessary, are provided in a smaller font below the requirement.

Anatomical and Physiological

- ☑ The model should represent the dimensions of the abdominopelvic cavity of a 24-week-old fetus.
  - ➔ The dimensions of the model were derived from US and MRI images of a 24-week-old fetus, and *medical experts* have verified their accuracy.
- ☑ The model should mimic the tissue characteristics of the fetal abdominal wall in a 24-week-old fetus.
  - ➔ Although clear characteristics of the fetal abdominal wall are lacking in existing literature, the abdominal wall was deemed sufficiently realistic for its intended purpose based on feedback from *medical experts*.
- ☑ The model should represent the anatomical position and dimension of a gastroschisis abdominal wall defect in a 24-week-old fetus.
  - ➔ To represent a variety of defect sizes, five different abdominal wall configurations were manufactured, with defect sizes spanning from 12 mm to 26 mm.
- ☑ The model should represent the anatomical trajectory and dimensions of the UC and vessels in a 24-week-old fetus.
  - ➔ The trajectory and dimensions of the UC and vessels are grounded in existing literature and were deemed sufficiently realistic for their intended purpose based on feedback from *medical experts*.
- ☑ The model should represent the anatomical position of the UC in relation to the abdominal wall defect.
  - ➔ The anatomical position of the UC relative to the abdominal wall defect was established through multiple clinical observations and was deemed sufficiently realistic for its intended purpose based on feedback from *medical experts*.

- ☑ The model should simulate the wet environment of the amniotic fluid.
  - ➔ The model is not intended for submersion in water to simulate the amniotic fluid. Instead, a water-based lubricant is used to mimic the wet environment akin to that of amniotic fluid.
- ☑ The model should accurately simulate and regulate the IAP within a clinically relevant range.
  - ➔ While the absence of fetal IAP data due to measurement constraints is acknowledged, the proposed IAP range of 0 to 20 mmHg following intestinal repositioning can be effectively simulated using the IAP regulation setup, achieving an accuracy of 3 mmHg.

Manufacturing Process

- ☑ The materials and equipment required for producing the model should be readily available commercially.
- ☑ The manufacturing process for the model should be replicable to ensure consistent quality.
  - ➔ The abdominal wall is the only component that shows some variability in production, with minor differences in thickness and uniformity. Nevertheless, following the production protocol precisely and conducting subsequent thickness measurements with an electronic caliper can ensure the quality of the manufactured abdominal wall.

5

Validation Experiments

This chapter presents the validation experiments conducted to assess the silicone ring with membrane in accordance with the predefined requirements outlined in Section 2.2.2. Experiment 1 (Section 5.1) aimed to evaluate the feasibility and effectiveness of the closure method using the validation model developed in Chapter 4. Experiment 2 (Section 5.2) served as a supplementary study designed to provide further insight into the findings from Experiment 1. Finally, Experiment 3 (Section 5.3) was conducted to assess the feasibility of introducing the silicone ring through a 14 Fr or 12 Fr port.

This chapter includes the introduction, methods, and results of these experiments. The discussion of the results is presented in Chapter 6.

5.1. Experiment 1: Proof of Principle

5.1.1. Introduction

To evaluate the feasibility and efficacy of the silicone ring with membrane as a closure method, an experiment was conducted using the validation model developed in Chapter 4. The predefined performance requirements, as outlined in Section 2.2.2, specify that the design should the intestines from protruding into the amniotic cavity and should shield them from exposure to the amniotic fluid. To achieve this, the silicone ring must remain within the abdominopelvic cavity and completely cover the abdominal wall defect with its membrane within a clinically relevant range of IAP. The primary objective of this experiment was to address the following main research question:

- Does the silicone ring with membrane remain securely in place, effectively closing the abdominal wall defect, during and immediately after a fetal intervention in a 24-week-old fetus with CG following intestinal repositioning?

Furthermore, the experiment aimed to investigate the impact of different parameters such as shape, diameter, and stiffness on the performance of the silicone ring with membrane, leading to the following sub-research question:

- Do ring shape, diameter, and stiffness influence the ability of the silicone ring with a membrane to remain securely in place?

Table 5.1: The experimental conditions (ECs) for Experiment 1 and Experiment 3.

Independent variable	Level		EC	Independent variable level		
	1	2		Shape	Diameter	Stiffness
Shape	Round	Rusk	111	1	1	1
Diameter (mm)	20	30	112	1	1	2
Stiffness[a]	A25	A40	121	1	2	1
			122	1	2	2
			211	2	1	1
			212	2	1	2
			221	2	2	1
			222	2	2	2

[a] Shore hardness

5.1.2. Methods

Materials and Equipment

The following materials and equipment were used in the experimental setup:

- **Validation model:** Assembled according to Appendix M, with abdominal wall prototypes AW9, AW10, and AW11 (see Appendix J).
- **8 × Silicone ring with membrane:** Produced according to Appendix F.
- **Water-based lubricant** (EasyGlide, Veendam, The Netherlands)

Experimental Design

To explore the impact of ring shape, diameter, and stiffness on the performance of the silicone ring with membrane, an experiment was structured around three independent variables: ring shape, ring diameter, and ring stiffness. Each of these variables consisted of two levels: round and rusk shapes for ring shape, 20 mm and 30 mm for ring diameter, and shore hardness A25 and A40 for ring stiffness. This configuration led to a total of 8 experimental conditions (ECs), as depicted in Table 5.1.

To maintain clinical relevance, the effectiveness of the silicone ring was assessed across various abdominal wall defect diameters — specifically, 12 mm, 16 mm, and 20 mm. To accomplish this, three sub-experiments were executed, each utilizing a distinct abdominal wall in the validation model: AW9, AW10, and AW11, correspondingly.

For sub-experiments 1A and 1B, involving defect diameters of 12 mm and 16 mm, a target sample size of 5 experimental units (EUs) was set for each EC. Consequently, each sub-experiment comprised a total of 40 EUs. However, due to the inability of the 20 mm diameter rings to adequately cover the 20 mm abdominal wall defect in sub-experiment 1C, these ECs were excluded from sub-experiment 1C. As a result, a sample size of 5 EUs was maintained for the remaining 4 ECs, culminating in 20 EUs for this sub-experiment.

To minimize the potential impact of nuisance variables, the ECs were assigned randomly to the EUs using an online automated randomizer [47]. The EUs with the assigned ECs were documented in an SPSS run-table prior to the start of each sub-experiment.

Protocol

Prior to each sub-experiment, the validation model was assembled according to the instructions provided in Appendix M, using either AW9 for sub-experiment 1A, AW10 for sub-experiment 1B, and AW11 for sub-experiment 1C.

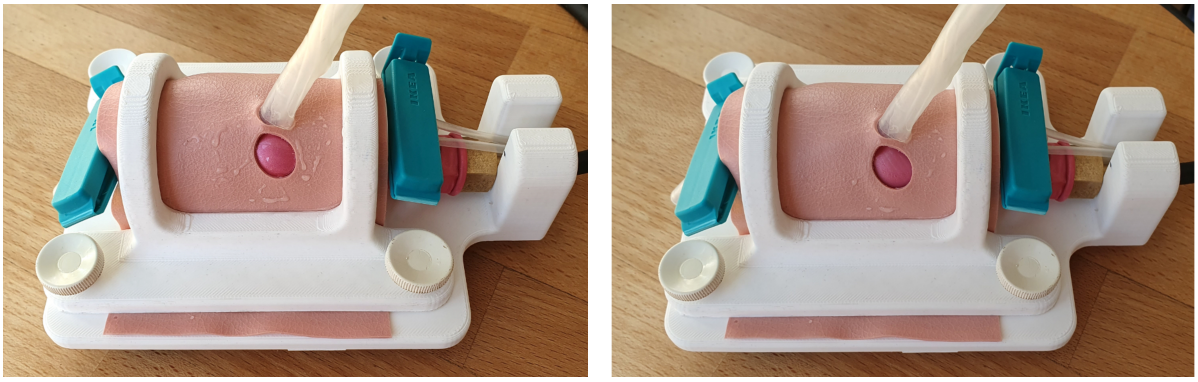

(a) Before insertion (b) After insertion

Figure 5.1: The validation model immediately before and after the insertion of the silicone ring during validation experiment 1, featuring AW9 (12 mm defect) and a round-shaped 20 mm ring.

In each sub-experiment, the following protocol was applied for each EU: to start, for each EU, the appropriate EC was obtained. Subsequently, it was verified whether the air release valve was closed and the sphygmomanometer displayed a pressure of 20 mmHg. In cases where the pressure deviated from 20 mmHg, the air release valve and inflation bulb were utilized to bring the pressure to the desired level before proceeding.

Next, the silicone ring with was lightly moistened with the water-based lubricant. Subsequently, the silicone ring was carefully inserted into the abdominal wall defect using a single finger. The aim was to position the ring precisely in the middle of the defect. For the rusk-shaped rings, special attention was paid to orient them in such a way that the cut-out was positioned at the side of the UC. It was ensured that only the membrane of the ring was visible once it was inserted. Figure 5.1 provides a visual representation of the model both immediately before and after insertion of the silicone ring.

After ensuring that the ring was properly inserted, the pressure in the abdominopelvic cavity was increased using the inflation bulb to 40 mmHg at a rate of approximately 2 mmHg/sec. Subsequently, the pressure was released using the air release valve, gradually decreasing it to 0 mmHg at a rate of approximately 2 mmHg/sec. Once the pressure reached 0 mmHg, the air release valve was closed.

Subsequently, the presence and position of the ring within the abdominopelvic cavity were visually assessed. Once the data was recorded, the silicone ring was gently removed using one finger.

Following each EU, to ensure consistent conditions for the subsequent EU, the water-based lubricant on the validation model was evenly spread out using one finger, covering the area surrounding the defect and extending between the balloon and the abdominal wall. Furthermore, after every four EUs, one drop of water-based lubricant was applied to the validation model and evenly spread out in the same manner to maintain uniform lubrication throughout the experiment.

Data Processing

The presence of the ring inside the abdominopelvic cavity was recorded as either ”yes” if it remained securely in the cavity or ”no” if it popped out of the abdominal wall defect. To assess the position of the ring within the abdominopelvic cavity, a scoring system was employed, consisting of three levels: (1) only the membrane is visible, (2) the cord of the ring is visible, but no direct view of the balloon, or (3) the cord of the ring is visible, with a direct view of the balloon. Figure 5.2 illustrates these three levels of the scoring system. The data collected during the experiment were directly entered into the SPSS run-table.

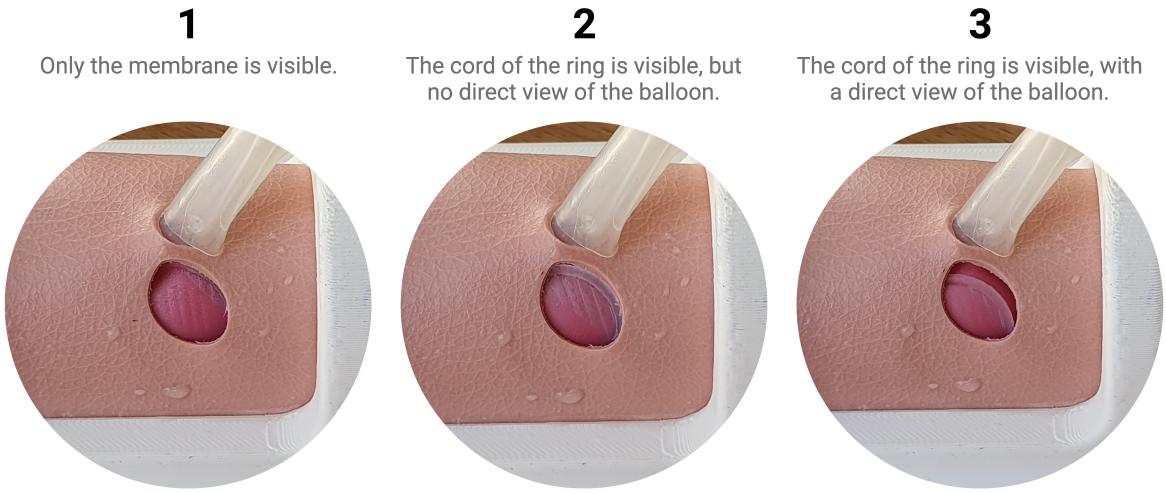

Figure 5.2: The three levels of the scoring system employed to assess the position of the ring within the abdominopelvic cavity.

Data Analysis

In SPSS, contingency tables were generated for each sub-experiment to analyze the relationship between the ECs and the presence and displacement of the silicone ring.

5.1.3. Results

Data

Throughout sub-experiments 1A to 1C, the silicone ring remained securely positioned within the abdominopelvic cavity under varying IAP conditions for all EUs.

A summary of the results regarding the position of the silicone ring within the abdominopelvic cavity are presented in Table 5.2.

Sub-Experiment 1A In sub-experiment 1A (12 mm defect) there were no differences observed between the ECs. Across all EUs and ECs, only the membrane was visible through the defect.

Sub-Experiment 1B Sub-experiment 1B (16 mm defect) revealed noticeable differences between the ECs. For EC_{111} and EC_{112} (round-shaped, 20 mm), the cord of the ring was visible in all 5 EUs, but the balloon was not directly visible. For EC_{211} and EC_{212} (rusk-shaped, 20 mm), the cord of the ring was visible in all 5 EUs, with a direct view of the balloon. However, for EC_{221} (rusk-shaped, 30 mm, flexible), the cord of the ring was visible in only 1 out of 5 EUs, without a direct view of the balloon. For all other ECs, only the membrane was visible for all EUs.

Sub-Experiment 1C Sub-experiment 1C (20 mm defect) also showed noticeable differences between the ECs. For EC_{221} (rusk-shaped, 30 mm, flexible), the cord of the ring was visible in all 5 EUs, with a direct view of the balloon. In contrast, for EC_{222} (rusk-shaped, 30 mm, stiff), the cord of the ring was visible in 3 out of 5 EUs without a direct view of the balloon, and in 2 out of 5 EUs with a direct view of the balloon. For EC_{121} and EC_{122} (round-shaped, 30 mm), only the membrane was visible for all EUs.

Remarkable Observations

Validation Model During the experiment, the stiffness of the shrink sleeve of the UC caused the defect to be slightly pulled in one direction, leading to incomplete contact between the abdominal wall

Table 5.2: Position of the silicone ring with membrane within the abdominopelvic cavity: summary of the results of Experiment 1.

EC	Sub-experiment: defect size								
	1A: 12 mm			1B: 16 mm			1C: 20 mm		
	(1)	(2)	(3)	(1)	(2)	(3)	(1)	(2)	(3)
111	5	0	0	0	5	0	-	-	-
112	5	0	0	0	5	0	-	-	-
121	5	0	0	5	0	0	5	0	0
122	5	0	0	5	0	0	5	0	0
211	5	0	0	0	0	5	-	-	-
212	5	0	0	0	0	5	-	-	-
221	5	0	0	4	1	0	0	0	5
222	5	0	0	5	0	0	0	3	2
Total	40	0	0	19	11	10	10	3	7

(1) Only the membrane was visible
(2) The cord of the ring was visible, but no direct view of the balloon.
(3) The cord of the ring was visible, with a direct view of the balloon.

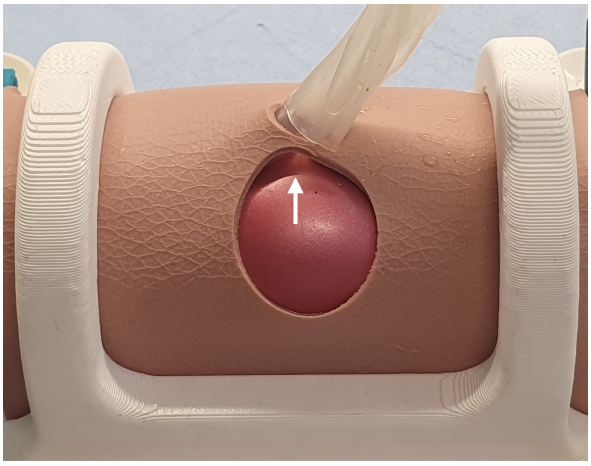

Figure 5.3: Validation model with AW11 (20 mm defect) illustrating incomplete contact between the abdominal wall and the balloon at the site of the umbilical cord, as indicated by the arrow.

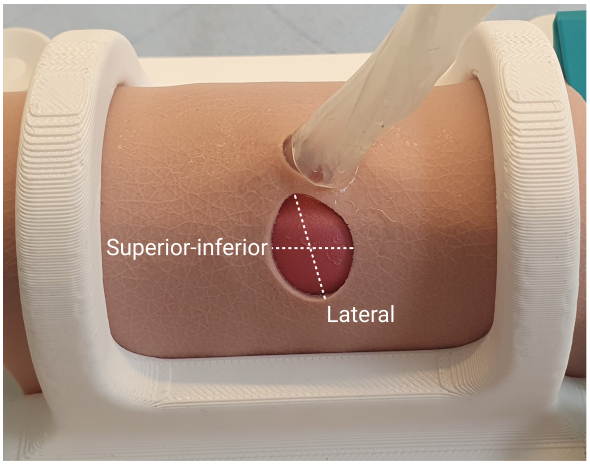

Figure 5.4: Validation model with AW9 (12 mm defect) illustrating stretching of the abdominal wall defect, particularly noticeable in the lateral direction.

and the balloon at the site of the UC, as depicted in Figure 5.3. Additionally, it was noted that the defect exhibited some stretching, particularly in the lateral direction, as shown in Figure 5.4. Furthermore, it was observed that as the defect size increased, the protrusion of the balloon through the defect became more pronounced, as evident when comparing Figure 5.3 and 5.4.

Placement of the Silicone Rings It was observed that the 20 mm rings were the most easily to position, while the 30 mm rings required slightly more effort and additionally, assessing whether the 30 mm rings were adequately positioned in the middle posed more of a challenge. Moreover, the stiff 30 mm rings were easier to position compared to the flexible 30 mm rings, as they showed less folding and returned more quickly to their original shape. Moreover, it was noted that the rusk-shaped rings were positioned between the balloon and the umbilical vessels after insertion, deviating from the intended placement between the abdominal wall and the vessels.

Incomplete Coverage Stretching of the abdominal wall defect during sub-experiments 1B and 1C resulted in incomplete coverage of the defect directly after insertion for certain ECs. In sub-experiment 1B, for EC_{111} and EC_{112} (round-shaped, 20 mm), the cord of the ring was already visible without a direct view of the balloon immediately after insertion. Additionally, for EC_{211} and EC_{212} (rusk-shaped, 20 mm), the cord of the ring was already visible with a direct view of the balloon at the site of the cut-out immediately after insertion. In sub-experiment 1C, for EC_{221} and EC_{222} (rusk-shaped, 30 mm), the cord of the ring was visible with a direct view of the balloon at the site of the cut-out immediately after insertion.

5.2. Experiment 2: Increase Abdominal Wall Defect Diameter

5.2.1. Introduction

In Experiment 1, it was observed that the abdominal wall defect, when placed in the validation model, exhibited an increased diameter compared to its original size due to the stretching of the abdominal wall. This stretching led to situations in sub-experiments 1B and 1C where certain configurations of the silicone rings were unable to fully cover the abdominal wall defect with their membranes immediately after insertion. To gain a better understanding of the results of Experiment 1, an additional experiment was conducted with a specific goal of evaluating the extent of diameter increase in the abdominal wall defect upon placement in the validation model. The research question addressed by this supplementary experiment was:

- How much does the diameter of the abdominal wall defect increase when the abdominal wall is positioned in the validation model?

5.2.2. Methods

Materials and Equipment

The following materials and equipment were used in the experimental setup:

- **Validation model:** Partially assembled according to Appendix M, with abdominal wall prototypes AW9, AW10, AW11 and AW12 (see Appendix J).
- **Water-based lubricant** (EasyGlide, Veendam, The Netherlands)
- **Electronic caliper** (500-752-20, Mitutoyo Corporation, Kawasaki, Japan)
- **Paper towels**

Experimental Design

An experiment was designed to evaluate the increase in diameter of the abdominal wall defect when positioned in the validation model, with the independent variable being the original abdominal wall defect diameter. This independent variable encompassed four different levels: 12 mm, 16 mm, 20 mm, and 24 mm. The first three values corresponded to the defect sizes of AW9, AW10, and AW11 as utilized in Experiment 1. The dimension of 24 mm corresponds to AW12, originally intended for Experiment 1. However, a pilot test conducted before Experiment 1 indicated that the 30 mm rings could not entirely cover the 24 mm defect, necessitating an evaluation of the increase in defect diameter for this specific defect size. This resulted in 4 ECs, as shown in Table 5.3. Each EC was intended to have a sample size of 3, resulting in a total of 12 EUs.

Table 5.3: Experimental conditions (ECs) for Experiment 2.

EC	Defect diameter (mm)	Abdominal wall prototype[a]
1	12	AW9
2	16	AW10
3	20	AW11
4	24	AW12

[a] Refer to Appendix J

To minimize the potential impact of nuisance variables, the ECs were assigned randomly to the EUs using an online automated randomizer [47]. The EUs with the assigned ECs were documented in an SPSS run-table prior to the start of the experiment.

Protocol

Before the start of the experiment, the validation model was partially assembled following the instructions in Section M.3 up to step 4, stopping before placing the abdominal wall over the base.

The following protocol was applied for each EU: to start, for each EU, the appropriate EC was obtained. Subsequently, it was verified whether the air release valve was closed and the sphygmomanometer displayed a pressure of 10 mmHg. In cases where the pressure deviated from 10 mmHg, the air release valve and inflation bulb were utilized to bring the pressure to the desired level before proceeding.

Next, steps 5 to 8 of the instructions for assembling the validation model (according to Section M) were followed. This involved inserting the UC through the 6 mm hole from the underside of the abdominal wall. Then, the abdominal wall was placed over the base, ensuring that the abdominal wall defect was located on the right side of the UC. The top was aligned over the abdominal wall, matching the 5 mm holes for the screws in the top and base. Care was taken to ensure that the abdominal wall conformed nicely to the shape of the arches of the top and base, without any indentation in the middle, while also minimizing stretching of the defect to maintain a circular shape. Subsequently, the top and base were securely fastened together using the knurled-headed thumb screws and wing nuts. Finally, the pressure inside the abdominopelvic cavity was raised to 20 mmHg using the inflation bulb.

After completing these steps, the diameter of the defect was measured in the lateral and superior-inferior directions (as depicted in Figure 5.4) using an electronic caliper.

Data Processing

Prior to each measurement, the outside jaws of the electronic caliper were brought together to ensure they were fully closed. Then, the zero button was pressed to reset the LCD display to zero. The inside jaws were subsequently positioned inside the abdominal wall defect, perpendicular to the balloon.

To measure the diameter of the defect in both the lateral and superior-inferior directions, the manual slider was employed to separate the inside jaws until they precisely made contact with the silicone borders of the defect. This was done in a way that captured the maximum distance in each respective direction. The resulting data was recorded in the SPSS run-table with a precision of 0.1 mm.

The stretch ratio in each direction was calculated using equation 5.1 and entered in the run-table.

$$\text{Stretch ratio} = \frac{\text{Measured defect diameter}}{\text{Original defect diameter}} \tag{5.1}$$

Table 5.4: Increase of the abdominal wall defect diameter in the validation model: summary of the results of Experiment 2.

EC	Original defect diameter (mm)	Measured defect diameter (mm)							
		Lateral				Superior-inferior			
		Min.	Max.	Mean	Ratio[a]	Min.	Max.	Mean	Ratio[a]
1	12	13.2	14.0	13.5	1.13	12.5	12.9	12.7	1.06
2	16	18.8	20.9	19.6	1.23	15.9	16.8	16.5	1.03
3	20	24.6	24.9	24.7	1.24	20.3	20.7	20.5	1.03
4	24	28.9	31.0	29.9	1.24	24.0	24.6	24.3	1.01

[a] Stretch ratio = $\frac{\text{Measured defect diameter}}{\text{Original defect diameter}}$

Data Analysis

In SPSS, the mean was calculated per data set - lateral defect diameter, superior-inferior defect diameter, lateral stretch ratio, and superior-inferior stretch ratio - for each EC.

5.2.3. Results

Table 5.4 provides a comprehensive summary of the experiment's results, presenting the minimum, maximum, and mean values for the measured defect diameter in both directions, as well as the stretch ratio for each EC.

5.3. Experiment 3: Compatibility Surgical Ports

5.3.1. Introduction

To evaluate the silicone ring with a membrane in accordance with one of the predefined surgical context requirements, as outlined in Section 2.2.2, an experiment was conducted. These requirements primarily pertain to the placement of the silicone ring during the fetoscopic procedure. However, due to time constraints and the project's scope, the primary focus was not on optimizing ring placement during the fetoscopic procedure but rather on demonstrating the ring's effectiveness in closing the abdominal wall defect.

Nevertheless, for the design to be applicable within the presented surgical context, it should be compatible with surgical ports featuring a maximum inner diameter of 14 Fr (≈ 4.7 mm), with a preference for 12 Fr (4.0 mm) or smaller. Thus, it was essential to ensure that the silicone ring with a membrane could be successfully introduced into the uterus through a 14 Fr port or smaller without sustaining any damage. The primary objective of this experiment was to address the following main research question:

- Can the silicone ring with membrane be successfully introduced through a 14 Fr port or smaller without sustaining any damage?

Additionally, the experiment aimed to explore the influence of different shape, diameter, and stiffness parameters on the ease of insertion of the silicone ring with membrane, leading to the following sub-research question:

- Do ring shape, diameter, and stiffness influence the ease of inserting the silicone ring with a membrane?

5.3.2. Methods

Materials and Equipment

The following materials and equipment were used in the experimental setup:

- **Aluminum block** (20 mm height) with a 4.0 mm and a 4.5 mm hole (as described in Section 3.1.2)
- **8 × Silicone ring with membrane:** Produced according to Appendix F.
- **Water-based lubricant** (EasyGlide, Veendam, The Netherlands)
- **10 Fr Dilator** (JCD10.0-38-20, Cook Inc., Bloomington, IN, USA)
- **12 Fr Dilator** (JCD12.0-38-20, Cook Inc., Bloomington, IN, USA)

Experimental Design

An experiment was designed to explore the effect of ring shape, diameter, and stiffness on the feasibility of introducing the silicone ring with a membrane through a 14 Fr trocar or smaller. Similar to Experiment 1, three independent variables were considered, resulting in a total of 8 ECs, as outlined in Table 5.1.

For silicone rings with a diameter of 20 mm (EC_{111}, EC_{112}, EC_{211}, EC_{212}), attempts were made to introduce the ring through the 4.0 mm hole in the aluminum block, as preliminary tests (as described in Section 3.1.3) had already shown that these rings could not be introduced through the 3.5 mm hole. On the other hand, for silicone rings with a diameter of 30 mm (EC_{121}, EC_{122}, EC_{221}, EC_{222}), attempts were made to insert the ring through the 4.5 mm hole. This decision was based on a pilot test, which demonstrated that none of the 30 mm rings could be successfully introduced through the 4.0 mm hole.

To minimize potential interference from nuisance variables, the ECs were randomly assigned to the EUs using an online automated randomizer [47]. The EUs with their respective assigned ECs were documented in an SPSS run-table before the start of the experiment.

Protocol

During the experiment, the insertion process for the silicone rings varied per EC. For EC_{111}, EC_{112}, EC_{211}, EC_{212}, attempts were made to introduce the ring through the 4.0 mm hole in the aluminum block using the 10 Fr dilator. On the other hand, for EC_{121}, EC_{122}, EC_{221}, EC_{222}, attempts were made to introduce the ring through the 4.5 mm hole with the 12 Fr dilator.

For each EU, the appropriate EC was obtained. Subsequently, a drop of water-based lubricant was applied to the relevant hole in the aluminum block. The block was then positioned on a table with the downside of the hole left free, and the dilator was moved up and down the hole once to ensure the lubricant was evenly distributed.

Next, the silicone ring was manually rolled up between the thumb and index finger, using both hands. The rusk-shaped rings were rolled with the cut-out positioned at one end of the roll. Then, the ring was manually introduced into the lubricated hole with pushing and twisting motions. In cases where manual movement was insufficient, the dilator was carefully used to push the ring through the hole.

Following each EUs, the silicone ring was dried using paper towels. Additionally, the researchers' hands were dried with paper towels.

Data Processing

The outcome of ring insertion was recorded in the SPSS run-table as either "yes," indicating successfully introduced through the hole, or "no," indicating that the ring could not be introduced or was only partially inserted in the hole.

5.3.3. Results

Data

Throughout all EUs, all 20 mm rings (EC_{111}, EC_{112}, EC_{211}, EC_{212}) were successfully introduced through the 4.0 mm hole. Similarly, all 30 mm rings (EC_{121}, EC_{122}, EC_{221}, EC_{222}) were successfully introduced through the 4.5 mm hole in all EUs.

Remarkable Observations

It was challenging to maintain the rings in their rolled-up state after manual rolling, and this was particularly noticeable for the rusk-shaped rings. The round-shaped rings, on the other hand, proved to be easier to tightly roll up. Additionally, it was noticed that the flexibility of the material allowed the flexible rings to be rolled up with a smaller crossing profile.

Consequently, it was observed that the flexible 30 mm rings were easier to insert compared to the stiff 30 mm rings. However, for the 20 mm rings, no significant difference in ease of insertion was noticed between the flexible and stiff variants. Furthermore, it was noted that the 20 mm rings were easier to insert through the 4.0 mm holes compared to the 30 mm rings through the 4.5 mm holes.

Lastly, in EC_{122}, a small hole was punctured in the membrane during insertion with the dilator.

6

Discussion

This chapter presents the discussion of this thesis, starting with an analysis of the results derived from the validation experiments, outlined in Section 6.1 and Section 6.2. The interpretation of these results, along with their implications, will be thoroughly explored, while also addressing the limitations of this study. Subsequently, the silicone ring with membrane will be evaluated against the predetermined design requirements in Section 6.3. In addition, future recommendations will be discussed in Section 6.4.

6.1. Validation Experiment 1 and 2: Proof of Principle

6.1.1. Interpretation of the Results

Increased Abdominal Wall Defect Diameter

The observations made in Experiment 1 were confirmed by the findings of supplementary Experiment 2, which demonstrated that the diameter of the abdominal wall defect indeed increased when positioned in the validation model, especially in the lateral direction, resulting in an oval-shaped abdominal wall defect. Consequently, the outcomes of Experiment 1 will be interpreted in light of the insights obtained from Experiment 2, considering the deformed shape and increased diameter of the abdominal wall defect.

The observed increase in diameter can likely be attributed to the tight fit between the 3D-printed top and base components (1 mm), which sets the abdominal wall under tension in the lateral direction even before the top and base are fastened together with the screws and nuts. Furthermore, this tight fit may also explain why the deformation of the abdominal wall defect is slightly more pronounced in AW10, AW11 and AW12 compared to AW9. Due to variety inherent to the production process of the abdominal wall prototypes, AW10, AW11 and AW12 are respectively 0.3 mm, 0.2 mm and 0.4 mm thicker than AW9 (see Appendix J), leading to an even tighter fit between the top and base components

Retention of the Silicone Ring

The findings of Experiment 1 revealed that the independent variables ring shape and ring stiffness had no significant impact on the silicone ring's ability to remain inside the abdominal cavity during and immediately after the fetal intervention. However, a notable difference was observed for the independent

variable ring diameter. The 30 mm rings could successfully remain inside the abdominopelvic cavity even with larger (oval-shaped) defects measuring up to 24.7 × 20.5 mm, while the 20 mm rings accommodated defects up to 19.6 × 16.5 mm. This result was to be expected, as a larger membrane can cover a larger defect, therefore remaining more securely inside the abdominopelvic cavity when subjected to increasing and decreasing IAP.

Interestingly, based on the results obtained from the preliminary tests (Section 3.1.3), it was expected that there would be a noticeable difference concerning the shape of the ring. During these preliminary tests, it was observed that (round-shaped) rings tended to protrude through the defect near the UC, indicating a potential influence of the umbilical vessels' position on this protrusion.

The rusk-shaped rings were designed with a cut-out specifically to accommodate the initiation of the umbilical vessels and prevent their compression. Consequently, the anticipation was that this cut-out would result in reduced pressure exerted by the umbilical vessels on the silicone ring, particularly in the lateral and posterior directions compared to the round-shaped rings. This, in turn, was expected to lower the risk of ring displacement and, consequently, the likelihood of the ring protruding through the defect. However, in practice, no noticeable difference was observed as all rings, regardless of their shape, remained within the abdominal cavity under varying IAP conditions.

It is important to note that the preliminary tests involved raising the IAP significantly higher than the maximum of 40 mmHg used in Experiment 1. Therefore, the effect of ring shape might not be observable under the IAP conditions employed in Experiment 1.

Position of the Silicone Ring

Regarding the position of the rings within the abdominopelvic cavity, no significant difference was observed for any of the independent variables concerning the 13.5 × 12.7 mm oval-shaped defect. Irrespective of the ring configurations, the membrane of the rings consistently provided complete coverage of the defect, both immediately after insertion and following variations in IAP, with no observable displacement.

In contrast, significant differences in the position of rings were observed for larger defect sizes. Regarding the diameter of the rings, the 30 mm rings could cover larger defect sizes solely with their membrane both immediately after insertion and after varying IAP conditions, up to the oval-shaped defect of 24.7 × 20.5 mm. In contrast, the 20 mm rings had difficulty in fully covering the abdominal wall defect solely with their membrane for the oval-shaped defect of 19.6 × 16.5 mm immediately after insertion.

The observed differences regarding ring diameter align with expectations, as a larger membrane naturally affords better coverage for larger defects. Nevertheless, it was assumed that the 20 mm rings could still adequately cover the originally 16 mm defect in sub-experiment 1B. However, this assumption proved incorrect as the defect's diameter increased due to stretching of the abdominal wall.

Moreover, in contrast to expectations, the rusk-shaped rings consistently displayed partial exposure of the balloon, either immediately after insertion or following changes in IAP. This exposure was consistently observed on the side of the cut-out. The initial expectation was that rusk-shaped rings would provide equivalent or superior coverage of the defect when compared to the round-shaped rings. This expectation was based on the assumption that, due to the presence of the cut-out, the umbilical vessels would exert less pressure on the rusk-shaped rings, reducing the likelihood of ring displacement.

The deviation from the expected behavior can be attributed to two primary factors. Firstly, during Experiment 1, it was consistently observed that the corners of the rusk-shaped rings were positioned between the umbilical vessels and the balloon. Consequently, the umbilical vessels could still exert

pressure on the ring. Secondly, the defect underwent significant enlargement primarily in the lateral direction, aligning with the orientation of the cut-out. As a result, it is reasonable to deduce that the rusk-shaped rings, with their smaller membrane size, provided less effective coverage of the defect under these conditions compared to the round-shaped rings.

Finally, with regard to the stiffness of the rings, minor differences were observed between the flexible and stiff variants only in sub-experiment 1C. Specifically, the rusk-shaped 30 mm flexible rings exhibited a less effective coverage of the 24.7 × 20.5 mm oval-shaped defect when compared to their stiff counterparts, both immediately after insertion and following variations in IAP. This discrepancy can potentially be attributed to the fact that the stiff rings were easier to position correctly as they showed less folding and had a tendency to return to their original shape more quickly.

6.1.2. Implications

The experimental results have provided a proof of principle for the silicone ring with membrane as a novel dedicated method that enables the swift closure of the abdominal wall defect during a fetoscopic repair procedure for CG, fulfilling the primary goal of this graduation project. During the experiments the silicone ring with membrane remained securely in place, effectively closing the abdominal wall defect, under IAP conditions ranging from 0 to 40 mmHg. Conducted using a validation model, the experiments were designed to replicate the conditions encountered during and immediately after a fetal intervention in a 24-week-old fetus with CG following intestinal repositioning.

Notably, previous research efforts have predominantly focused on developing fetoscopic procedures for gastroschisis relying on the time-consuming process of suturing to close or cover the abdominal wall defect. In contrast, this thesis stands out as the pioneering work introducing an alternative approach for closure, potentially reducing the duration of in utero surgery. This marks a significant step towards developing a fetoscopic procedure that addresses both causes of secondary bowel damage in CG while minimizing risks to both the mother and the fetus.

Concerning the parameters of shape, diameter, and stiffness for the silicone ring, the experimental results indicate a preference for the use of a round-shaped ring, which provides better coverage of the defect compared to a rusk-shaped due to its larger membrane. Additionally, the clinical insights gained during the later stages of this project have unveiled that the umbilical vessels are enveloped in a protective layer of connective tissue (Appendix D). This layer is presumed to safeguard the vessels from potential compression that could be caused by the round-shaped silicone ring.

Additionally, the experiments have shown that larger ring diameters correspondingly allow coverage of larger defects. It is noteworthy that the 20 mm round ring effectively covered an oval-shaped defect measuring 13.5 × 12.7 mm, which aligns with the mean defect size reported in CG by previous studies [19], [21].

As for the stiffness of the ring, firm conclusions cannot be drawn from these experiments. Nonetheless, a slight preference for a stiffer silicone ring can be deduced, as it was found to be more easily positionable.

6.1.3. Limitations

The limitations of these experiments primarily arise from the simplified nature of the validation model. The model's focus was solely on the moment of the fetal intervention, which restricts the generalization of results to the subsequent period until birth. As the model lacks a simulation of fetal growth and movement, a more comprehensive understanding can only be achieved through realistic simulations using animal models such as sheep [37].

Furthermore, the reliability of the data may be impacted by the unintentional characteristics of the validation model, specifically the presence of an oval-shaped defect and a stiff UC. It is presumed that these factors did not influence the proof of principle of the closure method, as they made it even more challenging to effectively close the abdominal wall defect. Nevertheless, they could have influenced the results regarding the preference for the round-shaped ring.

Moreover, the prototyping and testing process was limited to only a few configurations of the silicone ring, which makes it more difficult to draw definitive conclusions about the preferred ring parameters. This limitation particularly impacted the ability to identify a clear preference regarding the stiffness of the ring. It is plausible that exploring extreme values for this parameter could unveil more substantial differences in the ring's performance.

6.2. Validation Experiment 3: Compatibility Surgical Ports

6.2.1. Interpretation of the Results

The experiment demonstrated that all 20 mm rings, regardless of their shape or stiffness, could be successfully introduced through a 4.0 mm hole without sustaining any damage. These findings were anticipated, considering the diameter of the rings, the 1.5 mm cord size, and the 0.4 mm membrane thickness.

Similarly, the 30 mm rings could be introduced through the 4.5 mm hole without issues, except for one instance where a small hole was punctured in a round, stiff ring.

The observed difference in the diameter of the rings is explained by the fact that the 30 mm rings require more rolling over, resulting in the addition of more layers of membrane to their crossing profile. Hence, it is understandable why a slightly larger port is necessary to introduce them.

Moreover, the experiments revealed that the round-shaped rings were more manageable to tightly roll up manually, leading to a smaller crossing profile compared to the rusk-shaped rings. This discrepancy can be attributed to the double kink in the cord of the rusk-shaped rings caused by the cut-out, which presents an additional challenge in achieving a tight roll-up.

Additionally, it was demonstrated that the flexible rings could be rolled up with a smaller crossing profile. This observation can be explained by the fact that the flexible silicone can be stretched more easily, allowing for a tighter roll-up of the ring.

6.2.2. Implications

The findings of this experiment hold significant implications for the use of the silicone ring with membrane in a fetoscopic intervention for CG. The results indicate that the 20 mm ring can be effectively introduced through a 4.0 mm hole, establishing compatibility with the use of a 12 Fr port. Moreover, the 30 mm ring can be effectively introduced through a 14 Fr port, in line with Erasmus MC's procedural preferences.

Regarding the ring's parameters, the preference for a round-shaped ring becomes apparent, as it facilitates easier insertion. Additionally, a smaller diameter and a flexible material are favored, as they contribute to the ease of tightly rolling up the ring, ultimately reducing its crossing profile. These insights provide valuable guidance for optimizing the design and usability of the silicone ring in future clinical applications.

6.2.3. Limitations

The experiment's findings regarding the hole size cannot be directly extrapolated to the size of the surgical ports that can be used in practice because the silicone ring cannot be introduced directly through the surgical port. The seal of the port, designed to prevent CO_2 leakage, poses a hindrance. As a result, the silicone ring must be encapsulated in a yet undetermined material or instrument to facilitate its introduction through the port, which will inevitably add to its crossing profile. Furthermore, encapsulating the silicone ring can reduce the frictional forces exerted on the ring when pushing it through the entire length of the surgical port.

Furthermore, the experiment was constrained by material limitations, leading to the availability of only 3.5 mm, 4.0 mm, and 4.5 mm hole sizes for testing. This limitation prevented testing sizes in between, making it impossible to establish a more precise relationship between ring diameter and its crossing profile.

6.3. Requirements Evaluation

Based on the outcomes of the validation experiments, the silicone ring with membrane was assessed against the predefined list of requirements outlined in Section 2.2.2. The evaluation is presented below, with each requirement indicated as fulfilled by checking the corresponding boxes. In cases where a requirement is not yet met, the box remains unchecked. Additional explanations, if necessary, are provided in a smaller font below the respective requirement.

Performance

- ☑ The design should prevent the intestines from protruding into the amniotic cavity.
  - ➔ The silicone ring with membrane effectively closed the abdominal wall defect under IAP conditions ranging from 0 to 40 mmHg. Based on literature, it is presumed that the IAP after intestinal repositioning does not exceed 20 mmHg, thereby preventing the intestines from protruding into the amniotic cavity.
- ☑ The design should shield the intestines from exposure to amniotic fluid.
  - ➔ The silicone ring with a membrane functions as a physical barrier shielding the intestines from the amniotic fluid.
- ☐ The design should maintain its intended functionality from the fetal intervention (20-25 weeks GA) until birth (38-40 weeks GA).
  - ➔ Verification of this requirement can only be conclusively established through animal studies.
- ☑ The design should be suitable for abdominal wall defects with diameters ranging from 12 mm to 20 mm.
  - ➔ The 20 mm rings effectively covered an oval-shaped defect measuring 13.5 × 12.7 mm, whereas the 30 mm rings could cover an oval-shaped defect measuring 24.7 × 20.5 mm.
- ☑ The design should function effectively in the wet environment of the amniotic fluid.
  - ➔ The validation experiments were not carried out underwater to mimic the amniotic fluid. Instead, a water-based lubricant was employed to replicate the wet environment.

Safety

- ☑ The design should not compromise the blood flow through the UC or its vessels.
  - ➔ Clinical observations made while examining a newborn with gastroschisis, which revealed that the umbilical vessels are embedded in a layer of connective tissue, support the assumption that the silicone ring with a membrane will not compromise the blood flow through the UC or its vessels. In animal (and human) studies, it is recommended to monitor fetal hemodynamic changes using Doppler studies of the UC and its vessels.
- ☑ All materials used in the design should comply with biological safety standards as defined in ISO 10993-1 [25].
  - ➔ Several commercial companies offer 'biomedical grade' LSRs that have undergone biological safety testing in accordance with ISO 10993-1 standards, including a 12-week implant test [29], [30].
- ☑ The design should be capable of undergoing terminal sterilization, as defined in EN 556-1 [26].
  - ➔ For LSRs implants, the most effective and safe method of terminal sterilization is typically steam sterilization using an autoclave [28].

Surgical Context

- ☐ The design should facilitate a surgical procedure with a maximum in utero time of 30 minutes.
  - ➔ Verification of this requirement can only be conclusively established through future user studies conducted in a training model. Nonetheless, the quick and easy manual placement of the ring during the validation experiments has offered a promising indication that achieving this requirement is feasible.
- ☐ The design should be operable solely with indirect visual feedback provided by an endoscopic camera.
  - ➔ Verification of this requirement can only be conclusively established through future user studies conducted in a training model. However, considering that surgical tasks such as suturing require an equivalent or even greater level of depth perception, it is anticipated that the silicone ring with a membrane can also be placed with solely endoscopic visual feedback.
- ☐ The design should require the use of a maximum of two working instruments simultaneously, excluding the endoscopic camera.
  - ➔ Verification of this requirement can only be conclusively established through future user studies conducted in a training model. Nonetheless, the quick and easy manual placement of the ring during the validation experiments has offered a promising indication that achieving this requirement is feasible.
- ☑ The design should be compatible with surgical ports with a maximum inner diameter of 14 Fr (≈4.7 mm), with a preference for 12 Fr (4.0 mm) or smaller.
  - ➔ The crossing profile of the silicone rings is suitable for the 12 Fr and 14 Fr ports. However, when introduced through the surgical port, an encapsulation material or instrument will be required, and the increase in the crossing profile caused by this component is currently undetermined.

Manufacturing Process

- ☑ The materials and equipment required for producing the design should be readily available commercially.
- ☑ The manufacturing process for the design should be replicable to ensure consistent quality.
  - ➔ The production protocol employed for prototyping the design yielded rings of generally good quality, with minor variations noted. Employing a professional injection molding process will ensure a more consistent quality for the rings.

6.4. Future Recommendations

As this study marks the initial exploration of the silicone ring with membrane as a closure method in a fetal intervention for CG, various components of this project necessitate further research to pave the way for its eventual clinical application.

6.4.1. Clinical Research

To ensure the suitability of the silicone ring with membrane for CG fetuses, further clinical research is warranted to investigate the defect diameter in CG and its developmental changes during gestation. Understanding the dynamic nature of the defect size will contribute to the optimal design and application of the silicone ring in a clinical setting.

6.4.2. Silicone Ring Design Parameters

To optimize the design of the silicone ring, conducting a more thorough investigation into the material's stiffness and its impact on the ring's performance and crossing profile is highly recommended. The current range of silicone stiffnesses tested might not be extensive enough to yield conclusive results, and exploring a wider spectrum of stiffness variations could provide valuable insights.

To further reduce the crossing profile of the rings and enable insertion through smaller ports, investigating variations of the ring with a smaller cord size or with varying cord dimensions would be useful. Exploring these alternatives could lead to the development of more compact ring, facilitating the use of smaller surgical ports and ultimately minimizing the risks to both the mother and the fetus during fetoscopic interventions.

Additionally, a thorough investigation of rings with a wider range of diameters in the context of multiple defect diameters would establish a clearer relationship between the ring's diameter and its effectiveness in covering specific defect sizes.

6.4.3. Validation Model

In future research, the validation model can be enhanced to fulfill a dual role as both a validation model as well as a training model for conducting user tests. To achieve this, improvements can be made to simulate the tissue characteristics of the UC and vessels more realistically by embedding them in a layer of connective tissue. Additionally, the simulation of the intestines can be refined to accurately represent multiple bowel loops.

Furthermore, adjustments should be made to the tight fit between the 3D-printed top and base components to prevent stretching of the abdominal wall and ensure that the abdominal wall defect

remains circular in shape.

To transform it into a training model, efforts can be undertaken to make the model suitable for underwater use within a laparascopic box trainer. This adaptation would facilitate the replication of the amniotic fluid environment and enable training that closely mimics the fetoscopic setting, involving solely endoscopic feedback and two working instruments.

6.4.4. Introducing the Ring

To progress towards clinical application, it is essential to explore the method of introducing the silicone ring with membrane into the uterus through a surgical port. As discussed earlier, the ring currently requires encapsulation by a different material or instrument for successful insertion. The main focus in this application should be on minimizing any addition to the ring's crossing profile while ensuring successful and safe introduction.

6.4.5. Placing the Ring

Furthermore, to meet all predetermined design requirements, addressing the precise placement procedure of the ring is of utmost importance. Early-stage user tests involving clinical experts can provide valuable feedback for refining the design of the ring and collaboratively developing the necessary surgical techniques for accurate placement. It may be necessary to devise a new instrument that facilitates the easy and precise placement of the ring, potentially in conjunction with the instrument developed for insertion. Such efforts will significantly increase the chances of successful and accurate positioning of the ring during a fetoscopic intervention for CG.

6.5. Conclusion

This thesis has successfully achieved its primary goal of providing a proof of principle for a novel dedicated method that enables the swift closure of the abdominal wall defect during a fetoscopic repair procedure for CG. The development of this innovative method began with a thorough analysis of the clinical context, leading to the design of the silicone ring with membrane as the key concept. Multiple configurations of the concept were prototyped, exploring various shapes, diameters, and stiffness levels to assess their impact on the performance of the ring. Additionally, a validation model was created, simulating a 24-week-old fetus with CG. The subsequent validation experiments demonstrated the effectiveness of the silicone ring with membrane in closing the abdominal wall defect, while also affirming its feasibility for introduction through a 12 Fr or 14 Fr surgical port.

Looking ahead, future research is needed to clinically investigate the defect diameter in CG and optimize the design of the silicone ring with membrane. Additionally, enhancing the validation model to serve as both a validation and training model will be valuable for conducting user tests. Furthermore, the development of an instrument for introducing the ring into the uterus and refining the surgical technique for accurate positioning of the ring will be essential.

The achievements in this work mark the initial exploration of a novel closure method and a new procedure for fetoscopic repair of CG. This innovative approach addresses both causes of secondary bowel damage while minimizing risks to both the mother and fetus, presenting the potential to improve gastrointestinal health at birth and potentially reduce the need for multiple neonatal surgeries and general anesthesia. By doing so, it would lessen the medical and emotional burden on patients and their families, representing a significant advancement in the field of fetoscopic repair of CG.

References

[1] R. C. Sun, K. Hessami, E. Krispin, *et al.*, "Prenatal ultrasonographic markers for prediction of complex gastroschisis and adverse perinatal outcomes: A systematic review and meta-analysis," *Archives of Disease in Childhood. Fetal and Neonatal Edition*, vol. 107, no. 4, pp. 371–379, Jul. 2022. DOI: 10.1136/archdischild-2021-322612.

[2] R. G. Ferreira, C. R. Mendonça, L. L. Gonçalves Ramos, F. S. de Abreu Tacon, W. Naves do Amaral, and R. Ruano, "Gastroschisis: A systematic review of diagnosis, prognosis and treatment," *The Journal of Maternal-Fetal & Neonatal Medicine*, vol. 35, no. 25, pp. 6199–6212, Dec. 12, 2022. DOI: 10.1080/14767058.2021.1909563.

[3] L.-O. Durmaz, S. E. Brunner, A. Meinzer, T. F. Krebs, and R. Bergholz, "Fetal surgery for gastroschisis—a review with emphasis on minimally invasive procedures," *Children*, vol. 9, no. 3, p. 416, Mar. 15, 2022. DOI: 10.3390/children9030416.

[4] B. E. Willborg, E. R. Ibirogba, A. T. A. Trad, L. Sbragia, D. Potter, and R. Ruano, "Is there a role for fetal interventions in gastroschisis management? – an updated comprehensive review," *Prenatal Diagnosis*, vol. 41, no. 1, pp. 159–176, Aug. 2021. DOI: 10.1002/pd.5820.

[5] L. Joyeux, M. A. Belfort, P. De Coppi, *et al.*, "Complex gastroschisis: A new indication for fetal surgery?" *Ultrasound in Obstetrics & Gynecology*, vol. 58, no. 6, pp. 804–812, Sep. 2021. DOI: 10.1002/uog.24759.

[6] "Facts about gastroschisis," Centers for Disease Control and Prevention, National Center on Birth Defects and Developmental Disabilities, [Online]. Available: https://www.cdc.gov/ncbddd/birthdefects/gastroschisis.html (accessed Jan. 7, 2023).

[7] M. A. Belfort, W. E. Whitehead, A. A. Shamshirsaz, *et al.*, "Comparison of two fetoscopic open neural tube defect repair techniques: Single- vs three-layer closure," *Ultrasound in Obstetrics & Gynecology*, vol. 56, no. 4, pp. 532–540, 2020. DOI: 10.1002/uog.21915.

[8] D. Lapa, R. Chmait, Y. Gielchinsky, *et al.*, "Percutaneous fetoscopic spina bifida repair: Effect on ambulation and need for postnatal cerebrospinal fluid diversion and bladder catheterization," *Ultrasound in Obstetrics & Gynecology*, vol. 58, no. 4, pp. 582–589, Oct. 2021. DOI: 10.1002/uog.23658.

[9] T. Kohl, K. Tchatcheva, R. Stressig, U. Gembruch, and P. Kahl, "Is there a therapeutic role for fetoscopic surgery in the prenatal treatment of gastroschisis? a feasibility study in sheep.," *Surgical endoscopy*, vol. 23, no. 7, pp. 1499–1505, Jul. 2009. DOI: 10.1007/s00464-009-0394-6.

[10] R. Bergholz, T. Krebs, K. Wenke, *et al.*, "Fetoscopic management of gastroschisis in a lamb model.," *Surgical endoscopy*, vol. 26, no. 5, pp. 1412–1416, May 2012. DOI: 10.1007/s00464-011-2048-8.

[11] T. Krebs, M. Boettcher, H. Schäfer, *et al.*, "Gut inflammation and expression of ICC in a fetal lamb model of fetoscopic intervention for gastroschisis.," *Surgical endoscopy*, vol. 28, no. 8, pp. 2437–2442, Aug. 2014. DOI: 10.1007/s00464-014-3494-x.

[12] R. Bergholz, T. Krebs, B. Cremieux, *et al.*, “Fetoscopic techniques for prenatal covering of gastroschisis in an ovine model are technically demanding and do not lead to permanent anchoring on the fetus until the end of gestation.,” *Surgical endoscopy*, vol. 35, no. 2, pp. 745–753, Feb. 2020. DOI: 10.1007/s00464-020-07441-7.

[13] “Fetal medicine webinar - updates on gastroschisis and trial for in utero repair,” YouTube. in collab. with A. King, M. Belfort, L. Joyeux, S. Keswani, and M. S. Cortes, [Online]. Available: https://www.youtube.com/watch?v=SMj2GBDlxSk (accessed Apr. 11, 2023).

[14] S. Keswani. “Fetal repair of complex gastroschisis: A safety and feasibility trial,” Clinical Trials, [Online]. Available: https://clinicaltrials.gov/ct2/show/study/NCT05704257 (accessed Apr. 11, 2023).

[15] M. Sanz Cortes, D. A. Lapa, G. L. Acacio, *et al.*, “Proceedings of the first annual meeting of the international fetoscopic myelomeningocele repair consortium,” *Ultrasound in Obstetrics & Gynecology*, vol. 53, no. 6, pp. 855–863, 2019. DOI: 10.1002/uog.20308.

[16] S. Keswani, M. Belfort, L. Joyeux, A. King, and M. S. Cortes. “Updates on gastroschisis and trial for in utero repair (official flyer),” Baylor College of Medicine, [Online]. Available: https://cdn.bcm.edu/sites/default/files/gastroschisis.webinar_flyer-final2.pdf (accessed Apr. 11, 2023).

[17] H. Cheng, J. W. Clymer, B. Po-Han Chen, *et al.*, “Prolonged operative duration is associated with complications: A systematic review and meta-analysis,” *Journal of Surgical Research*, vol. 229, pp. 134–144, Sep. 1, 2018. DOI: 10.1016/j.jss.2018.03.022.

[18] K. L. Moore, A. M. Agur, and A. F. Dalley II, *Essential Clinical Anatomy*, Fifth, International edition. Philadelphia, PA, USA: Lippincott Williams & Wilkins, 2015.

[19] G. Mazzoni, D. Alberti, F. Torri, *et al.*, “Prediction of complex gastroschisis: The evolution of therapeutic techniques and their relation with fetal sonographic features,” *Journal of Neonatal-Perinatal Medicine*, vol. 15, no. 1, pp. 137–145, Jan. 1, 2022. DOI: 10.3233/NPM-210746.

[20] P. C. Brugger and D. Prayer, “Development of gastroschisis as seen by magnetic resonance imaging,” *Ultrasound in Obstetrics & Gynecology*, vol. 37, no. 4, pp. 463–470, 2011. DOI: 10.1002/uog.8894.

[21] T. Gelas, D. Gorduza, S. Devonec, *et al.*, “Scheduled preterm delivery for gastroschisis improves postoperative outcome,” *Pediatric Surgery International*, vol. 24, no. 9, pp. 1023–1029, Sep. 1, 2008. DOI: 10.1007/s00383-008-2204-y.

[22] R. P. Davis, M. C. Treadwell, R. A. Drongowski, D. H. Teitelbaum, and G. B. Mychaliska, “Risk stratification in gastroschisis: Can prenatal evaluation or early postnatal factors predict outcome?” *Pediatric Surgery International*, vol. 25, no. 4, pp. 319–325, Apr. 1, 2009. DOI: 10.1007/s00383-009-2342-x.

[23] K. L. Moore, T. Persaud, and M. G. Torchia, *The Developing Human: Clinically Oriented Embryology*, Tenth, International Edition. Philadelphia, PA, USA: Elsevier, Inc., 2016.

[24] J. W. Rohen, C. Yokochi, and E. Lütjen-Drecoll, *Color Atlas of Anatomy: A Photographic Study of the Human Body*, Seventh Edition. Philadelphia, PA, USA: Lippincott Williams & Wilkins, 2011.

[25] “Biological evaluation of medical devices — Part 1: Evaluation and testing within a risk management process,” ISO 10993-1:2018, International Organization for Standardization (ISO), 2018.

[26] “Sterilization of medical devices - Requirements for medical devices to be designated “STERILE” - Part 1: Requirements for terminally sterilized medical devices,” EN 556-1:2001, European Committee for Standardization (CEN), 2001.

[27] N. F. M. Roozenburg and J. Eekels, *Product Design: Fundamentals and Methods*. Chichester, NY, USA: John Wiley & Sons, 1995.

[28] N. P. Tipnis and D. J. Burgess, “Sterilization of implantable polymer-based medical devices: A review,” *International Journal of Pharmaceutics*, vol. 544, no. 2, pp. 455–460, Jun. 15, 2018. DOI: 10.1016/j.ijpharm.2017.12.003.

[29] “Liquid silicone rubber - application and product selection guide,” DuPont, 2022. [Online]. Available: https://www.dupont.com/content/dam/dupont/amer/us/en/liveo/public/documents/en/Liquid%20Silicone%20Rubber_001-20385-CDP-REV2-0522_Letter-spreads.pdf (accessed Sep. 5, 2023).

[30] “Medical grade liquid silicone rubbers (lsr) for healthcare applications - lsr selector guide,” Elkem. [Online]. Available: https://content.elkem.com/lsr-selector-guide (accessed Sep. 5, 2023).

[31] “Design specifications for 3d models (form 3/form 3b),” Formlabs Customer Support. (Jun. 17, 2020), [Online]. Available: https://support.formlabs.com/s/article/Design-specifications-for-3D-models-form-3?language=en_US (accessed Sep. 8, 2023).

[32] “Which formlabs resins print with the form 3/form 3b?” Formlabs Customer Support. (Mar. 5, 2020), [Online]. Available: https://support.formlabs.com/s/article/What-Formlabs-resins-work-with-the-new-Form-3?language=en_US#top (accessed Sep. 8, 2023).

[33] “General purpose resins - materials for high resolution models and rapid prototyping,” Formlabs, 2016. [Online]. Available: https://formlabs-media.formlabs.com/datasheets/1801089-TDS-ENUS-0P.pdf (accessed Sep. 8, 2023).

[34] “Form cure time and temperature settings,” Formlabs Customer Support. (Sep. 30, 2022), [Online]. Available: https://support.formlabs.com/s/article/Form-Cure-Time-and-Temperature-Settings?language=en_US (accessed Sep. 8, 2023).

[35] “Form wash/form wash l time settings,” Formlabs Customer Support. (Jun. 13, 2023), [Online]. Available: https://support.formlabs.com/s/article/Form-Wash-Time-Settings?language=en_US (accessed Sep. 8, 2023).

[36] “Deadener & hardener for PlatSil® gels - technical bulletin,” Polytek Development Corp., Dec. 9, 2020. [Online]. Available: https://polytek.com/content/pdf/technicalbulletin/Polytek_TB_Deadener_5-5-2021.pdf (accessed Jun. 15, 2023).

[37] S. K. Kabagambe, C. J. Lee, L. F. Goodman, Y. J. Chen, M. A. Vanover, and D. L. Farmer, “Lessons from the barn to the operating suite: A comprehensive review of animal models for fetal surgery,” *Annual Review of Animal Biosciences*, vol. 6, pp. 99–119, Feb. 15, 2018. DOI: 10.1146/annurev-animal-030117-014637.

[38] D. Ting, *Thermofluids: From Nature to Engineering*, First Edition. Cambridge, MA, USA: Academic Press, 2022.

[39] M. L. N. G. Malbrain, M. L. Cheatham, A. Kirkpatrick, *et al.*, "Results from the international conference of experts on intra-abdominal hypertension and abdominal compartment syndrome. i. definitions," *Intensive Care Medicine*, vol. 32, no. 11, pp. 1722–1732, Nov. 1, 2006. DOI: 10.1007/s00134-006-0349-5.

[40] A. W. Kirkpatrick, D. J. Roberts, J. De Waele, *et al.*, "Intra-abdominal hypertension and the abdominal compartment syndrome: Updated consensus definitions and clinical practice guidelines from the world society of the abdominal compartment syndrome," *Intensive Care Medicine*, vol. 39, no. 7, pp. 1190–1206, 2013. DOI: 10.1007/s00134-013-2906-z.

[41] "Pressure converter," UnitConverters.net, [Online]. Available: https://www.unitconverters.net/pressure-converter.html (accessed Sep. 7, 2023).

[42] C. Haddock and E. D. Skarsgard, "Understanding gastroschisis and its clinical management: Where are we?" *Expert Review of Gastroenterology & Hepatology*, vol. 12, no. 4, pp. 405–415, Apr. 3, 2018. DOI: 10.1080/17474124.2018.1438890.

[43] M. Olesevich, F. Alexander, M. Khan, and K. Cotman, "Gastroschisis revisited: Role of intraoperative measurement of abdominal pressure," *Journal of Pediatric Surgery*, vol. 40, no. 5, pp. 789–792, May 1, 2005. DOI: 10.1016/j.jpedsurg.2005.01.043.

[44] "PLA for s series," UltiMaker, [Online]. Available: https://ultimaker.com/materials/s-series-pla/ (accessed Sep. 8, 2023).

[45] "UltiMaker s5," UltiMaker, [Online]. Available: https://ultimaker.com/3d-printers/s-series/ultimaker-s5/ (accessed Sep. 6, 2023).

[46] "Handmatige bloeddrukmeter palm-type ST-a211 II," Stalt Medical, [Online]. Available: https://www.staltmedical.nl/handmatige-bloeddrukmeter-palm-type-st-a211-ii.html (accessed Jul. 20, 2023).

[47] "List randomizer," RANDOM.ORG, [Online]. Available: https://www.random.org/lists/?mode=advanced (accessed Jul. 21, 2023).

[48] S. M. Fateh, N. A. Mohammed, K. A. Mahmood, *et al.*, "Sonographic measurement of splenic size and its correlation with body parameters," *Medicine International*, vol. 3, no. 1, p. 7, Jan. 9, 2023. DOI: 10.3892/mi.2023.67.

[49] B. de Bakker and M. van den Hoff. "The dutch fetal biobank," Dutch Fetal Biobank, Amsterdam UMC, [Online]. Available: www.fetalbiobank.com (accessed May 15, 2023).

[50] F. Togni, E. Araujo Júnior, F. Vasques, A. Moron, M. Torloni, and L. Nardozza, "The cross-sectional area of umbilical cord components in normal pregnancy," *International Journal of Gynecology & Obstetrics*, vol. 96, no. 3, pp. 156–161, 2007. DOI: 10.1016/j.ijgo.2006.10.003.

A

Clinical Interview

On March 16, 2023, three medical professionals were interviewed to delve into the clinical perspective on gastroschisis. The aim was to gather insights into the visual appearance and tissue characteristics of the abdominal wall defect and the eviscerated intestines, as well as to explore their insights and ideas regarding a novel fetal intervention for gastroschisis. The interviewees were Prof. dr. R.M.H. Wijnen (pediatric surgeon and head of department pediatric surgery, Erasmus MC), Dr. H.R. Langeveld-Benders (pediatric surgeon, Erasmus MC) and Dr. P.L.J. DeKoninck (gynecologist-perinatologist, Erasmus MC). This appendix contains a comprehensive list of the main findings obtained from this interview.

A.1. Abdominal Wall Defect

- The shape of the defect is circular.
- The diameter of the defect does not vary significantly among babies and is estimated to be around 20-25 mm.
- The UC is positioned almost inside the defect.
- The fascia wall feels firm and forms a distinct ”hard” ring that can be felt after birth.
- The fascia and the skin are aligned at the same level, with the diameter of the defect being consistent in both layers.

A.2. Eviscerated Intestines

- Typically, the small intestines protrude through the defect. However, in some instances, a portion of the stomach or colon also protrudes alongside the small intestines.
- Postnatally, the appearance of the intestines varies significantly among each baby in terms of characteristics such as peeling or non-peeling, as well as the arrangement of the intestines, which can range from a solid tangle to loose loops.

A.3. Current Treatment Method

- The decision for primary closure, which involves pushing back the intestines and closing the defect, is determined through a trial-and-error approach. The medical professionals attempt the closure and assess its success. If the primary closure is not achieved within a 30-minute timeframe, they discontinue the attempt and opt for a silo, which is a secondary closure method.
- Based on the appearance of the intestines at birth, it is possible to assess whether primary closure is likely to be successful.
- In certain cases, it may be necessary to make an incision (upwards) to slightly enlarge the defect, allowing for easier maneuvering of the intestines back into the abdominal cavity.

A.4. Additional Insights

- DeKoninck suggested that a fetal gastroschisis intervention would likely occur between 20 to 25 weeks of gestation, similar to the timing of fetoscopic spina bifida interventions. When considering the timing of the fetal intervention, the approach depends on whether suturing is required or not. If suturing is necessary, it is preferable to perform the intervention as late as possible to take advantage of the less fragile tissue. Conversely, if suturing is not needed, it is recommended to intervene as early as possible to maximize its impact.
- The presence of the UC should be carefully considered during fetal interventions, as it naturally extends into the abdominal cavity. It is crucial to ensure that any fetal intervention does not cause any compression or compromise to the UC or the umbilical vessels.
- It is important to consider the potential risk of tissue necrosis in the abdominal wall due to prolonged pressure during or after a fetal intervention. However, it is worth noting that wound healing in fetuses seems to differ from that in newborn babies, which may mitigate some of the concerns.
- According to Wijnen's perspective, there is sufficient space within the abdominal cavity to perform a fetoscopic procedure for pushing back the eviscerated intestines.
- Langeveld-Benders speculates that the fetoscopic repositioning of the intestines may not be successful, considering the challenges encountered during postnatal efforts to return the intestines to the abdominal cavity. The process of repositioning is likely facilitated by gentle manual manipulation rather than using rigid pointed instruments.
- DeKoninck expresses a preference for a novel fixation technique that is compatible with a 12 Fr surgical port. If that is not feasible, an alternative option would be the utilization of a 14 Fr surgical port, according to DeKoninck's preference.
- DeKoninck expresses a preference for a surgical procedure with a maximum in utero time of 30 minutes.

B

Ultrasound Image Analysis

In the process of designing a novel closure method intended to remain in place until birth, it was essential to thoroughly understand the anatomical characteristics of the abdominal wall defect and the eviscerated bowel throughout gestation. To achieve this, US images were analyzed to assess the size of the abdominal wall defect and measure the volume of the eviscerated intestines throughout gestation. This appendix provides a detailed overview of the methods, results, and discussion of this US image analysis.

B.1. Methods

A retrospective analysis was conducted on US images of ten gastroschisis patients who received treatment at Erasmus MC, between 2018 and 2023. The primary objective was to determine the dimensions of the eviscerated intestines in both the transverse plane (length and width) and the sagittal plane (height). Figure B.1 illustrates the method used to measure the dimensions of the eviscerated intestines on US images in the transverse plane. Due to the lack of standardization in the US protocol for gastroschisis, not all patients had available US images in both planes. Multiple patients were missing sagittal plane images. In such cases, the closest alternative US image was used to estimate the height. Additionally, the maximum diameter of the abdominal wall defect in the transverse plane was measured for five patients. Furthermore, the gestational age of each fetus, expressed in weeks, was recorded.

All the collected data was recorded in a run-table using Microsoft Excel. Subsequently, the volume of the eviscerated bowel was computed for each patient using the standard ellipsoid formula (length x width x height x 0.523), commonly employed for estimating the volume of irregularly shaped organs [48]. The calculated volumes were then converted from mm^3 to mL and entered into run-table. Mean values for the dimensions and volumes were subsequently calculated per gestational age.

B.2. Results

The analysis included routine 20-week US scans from nine patients. In addition to these cases, one patient had additional US images available at 24 weeks' gestation, while another patient had images at 27 weeks' gestation. Furthermore, there was one patient whose US images were only analyzed at

Table B.1: Summary of the dimensions and volume of the eviscerated intestines and abdominal wall defect in gastroschisis fetuses according to gestational age (GA).

GA (weeks)	Eviscerated intestines								Defect	
	Length (mm)		Width (mm)		Height (mm)		Volume (ml)		Maximum diameter (mm)	
	mean (n)									
20	22.6	(9)	22.8	(9)	21.5	(9)	5.9	(9)	9.7	(4)
24	-	-	35.8	(1)	20.3	(1)	-	-	13.0	(1)
25	43.2	(1)	33.5	(1)	19.2	(1)	14.5	(1)	10.0	(1)
27	36.2	(1)	41.5	(1)	35.9	(1)	28.2	(1)	-	-

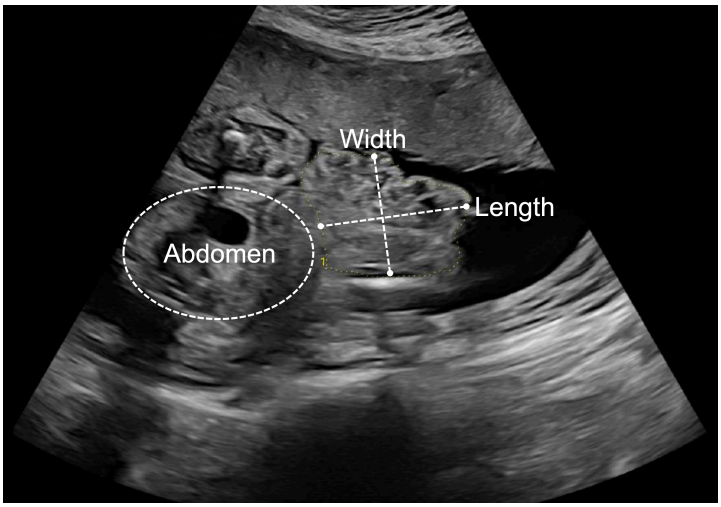

Figure B.1: Determining the length and width of the eviscerated intestines on an ultrasound image in the transverse plane.

25 weeks' gestation.

The mean values for length, width, and height at 20 weeks' gestation (n = 9) were found to be 22.6 mm, 22.8 mm, and 21.5 mm, respectively. The mean volume at 20 weeks of gestation was calculated to be 5.9 mL (n = 9), while the mean diameter of the defect was 9.7 mm (n = 4). All the dimensions and volumes are presented in Table B.1.

B.3. Discussion

B.3.1. Interpretation of the Results

At 20 weeks' gestation, the mean length, width, and height of the eviscerated intestines were all found to be approximately 22 mm. This suggests that there is no significant difference among these three dimensions, which can be attributed to the intestines floating freely within the amniotic cavity.

The volume of the eviscerated intestines increases clearly throughout gestation. For instance, when comparing the US images of a fetus at both 20 weeks and 27 weeks of gestation, the volume of the eviscerated intestines rose from 6.2 mL to 28.2 mL. Additionally, in the case of the fetus examined at

25 weeks' gestation, the volume measured 14.5 mL, more than double the mean volume at 20 weeks' gestation (5.9 mL). This outcome aligns with expectations, considering that the intestines grow along with the fetus during gestation, including the portions extending outside the abdomen.

Although not explicitly stated in the results, the US images at 20 weeks of gestation revealed scrunched intestines, making it difficult to discern the individual bowel loops and their lumens clearly. However, in contrast, the US images captured at 24, 25, and 27 weeks of gestation displayed a distinct lumen for each bowel loop, indicating more distended intestines. This observation highlights a developmental progression in the visibility and differentiation of the bowel loops over the course of gestation.

The defect diameter appears to consistently remain within a similar range throughout gestation, ≈10 mm, without significant increases observed over time.

B.3.2. Limitations

One notable limitation of this analysis is the small sample size, particularly for fetuses at 24, 25, and 27 weeks of gestation (n = 1). As a result, caution should be taken when interpreting the findings, as they may not fully represent the overall population.

Moreover, each dimension was measured only once per patient. To enhance accuracy, multiple measurements should ideally be taken for each dimension and the mean value calculated to provide a more precise result.

Another important limitation is the lack of standardization in the US imaging protocol for gastroschisis patients at Erasmus MC. Consequently, not all fetuses had available sagittal plane images, and the height measurements taken in a slightly different plane may be less accurate.

Lastly, it is worth noting that at the beginning of this US measurement process, there was no established experimental protocol. As a result, the measurement of defect diameter was not performed for all patients, leading to limited data available for this variable (n = 5).

B.3.3. Conclusion

Analysis of US images in gastroschisis patients reveals a noticeable increase in the volume of eviscerated intestines as gestation progresses. From week 20 to week 27, the volume expands from 5.9 mL to 28 mL. In contrast, the diameter of the abdominal wall defect shows no significant increase, remaining ≈10 mm between week 20 and week 25 of gestation. Notably, the intestines become more distended as the gestational age advances, resulting in improved visibility of individual bowel loops over time.

C

Dutch Fetal Biobank

The Dutch Fetal Biobank is a globally unique initiative where human embryos and fetuses are stored for medical scientific research. Inclusion in the biobank is carried out exclusively with explicit written permission from the donors [49].

In March 2023, a fetus diagnosed with gastroschisis was included in the Dutch Fetal Biobank. Table C.1 provides an overview of the general specifications of the fetus. The purpose of studying this fetus was to observe the positioning of the UC in relation to the defect and to gain insights into the shape and appearance of the eviscerated intestines. Apart from the small intestine, the liver had protruded through the defect in this fetus as well. Figure C.1 presents a photograph of the fetus' body captured from both the left and right sides.

Table C.1: General specifications on the gastroschisis fetus

Variable	Gastroschisis Fetus
Sex	Male
Gestational age (weeks+days)	15+0
Weight (gram)	67
Crown-rump length (cm)	8.9
Total length (cm)	12.8

(a) Left side of the fetus' body.

(b) Right side of the fetus' body.

Figure C.1: Aborted gastroschisis fetus at 15 0/7 weeks of gestation at the Dutch Fetal Biobank. *Labels:* (1) Liver, (2) Small intestine, (3) Umbilical cord.

D

Gastroschisis Newborn Examination

In July 2023, a male newborn with SG was delivered at Erasmus MC at a GA of 36 weeks. Dr. P.L.J. DeKoninck (gynecologist-perinatologist, Erasmus MC) was present during the surgery to repair the abdominal wall defect, which occurred on the same day as the birth, and conducted measurements of the abdominal wall defect.

A measuring rod was positioned beside the defect to capture measurements in both the lateral and superior-inferior directions, both before and after repositioning the intestines within the abdominal cavity. Photographs were taken to document these measurements; however, they are not included in this thesis due to privacy considerations.

The abdominal wall defect measured 20 mm in both dimensions, both before and after the intestines were repositioned. Furthermore, the following observations were noted: the fascia layers and the skin essentially formed a cohesive unit, the UC was positioned directly adjacent to the defect, and the umbilical vessels were enveloped in mucous connective tissue, creating a protective layer.

E

Ideated Concepts and Harris Profiles

Figure E.1 visually represents all the concepts generated during the ideation phase. Additionally, the concepts are listed below:

(A) Solid Silicone Plug

(B) Silicone Ring with Membrane

(C) Double Silicone Ring with Membrane

(D) Spring Loaded Ring with Membrane

(E) ASD-like Memory Metal Closure

(F) Membrane with Barbs

(G) Membrane with Bioglue

(H) Membrane with Ostomy-like Patch

The evaluation of all conceptual ideas was conducted using the Harris Profile methodology [27], taking into account the key properties outlined in Section 2.2.1. The Harris Profile utilizes a 4-point matrix scale (-2, -1, +1, +2) to visually represent the qualities demonstrated by each design concept. A score of -2 indicates poor performance in the evaluated key property, while +2 signifies excellent performance. Figure E.2 illustrates the Harris profiles for all conceptual ideas.

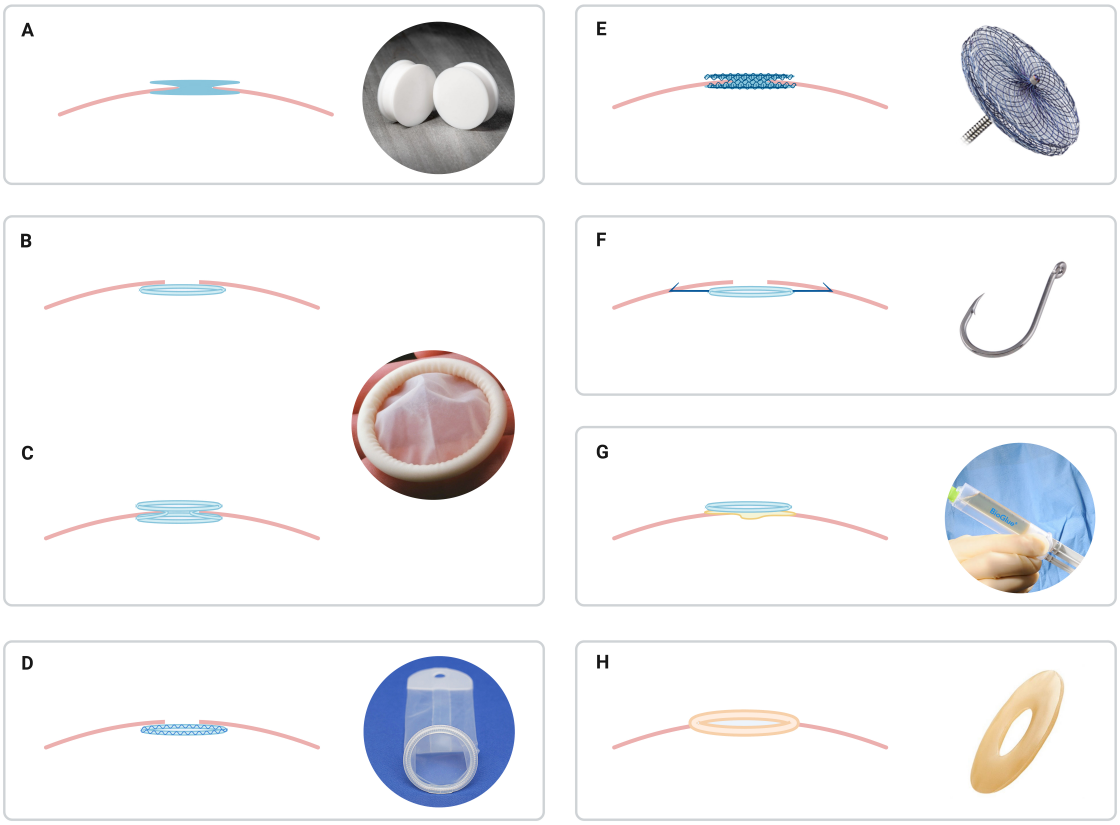

Figure E.1: All concepts generated during the ideation phase, depicted in relation to a simplified transverse view of an abdominal wall with a gastroschisis defect. Each concept is accompanied by a photograph depicting its inspiration. *Concepts:* (A) Solid silicone plug, (B) Silicone ring with membrane, (C) Double silicone ring with membrane, (D) Spring loaded ring with membrane, (E) ASD-like memory metal closure, (F) Membrane with barbs, (G) Membrane with bioglue, (H) Membrane with ostomy-like patch. Created with BioRender.com

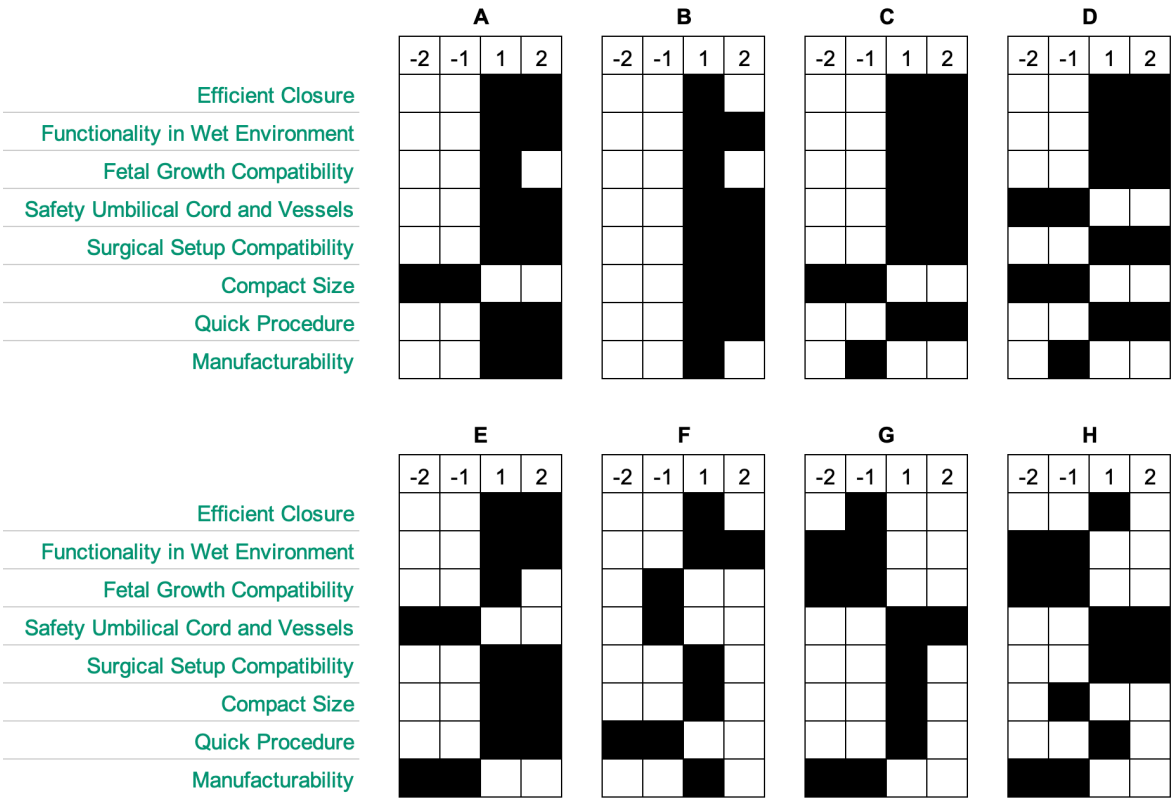

Figure E.2: Harris Profiles evaluating all ideated concepts based on the key properties. A score of -2 indicates poor performance in the evaluated key property, while +2 signifies excellent performance. *Concepts:* (A) Solid silicone plug, (B) Silicone ring with membrane, (C) Double silicone ring with membrane, (D) Spring loaded ring with membrane, (E) ASD-like memory metal closure, (F) Membrane with barbs, (G) Membrane with bioglue, (H) Membrane with ostomy-like patch.

F

Production Protocol Silicone Rings

This appendix provides a comprehensive outline of the production protocol implemented for the silicone ring with membrane during the second and final prototyping round. The protocol presented herein is the result of extensive testing and numerous iterations conducted during the first prototyping round.

F.1. Materials and Equipment

- Top and bottom mold silicone rings (produced according to Section 3.2.2)
- Release agent (Ease Release™200, Mann Release Technologies Inc., Macungie, PA, USA)
- 4 × Clamp (Holex Universal Clamp Clamping Hands (861900 25), Hoffmann Group, Knoxville, TN, USA)
- Bench vise 360°rotation
- 4 × Silicone tube (length 8 cm, inner ⌀ 4 mm, outer ⌀ 6 mm)
- PlatSil® Gel-25 Part A (Polytek® Development Corp., Easton, PA, USA)
- PlatSil® Gel-25 Part B (Polytek® Development Corp., Easton, PA, USA)
- PlatSil® Part H Hardener (Polytek® Development Corp., Easton, PA, USA)
- Labaratory balance (EMB 600-2, Kern, Balingen, Germany)
- Cardboard cup (300 ml capacity)
- Wooden paint stir stick (200 mm x 25 mm x 5 mm)
- Vacuumpump (EVD-VE260, Eurovacuum B.V., Oudewater, The Netherlands)
- De-gassing chamber (419115, Eurovacuum B.V., Oudewater, The Netherlands)
- Syringe without needle 50 mL (Terumo Corporation, Tokyo, Japan)
- 4 × Sealing clip (BEVARA Sealing clip (6 cm), IKEA, Delft, The Netherlands)

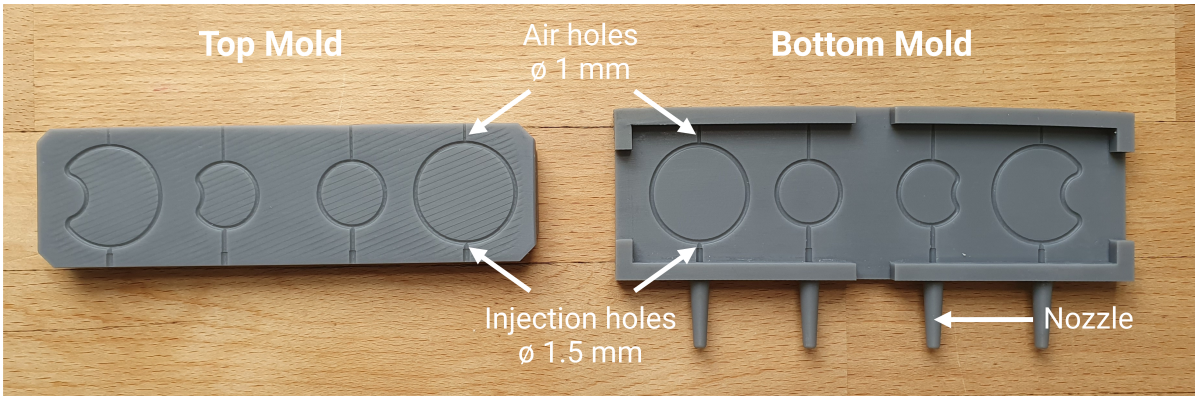

Figure F.1: Interior surface of both the top and bottom mold used for producing four configurations of the silicone ring with membrane during the final prototyping round. The membrane thickness of all rings equals 0.4 mm. The rings exhibit two different shapes: round or rusk (with a cut-out). Additionally, the outer diameter of the rings varies (20 mm or 30 mm).

- Stainless steel tailoring scissors (G-5150, Green Bell, Osaka, Japan)
- Drill with 0.9 mm drill bit
- Paper towels
- Compressed air

F.2. Production Protocol

F.2.1. Preparation Mold

Firstly, the release agent was evenly applied to the interior surfaces of both the top and bottom mold components (refer to Figure F.1). The release agent was sprayed onto the mold from a distance of 30 cm for a duration of 3 seconds. Subsequently, the release agent was allowed to dry for a minimum of 5 minutes before proceeding to the next step.

Next, the top and bottom mold components were carefully aligned and assembled, ensuring proper positioning of each part. To secure the mold in place, four clamps were utilized, tightly fastening the mold parts together according to the configuration depicted in Figure F.2. Additionally, a bench vise was employed to exert pressure on the mold parts. The bench vise was positioned at a 60°angle relative to the table surface, resulting in a 30°angle of inclination for the mold. The positioning of the mold guaranteed that the nozzles were directed towards the table, while the air holes were oriented upwards, as illustrated in Figure F.3. This specific position ensured the proper alignment of the mold with the desired direction of material flow.

Finally, silicone tubes were inserted over the nozzles, extending them as far as possible to ensure a secure connection.

F.2.2. Preparation Liquid Silicone Rubber

Two distinct silicone rubbers, referred to as the *flexible* and *stiff* silicone rubbers, were prepared separately. The specifications for each silicone rubber can be found in Table F.1. It is important to note that the entire production protocol must be followed individually for each silicone rubber.

To accurately measure and combine the PlatSil® components, a cardboard cup was used. The process began by weighing Part A according to the specified quantity outlined in Table F.1. Subsequently, Part H was poured into the same cup and weighed to the designated quantity. Finally, Part B was

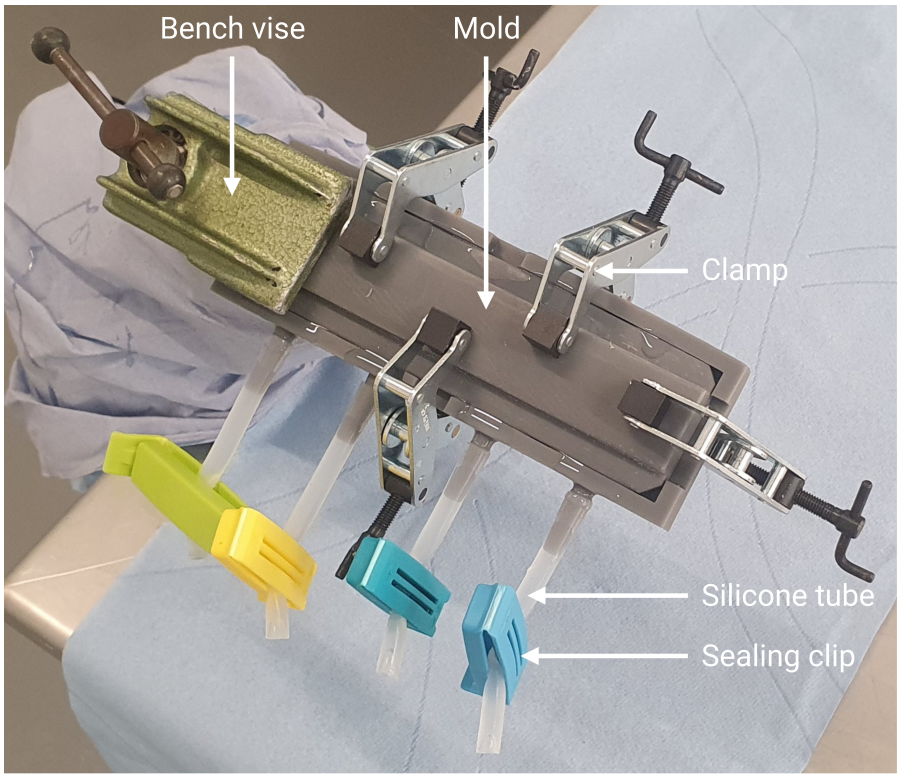

Figure F.2: Mold for silicone rings during curing process. The clamps securely press the top and bottom parts of the mold together, while the bench vise holds the mold in position. Silicone tubes are attached to the nozzles of the mold, facilitating the injection of the liquid silicone rubber. Sealing clips are employed to prevent any unintended pouring of the liquid silicone rubber out of the silicone tubes.

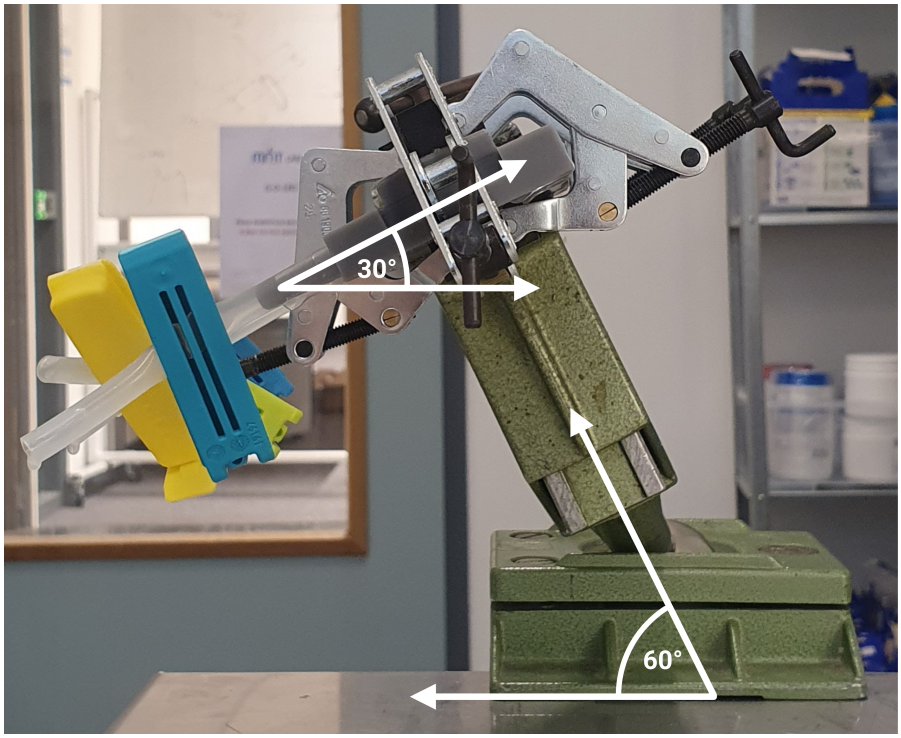

Figure F.3: Position of the bench vise and the mold within it. The bench vise is positioned at a 60°angle in relation to the table surface, resulting in a 30°angle of inclination for the mold. The nozzles of the mold are directed towards the table, while the air holes are oriented upwards, allowing for optimal material flow.

Table F.1: Specifications of the silicone rubbers used in the molding process of the silicone rings with membrane.

Silicone rubber	Shore hardness [36]	Proportion silicone components[a]	Quantity per component (gram)	Pour time (minutes)	Demold time (hours)
Flexible	A25	1A:1B	20.0	6	1
Stiff	A40	1A:1B:1H	15.0	8	2.5

[a] PlatSil® Gel-25 Part A and Part B, and PlatSil® Part H Hardener (Polytek® Development Corp., Easton, PA, USA).

added to the cup and weighed to the specified quantity. For the *flexible* silicone rubber, Part H was omitted from the process.

The pain stir stick was used to thoroughly mix the components together for approximately 30 seconds, ensuring a homogeneous mixture. Next, the cardboard cup containing the mixture was placed into a de-gassing chamber. The vacuum pump was activated, the vent closed, and the pump was allowed to operate for 60 seconds, starting from the point when the pressure gauge indicated -1 Bar pressure. Upon completion, the vacuum pump was deactivated, the vent was opened, and the cardboard cup was removed from the chamber. This process effectively eliminated any air bubbles within the silicone mixture.

F.2.3. Injection Liquid Silicone Rubber

The syringe utilized in the experiment consisted of two main components: the barrel and the plunger. Initially, the syringe was opened, separating the barrel from the plunger.

The liquid silicone mixture, previously prepared in the cardboard cup, was poured carefully into the barrel of the syringe. It was ensured that the needle was positioned upwards to prevent any leakage of the silicone mixture. Subsequently, the plunger was inserted into the barrel, with the syringe positioned in a manner that allowed the expulsion of all air from the needle. This step aimed to eliminate the presence of air bubbles within the silicone mixture.

Once the air was completely removed from the barrel, the needle was connected to the first silicone tube. The plunger was then pushed to inject the silicone mixture into the mold. Throughout the injection process, close attention was paid to the air hole of the mold. The injection continued until the silicone mixture flowing out of the air hole no longer contained any air bubbles. At this point, a sealing clip was applied to the silicone tube while maintaining pressure on the plunger.

Subsequently, the syringe was attached to the next silicone tube, and the injection procedure outlined above was iterated for each silicone tube. This process was carried out sequentially from left to right, guaranteeing the complete filling of each section of the mold, as illustrated in Figure F.2. Following the injection, the LSR was left to cure for a minimum duration as indicated by the demold time specified in Table F.1. During this period, the silicone rubber solidified and attained its desired physical properties.

F.2.4. Demolding and Post-processing

Once the minimum demold time had elapsed, the mold was carefully released from the bench vise. Subsequently, the clamps securing the mold were removed. The outer layer of cured silicone on the mold's exterior was meticulously removed by hand, excluding the silicone around the nozzles, which was left intact.

Next, the mold was cautiously opened manually. Tailoring scissors were employed to make precise

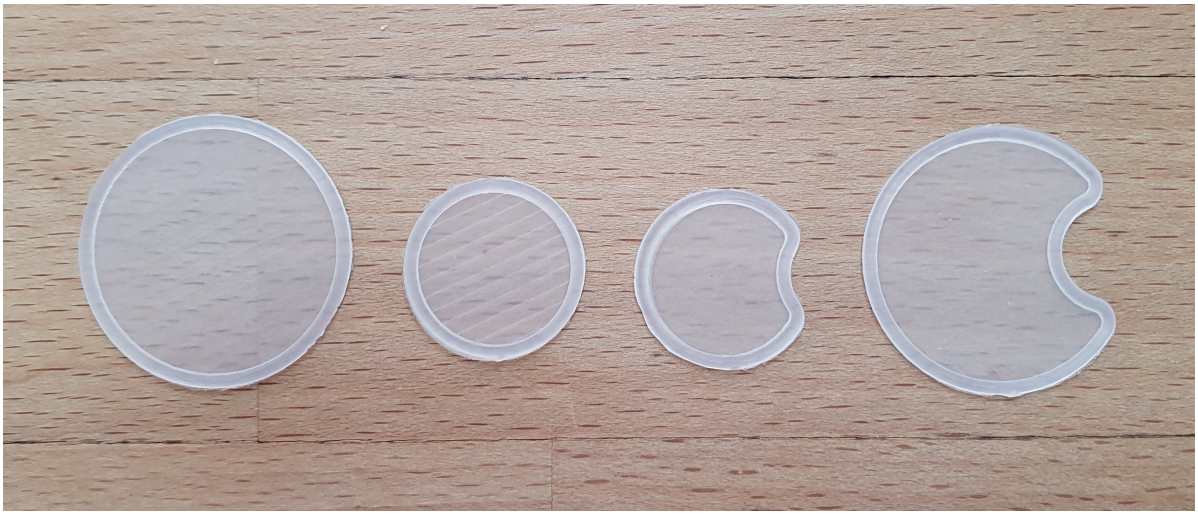

Figure F.4: The four different variations of silicone rings after the removal of all cured silicone from their exterior surfaces using tailoring scissors.

cuts on the cured silicone rods located outside the rings, particularly those connected to the air holes and injection holes. Following these cuts, the rings were detached from the mold. Lastly, all the cured silicone present on the exterior surface of the rings was diligently removed using the tailoring scissors, ensuring a clean and precise separation (see Figure F.4).

F.2.5. Cleaning the Mold

To prepare the mold for the next production process, thorough cleaning was performed. The first step involved carefully removing all cured silicone residue from the mold by hand. Sealing clips, used to secure the silicone tubes, were then detached and stored for future use, while the silicone tubes themselves were discarded as they are replaced for each new injection.

Next, paper towels were used to clean the mold's interior, paying close attention to the narrow indentations. This ensured the removal of any remaining debris. The air holes in the mold were checked to ensure they were open, and any blocked holes were carefully opened using a 0.9 mm drill bit. Compressed air was employed to remove any remaining small particles from the mold.

Once the cleaning process was completed, the mold was ready for the subsequent production, and the mold preparation could commence. By following this thorough cleaning procedure, the mold's performance and the quality of the produced items were maintained at their best.

G

Dimensions Umbilical Cord and Vessels

This appendix presents a comprehensive examination of the dimensions of the UC and vessels, which were essential for designing the rusk-shaped ring in the final prototyping round (Section 3.1.2) and developing the validation model (Chapter 4).

A thorough literature search was conducted to gather information on the diameter of the UC, UV, and UAs. Togni *et al.* conducted a study reporting the cross-sectional area of the Wharton jelly, UV, and UAs during weeks 24-40 of gestation [50]. The data extracted from this study was used to calculate the diameter of the Wharton jelly, UV, UAs, and a simplified total diameter of the collective umbilical vessels (excluding the Wharton jelly). Although these anatomical structures are not perfectly circular, as evident from Figure G.1, equation G.1 was employed to calculate the diameter assuming all structures were perfectly circular, for the sake of simplicity.

$$\text{Diameter} = 2 \times \sqrt{\frac{\text{cross-sectional area}}{\pi}} \tag{G.1}$$

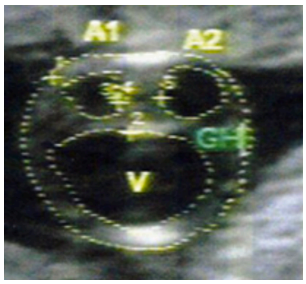

Figure G.1: Cross-section of the umbilical cord shown on an ultrasound image. (V) Umbilical vein. (A1 & A2) Umbilical arteries. Source: [50].

Table G.1: Mean cross-sectional area and diameter of the Wharton jelly, umbilical vein (UV), umbilical artery (UA) and the collective umbilical vessels at various gestational ages (GA).

GA (weeks)	Cross-sectional area (mm^2) [50]				Diameter[a] (mm)			
	Wharton jelly	UV	UA	Total vessels[b]	Wharton jelly	UV	UA	Total vessels
24-25	86.0	30.5	8.7	47.9	10.5	6.2	3.3	7.8
25-26	103.1	36.4	10.2	56.8	11.5	6.8	3.6	8.5
26-27	109.1	42.5	12.2	66.9	11.8	7.4	3.9	9.2
27-28	121.6	41.7	10.5	62.7	12.4	7.3	3.7	8.9
28-29	130.2	44.7	11.7	68.1	12.9	7.5	3.9	9.3
29-30	136.2	45.2	11.0	67.2	13.2	7.6	3.7	9.2
30-31	124.3	51.7	12.9	77.5	12.6	8.1	4.1	9.9
31-32	132.7	60.8	12.4	85.6	13.0	8.8	4.0	10.4
32-33	140.3	53.1	12.8	78.7	13.4	8.2	4.0	10.0
33-34	133.3	59.0	14.1	87.2	13.0	8.7	4.2	10.5
34-35	129.6	60.6	14.5	89.6	12.8	8.8	4.3	10.7
35-36	147.3	59.9	13.4	86.7	13.7	8.7	4.1	10.5
36-37	140.6	58.8	14.0	86.8	13.4	8.7	4.2	10.5
37-38	135.7	58.9	11.4	81.7	13.1	8.7	3.8	10.2
38-39	138.3	63.4	12.7	88.8	13.3	9.0	4.0	10.6
39-40	131.1	51.9	11.5	74.9	12.9	8.1	3.8	9.8

[a] Diameter = $2 \times \sqrt{\frac{\text{cross-sectional area}}{\pi}}$

[b] Total vessels = UV + $2 \times$ UA

H

Technical Specifications 3D-Printed Mold

Figure H.1 showcases the 3D-printed mold for the silicone ring with membrane in an isometric view. Figure H.2 and Figure H.3 offer technical illustrations of the bottom and top components, respectively.

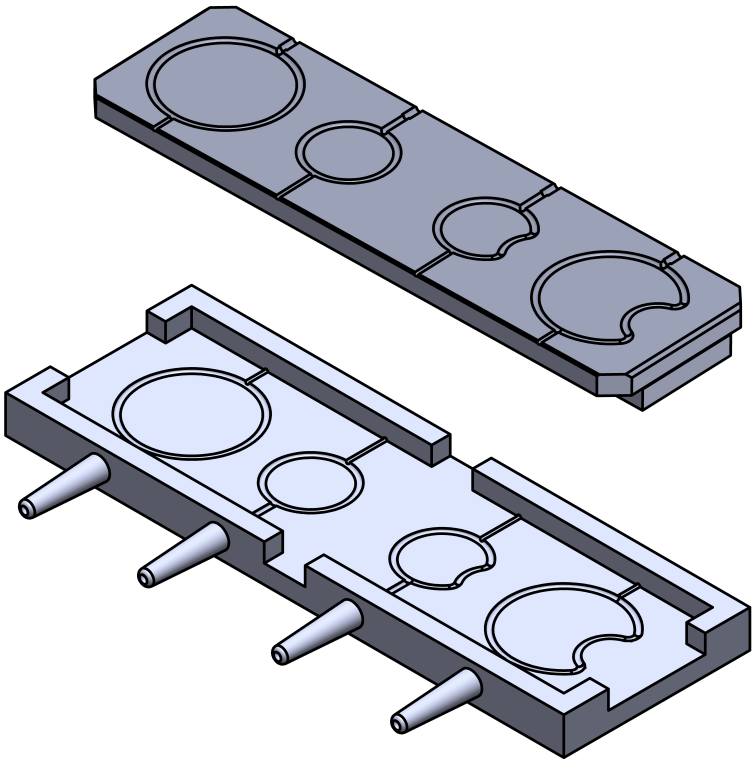

Figure H.1: Isometric view of the 3D-printed top and bottom mold for the silicone ring with membrane.

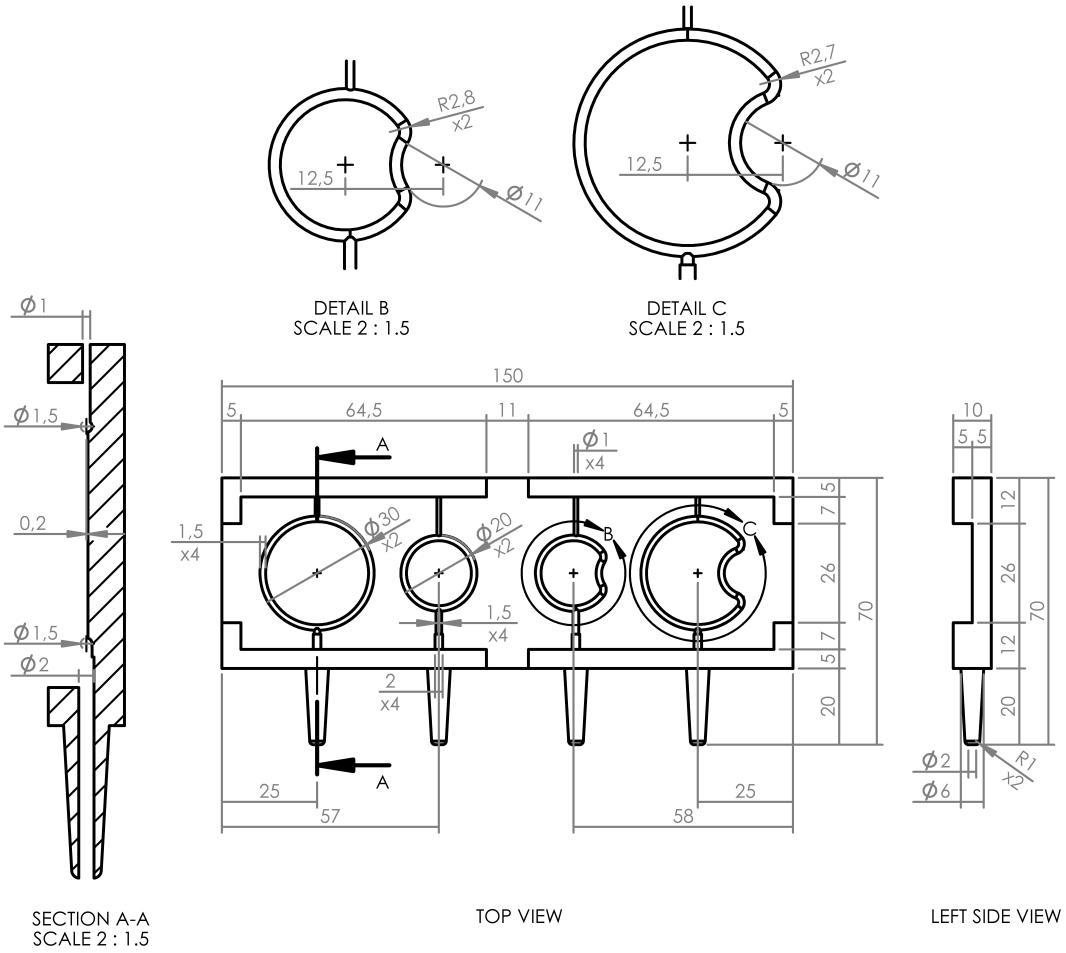

Figure H.2: Technical illustration depicting the 3D-printed bottom mold for the silicone ring with membrane. All dimensions are expressed in millimeters (mm).

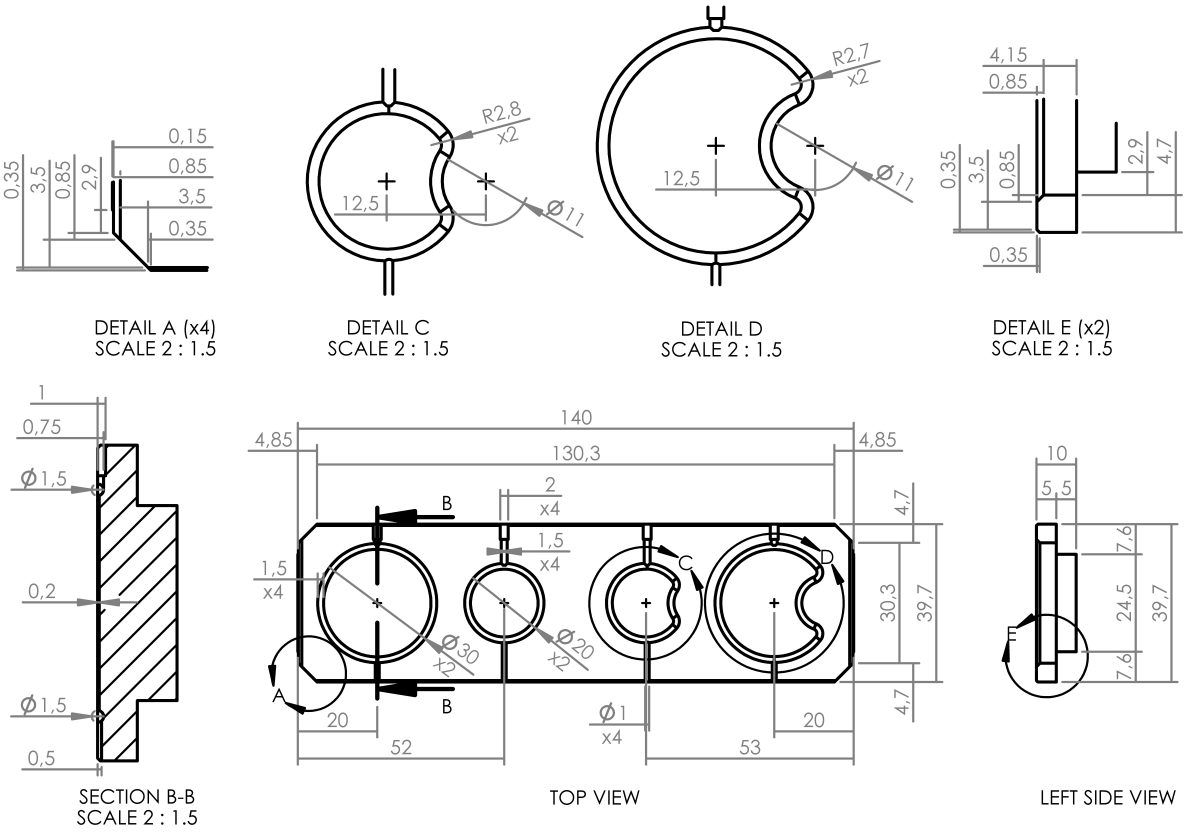

Figure H.3: Technical illustration depicting the 3D-printed bottom mold for the silicone ring with membrane. All dimensions are expressed in millimeters (mm)

Dimensions Fetal Abdominopelvic Cavity

To develop a realistic validation model, it was necessary to determine the dimensions of the fetal abdominopelvic cavity during the fetal intervention period (20-25 weeks of gestation). To obtain these dimensions, MRI images of a fetus with SBA and US images of a fetus with gastroschisis, both at 24 weeks of gestation, were analyzed at Erasmus MC. This appendix provides a comprehensive overview of the methods, results, and discussion of this US and MRI image analysis.

I.1. Methods

A retrospective analysis of MRI images of a 24-week-old fetus with SBA was conducted at Erasmus MC. The original purpose of capturing these images was unknown. Multiple measurements of the fetal abdominopelvic cavity were extracted from the MRI images in the sagittal, transversal, and coronal planes. The length, width, and height of the abdominopelvic cavity were determined. Specifically, the length was defined as the distance in the superior to inferior direction, extending from the top of the diaphragm to the pelvic floor [18]. The width was defined as the lateral distance, and the height was measured in the anterior to posterior direction, excluding the spine.

In addition, US images of a 24-week-old fetus with gastroschisis were captured and subsequently analyzed in collaboration with a perinatologist at Erasmus MC. Following a similar approach to the SBA fetus, multiple measurements of the length, width, and height of the fetal abdominopelvic cavity were extracted from the US images in the sagittal, transverse, and coronal planes.

All the collected data was recorded in a run-table using Microsoft Excel. Subsequently, the mean values for the dimensions were calculated.

I.2. Results

The mean values of the length, width, and height of the fetal abdominal cavity were determined to be 55.1 mm (n = 10), 46.9 mm (n = 4), and 41.1 mm (n = 3), respectively.

I.3. Discussion

Although this analysis is limited to only two cases, one of which is not a gastroschisis but a SBA fetus, the findings are considered sufficiently representative for the purpose of determining the dimensions of the fetal abdominopelvic cavity for the validation model. Therefore, for the validation model, a length of 55.1 mm, a width of 46.9 mm, and a height of 41.1 mm are assumed.

J

Abdominal Wall Prototypes

This appendix provides a comprehensive overview of the abdominal wall prototypes created during multiple prototyping rounds in the development of the final validation model. Table J.1 presents the details of each abdominal wall prototype.

Table J.1: Characteristics of the abdominal wall prototypes that were generated during the development of the final validation model.

Prototype	Proportion silicone components[a]	No. of silicone layers	Fascia component[b]	No. of fascia layers	Thickness[c] (mm)	Defect diameter (mm)	Distance defect to UC[c,d] (mm)
			Prototyping Round 1				
AW1	1A:1B	1	PowerMesh	1	1.4	12	1.1
AW2	1A:1B	1	PowerMesh	2	1.8	12	1.6
AW3	1A:1B	2	PowerMesh	1	3.3	12	2.4
AW4	1A:1B	2	PowerMesh	2	3.8	12	2.0
			Prototyping Round 2				
AW5	1A:1B:1H	1	PowerMesh	1	1.3	12	-
AW6	1A:1B	1	Cotton	1	1.6	12	-
AW7	1A:1B:1H	1	Cotton	1	1.5	12	-
			Prototyping Round 3				
AW8	1A:1B	1	Cotton	1	1.2	12	1.2
			Prototyping Round 4				
AW9	1A:1B	1	Cotton	1	1.0	12	2.0
AW10	1A:1B	1	Cotton	1	1.3	16	1.8
AW11	1A:1B	1	Cotton	1	1.2	20	1.8
AW12	1A:1B	1	Cotton	1	1.3	24	1.5
AW13	1A:1B	1	Cotton	1	1.4	26	2.0

[a] PlatSil Gel-25 Part A and Part B, and PlatSil Part H Hardener (Polytek® Development Corp., Easton, PA, USA).
[b] PowerMesh fabric (69% polyamide / 31% lycra). Cotton handkerchief (HEMA B.V., Amsterdam, The Netherlands)
[c] Measured with an electronic caliper (500-752-20, Mitutoyo Corporation, Kawasaki, Japan).
[d] UC: Umbilical cord.

K

Production Protocol Abdominal Wall

This appendix provides a comprehensive outline of the production protocol implemented for the abdominal wall during the fourth and final prototyping round. The protocol presented herein is the result of extensive testing and numerous iterations conducted during the preceding prototyping rounds.

K.1. Materials and Equipment

- Cotton handkerchief (HEMA B.V., Amsterdam, The Netherlands)
- PlatSil® Gel-25 Part A (Polytek® Development Corp., Easton, PA, USA)
- PlatSil® Gel-25 Part B (Polytek® Development Corp., Easton, PA, USA)
- Silicone color pigment 'White' (Silc Pig® Pigments, Smooth-On, Inc., Macungie, PA, USA)
- Silicone color pigment 'Light Flesh' (Silc Pig® Pigments, Smooth-On, Inc., Macungie, PA, USA)
- Silicone color pigment 'Blood' (Silc Pig® Pigments, Smooth-On, Inc., Macungie, PA, USA)
- Laboratory balance (EMB 600-2, Kern, Balingen, Germany)
- Cardboard cup (300 ml capacity)
- Wooden paint stir stick (200 mm x 25 mm x 5 mm)
- Cardboard shelf covered with fake leather (30 cm x 50 cm)
- Synthetic flat brush (25 mm)
- Punch kit (including 6 mm, 12 mm, 16 mm, 20 mm, 24 mm and 26 mm pieces)
- Mallet
- Wooden shelf
- Stainless steel tailoring scissors (G-5150, Green Bell, Osaka, Japan)

K.2. Production Protocol

K.2.1. Preparation Cotton Fascia

To begin, the cotton handkerchief was soaked with tap water and then carefully stretched out over a cardboard shelf, ensuring all folds and wrinkles were eliminated. It was left to air dry until completely dry and free of any creases.

Following that, a rectangular piece measuring 20 cm x 10 cm was carefully cut out from the center of the handkerchief, ensuring that the selected portion of the fabric did not include any woven patterns.

K.2.2. Preparation Silicone Rubber

A silicone rubber was prepared by combining the LSR components PlatSil® Gel-25 Part A (Polytek®) and Part B. To accurately measure and combine these PlatSil® components, a cardboard cup was used. The process commenced by weighing Part A, precisely measuring 15 grams. Subsequently, Part B was added to the same cup and weighed to 15 grams as well.

Next, two drops of the silicone color pigment 'White,' two drops of 'Light Flesh,' and one drop of 'Fresh Blood' were carefully added to the silicone mixture.

The pain stir stick was used to thoroughly mix the components together for approximately 30 seconds, ensuring a homogeneous mixture.

K.2.3. Pouring the Liquid Silicone Rubber

Subsequently, the prepared liquid silicone mixture was poured from the cardboard cup onto the center of the cardboard shelf, making sure not to exceed an area of 20 cm x 10 cm. A flat brush was used to carefully spread out the silicone in a rectangular shape, covering approximately 20 cm x 10 cm. Once the silicone was evenly distributed, the cut-out cotton piece of fabric was gently placed on top of the silicone mixture.

After waiting for about 30 seconds to allow the silicone to penetrate the fabric's pores any areas of the cotton fabric that were not yet fully embedded in the silicone were lightly tapped upon manually with fingertips. This ensured that the entire cotton piece became fully embedded in the silicone mixture, as depicted in Figure K.1. Subsequently, the model was left to cure for 1 hour.

K.2.4. Post-processing

After the 1-hour curing period, the silicone abdominal wall was carefully removed from the cardboard shelf. To ensure a proper fit between the 3D printed parts of the validation model, the abdominal wall was cut to a width of 9 cm. Additionally, the shorter ends of the abdominal wall were trimmed slightly for a clean appearance, leaving sufficient length to fit well inside the model.

A 6 mm hole was then punched in the middle of the abdominal wall to accommodate the UC. Adjacent to the 6 mm hole, a second hole was punched, ensuring alignment of the midpoints and leaving a distance of about 1-2 mm between the two holes. This second hole represented the abdominal wall defect, and its diameter varied among the last five prototypes, with sizes of 12 mm, 16 mm, 20 mm, 24 mm, and 26 mm, respectively. The abdominal wall prototypes created during the fourth and final prototyping round are depicted in Figure K.2.

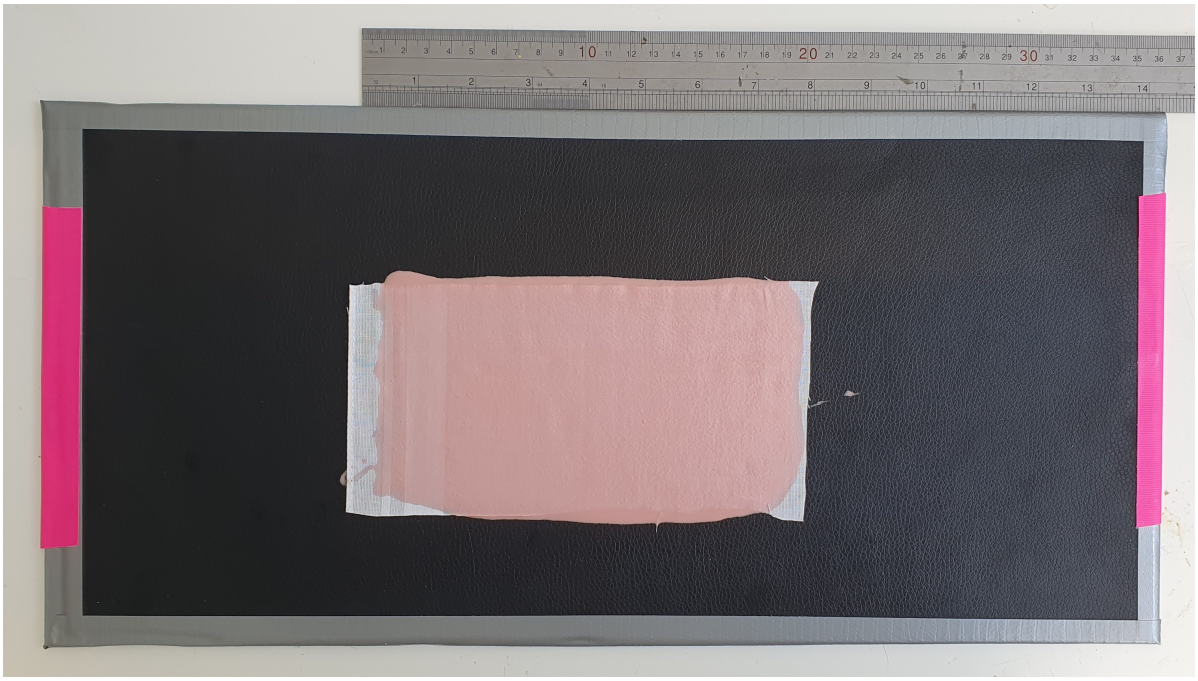

Figure K.1: Liquid silicone rubber (LSR) poured over a cardboard shelf covered with fake leather, with a 20 cm x 10 cm cotton piece embedded in the LSR during the production of the abdominal wall. Note that this particular piece of cotton fabric was not cut out of the middle of the handkerchief, as a woven pattern can be seen on the left side, as this photograph was taken during a preceding prototyping round.

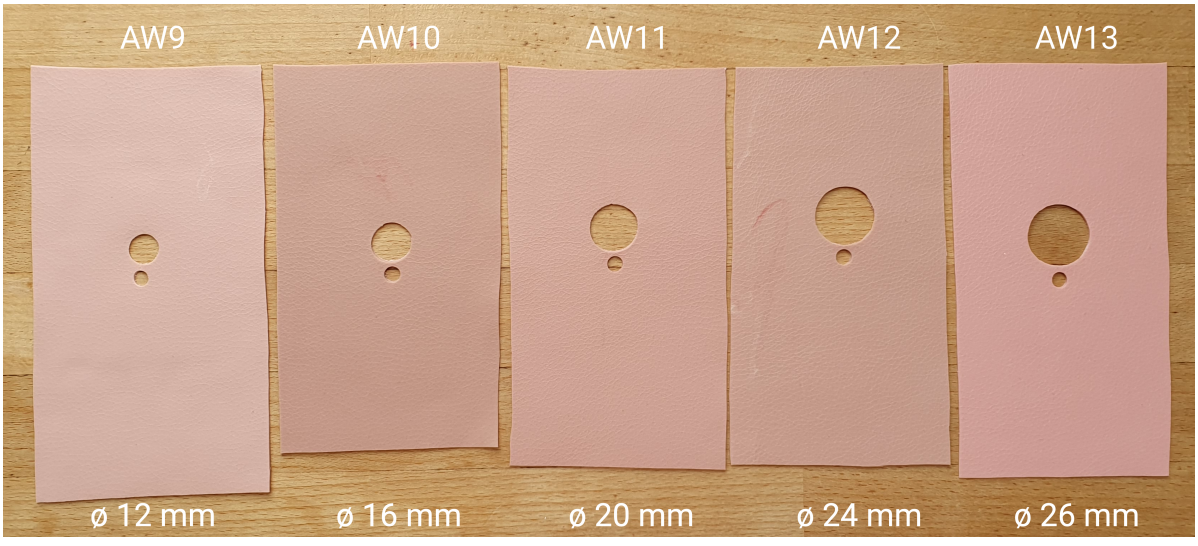

Figure K.2: Abdominal wall prototypes created during the fourth and final prototyping round with defect sizes ranging from 12 mm to 26 mm. All prototypes include a 6 mm hole for embedding the umbilical cord.

Technical Specifications 3D-Printed Components Validation Model

Figure L.1 showcases the 3D-printed components of the validation model in a trimetric view. Figure L.2 and Figure L.3 offer technical illustrations of the base and top components, respectively.

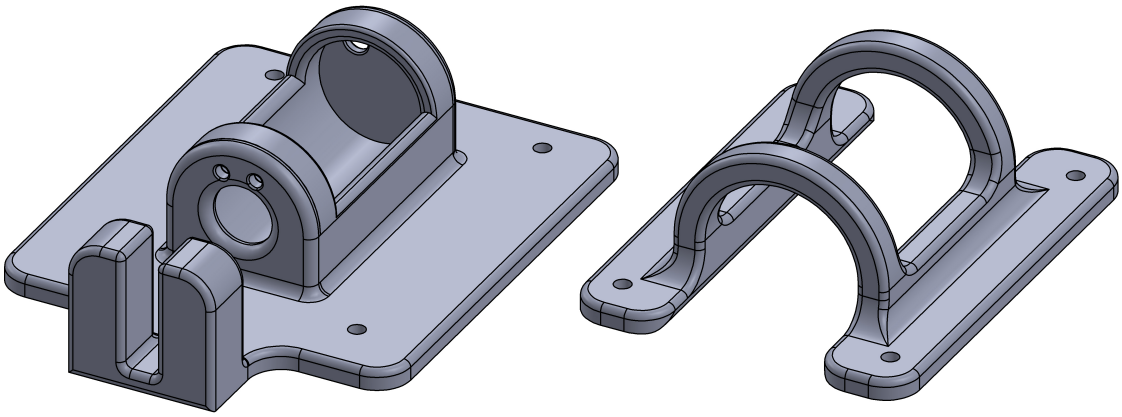

Figure L.1: Trimetric view of 3D-printed validation model components: base (left) and top (right).

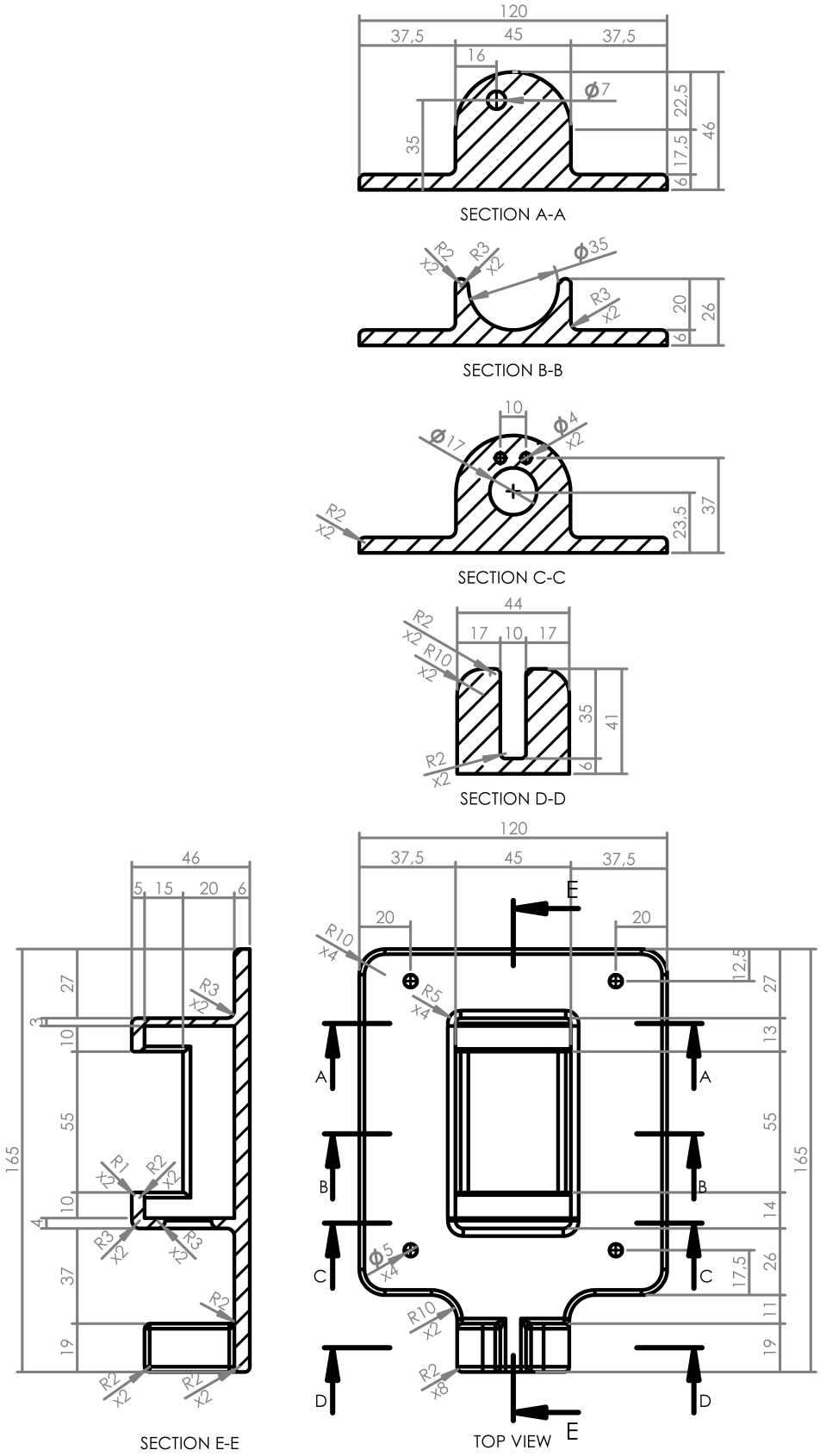

Figure L.2: Technical illustration depicting the 3D-printed base component of the validation model. All dimensions are expressed in millimeters (mm).

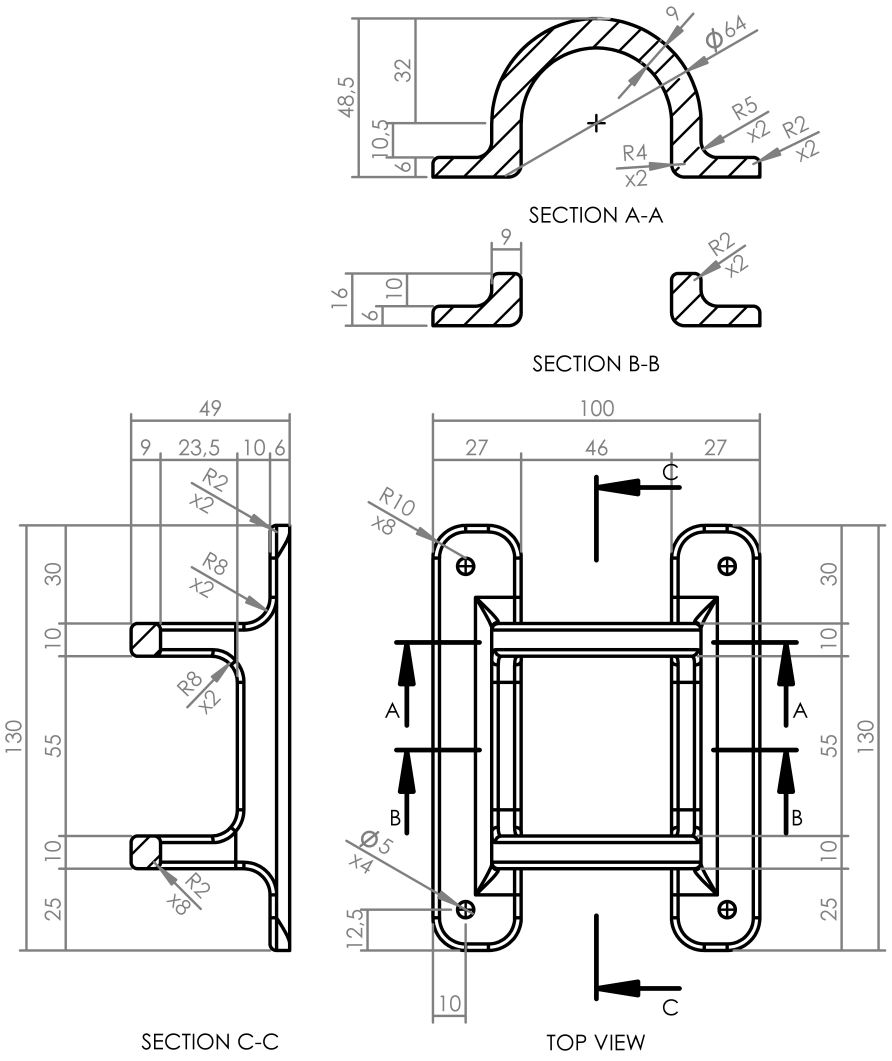

Figure L.3: Technical illustration depicting the 3D-printed top component of the validation model. All dimensions are expressed in millimeters (mm).

M

Assembly Instructions Validation Model

This appendix presents the assembly instructions for the validation model used in the validation experiments described in Chapter 5. Section M.1 presents a comprehensive list of all components and materials used in the validation model. Section M.2 provides step-by-step instructions for constructing specific components of the validation model. Lastly, Section M.3 offers detailed instructions for assembling the complete validation model.

M.1. Components and Materials

- 3D-printed components (produced according to Section 4.4.3)
  - Top
  - Base
- UC and its vessels
  - Silicone tube (ø 6 mm, length 20 cm)
  - 2 × Silicone tube (ø 3 mm, length 20 cm)
  - Transparent shrink sleeve (length 10 cm)
- IAP regulation setup
  - Manual blood pressure monitor (ST-A211-II, Stalt Medical, Dordrecht, The Netherlands)
  - Connection nipple (small side ø 5 mm, large side ø 18 mm)
  - Latex balloon (30 cm)
  - 2 × Zip tie
- Abdominal wall (produced according to Appendix K)
- 2 × Sealing clip (BEVARA Sealing clip (6 cm), IKEA, Delft, The Netherlands)
- 4 × Knurled-head thumb screw (M4, length 20 mm)
- 4 × Wing nut (M4)
- Water-based lubricant (EasyGlide, Veendam, The Netherlands)

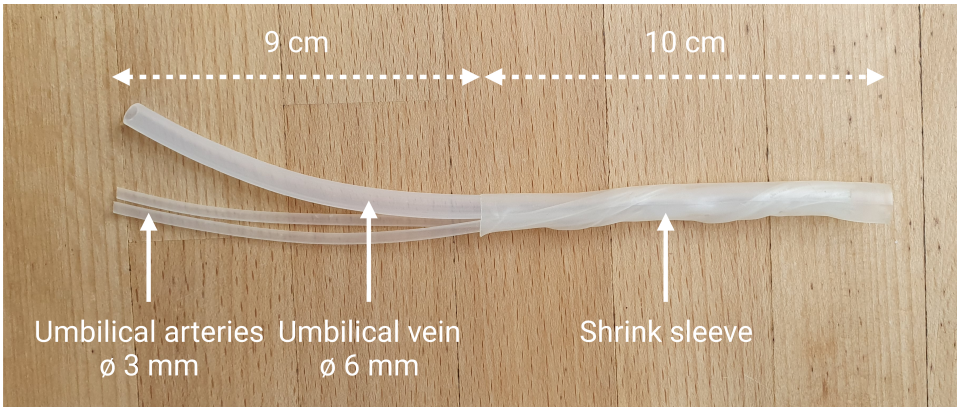

Figure M.1: Umbilical cord and vessels.

M.2. Preparation Components

M.2.1. Umbilical Cord and Vessels

To construct the UC and vessels presented in Figure M.1, take the following steps:

1. Take two 3 mm silicone tubes and tightly twist them around a 6 mm silicone tube.
2. Place the transparent shrink sleeve carefully over approximately half of the twisted tubes.
3. Using a blow dryer, gently heat the shrink sleeve until it tightly encloses the twisted tubes.

M.2.2. Intra-Abdominal Pressure Regulation Setup

To construct the IAP regulation setup presented in Figure M.2, take the following steps:

1. Cut the tube of the manual blood pressure monitor near the arm cuff.
2. Insert the small side of the connection nipple firmly into the tube.
3. Stretch the open end of the latex balloon over the larger side of the connection nipple.
4. Use two zip ties to fasten the balloon securely to the connection nipple, ensuring that the zip tie heads are positioned precisely opposite each other.
5. To check the seal, increase the pressure to 20 mmHg in the balloon using the inflation bulb while keeping the air release valve closed. Wait and observe if the pressure remains at 20 mmHg for one minute.
6. If the balloon is properly sealed, open the air release valve to decrease the pressure inside the balloon to 0 mmHg, and then close the air release valve.

M.3. Assembly Instructions

When the UC with vessels and the IAP regulation setup have been prepared, the following steps need to be taken to assemble the validaton model:

1. Insert the balloon into the abdominopelvic cavity through the 17 mm hole on the base's inferior side. Ensure the balloon is not twisted and place the slender part of the connection nipple into the slot, following the illustration in Figure M.3.

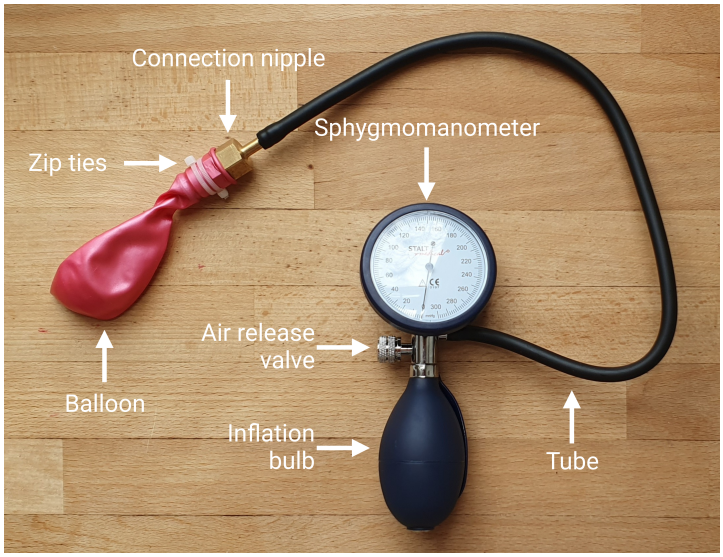

Figure M.2: Intra-abdominal pressure regulation setup.

2. Position the umbilical vessels in the base: insert the UV into the 7 mm hole on the base's superior side and the UAs into the 4 mm holes on the base's inferior side. Verify that the vessels are not twisted, and the UC is centered within the abdominopelvic cavity.

3. Use the inflation bulb to increase the pressure inside the balloon to 10 mmHg. Secure the position of the umbilical vessels with sealing clips on both the superior and inferior sides of the base. Ensure that the UC is centered, as depicted in Figure M.4, and that the vessels are not under tension.

4. Apply a few drops of water-based lubricant to the visible part of the balloon and evenly spread it manually to ensure proper lubrication.

5. Take the selected abdominal wall and insert the UC through the 6 mm hole from the underside of the abdominal wall. Place the abdominal wall over the base, ensuring the abdominal wall defect is located on the right side of the UC.

6. Align the top over the abdominal wall, matching the 5 mm holes for the screws in the top and base. Make sure the abdominal wall conforms nicely to the shape of the arches of the top and base, without any indentation in the middle of the abdominal wall. Additionally, ensure the defect stretches as minimally as possible, maintaining a circular shape.

7. Securely fasten the top and base together using the knurled-headed thumb screws and wing nuts.

8. Use the inflation bulb to raise the pressure inside the abdominopelvic cavity to 20 mmHg, as depicted in Figure M.5.

9. Apply a few drops of water-based lubricant to the area surrounding the abdominal wall defect, as depicted in Figure M.6.

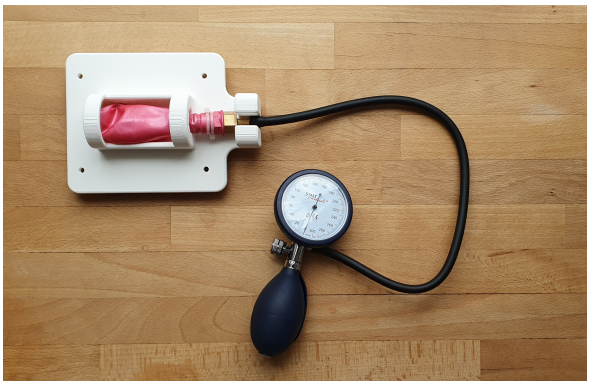

Figure M.3: The balloon is inserted into the abdominopelvic cavity, with the slender part of the connection nipple positioned in the slot of the base.

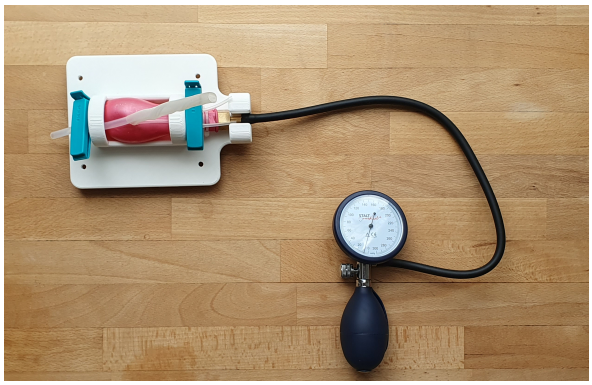

Figure M.4: The umbilical vessels are secured with the sealing clips, ensuring the umbilical cord is centered, and the pressure is set at 10 mmHg.

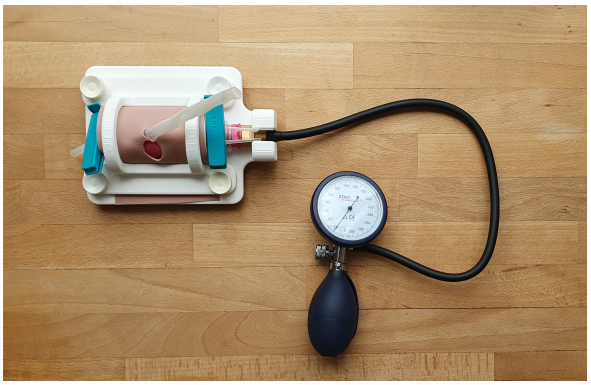

Figure M.5: The top and base are fastened together with the abdominal wall in between, and the pressure is set to 20 mmHg.

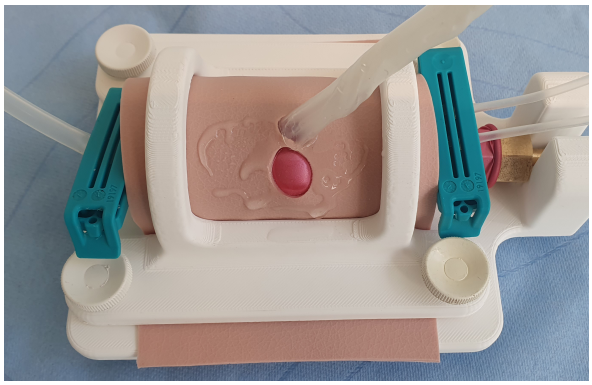

Figure M.6: The area surrounding the abdominal wall defect is lubricated with water-based lubricant.


Erasmus MC


TU Delft